Exploring Geospace Dynamics Through Ground Magnetic Perturbations during Substorms

Reham Elhawary

Thesis for the degree of Philosophiae Doctor (PhD)
University of Bergen, Norway
2024

UNIVERSITY OF BERGEN

Exploring Geospace Dynamics Through Ground Magnetic Perturbations during Substorms

Reham Elhawary

Thesis for the degree of Philosophiae Doctor (PhD)
at the University of Bergen

Date of defense: 18.06.2024

Year: 2024

Title: Exploring Geospace Dynamics Through Ground Magnetic Perturbations during Substorms

Name: Reham Elhawary

Print: Skipnes Kommunikasjon / University of Bergen

Acknowledgements

I am profoundly grateful to Allah for granting me the opportunity to be in this position and to be a part of this exceptional group. It has facilitated immense growth in my knowledge and perspective. I think of my journey as being like that of a worm, long in its cocoon, and now on the way to transforming into the vibrant butterfly I aspire to be.

I extend my deepest gratitude and appreciation to my supervisor, Dr. Karl Magnus Laundal, for his incredible support, guidance, and patience. I will forever be indebted to you. Additionally, my sincere thanks go to my co-supervisor, Dr. Jone Peter Reistad, for the precious discussions, insights, and comprehensive ideas that have greatly enhanced my research.

I am so grateful to Dr. Anders Ohma for his insightful discussions and excellent work, which has been a reference in my research.

To my colleagues, thank you all for being part of this journey. Amalie and Ingrid, thank you for making me feel welcome and included. Eldho, thank you for all the nice and kind situations that I will never forget, and also the jokes and good humor. Margot, thank you, my kind office mate. I will remember the twisted version of playing video games together, and that I always won :D.

On a personal note, my heartfelt thanks go to my family for their continuous support. Dad, Mum, Rnia, Rana, and Rawan - I am forever thankful. To my children, Zain and Hana, your presence and happiness are my daily motivation to be eager to do more. The joy of seeing you thrive pushes me to overcome all challenges and to strive to be the best version of myself, both as a researcher and a parent you deserve. To my dear friend Khadiga: your amazing support and our friendship have been essential for my journey. I could not have wished for a better friend. Khadiga, deeply from my heart, Thank you. To my dearest Ghadeer, Waad, Samar, Nour, Ayat, and Reham, thank you for brightening my days. Rawan and Mariam, thank you for being there for me at the most needed; I can never forget that. Last but by no means least, Thank you, Kavitha, for treating me and my kids as family. We will always remember that.

Reham Elhawary
Bergen, 2024

Abstract

Ionospheric dayside dynamics are primarily controlled by the interaction between the Interplanetary Magnetic Field (IMF) and Earth's magnetic field at the dayside magnetopause, while nightside ionospheric dynamics are mainly driven by magnetotail processes. This thesis investigates the impact of substorms on the ionospheric current system across dayside and nightside, under different orientations of IMF and across seasonal changes. By conducting superposed epoch analyses of ground magnetic field data, we offer a novel perspective on the influence of magnetotail activities on the behavior of the ionospheric currents on the dayside. Substorms occurring during northward IMF conditions offer a unique perspective on this because dayside reconnection is reduced, allowing for the isolation of magnetotail activity effects. Our findings reveal an enhancement in dayside ionospheric currents as the nightside activity increases, suggesting an impact of the nightside activity on the dayside dynamics during northward IMF substorms. We also observe that lobe cells become more pronounced post-onset, suggesting that the magnetospheric reconfiguration makes lobe reconnection more efficient.

Additionally, the study explores interhemispheric asymmetries in ionospheric dynamics. We show that during substorms, interhemispheric asymmetries induced by IMF B_y and dipole tilt reduce significantly in the nightside current, but this reduction is not observed in the dayside currents. This difference in response between the dayside and nightside ionospheric currents highlights the importance of integrating nightside dynamics into climatological models of ionospheric currents traditionally focused on upstream parameters. Furthermore, an investigation into auroral substorm onset locations uncovers that pre-substorm geomagnetic activity levels, as indicated by the AL index, significantly correlate with onset magnetic local time (MLT). This suggests that ionospheric conductance gradients lead to a duskward shift of magnetotail dynamics. By integrating these observations, the thesis offers novel insights into how substorms modulate ionospheric currents, highlighting the dynamic responses of the ionosphere to magnetospheric processes and laying a foundation for future modeling efforts that more accurately capture the magnetosphere-ionosphere coupling.

Abstrakt (Norsk)

Dynamikken på dagsiden av ionosfæren styres hovedsakelig av samspillet mellom det interplanetære magnetfeltet (IMF) og jordens magnetfelt på dagsiden av magnetopausen, mens dynamikken på nattsiden hovedsakelig drives av prosesser i magnetohalen. Denne avhandlingen undersøker effekten av substormer på strømsystemet i ionosfæren på både dagsiden og nattsiden, under ulike orienteringer av IMF og i forskjellige sesonger. Våre statistiske analyser av bakkebaserte magnetfeltdata gir et nytt bilde av hvordan magnetohaleaktiviteter påvirker ionosfærens strømmer på dagsiden. Substormer som oppstår når IMF peker nordover gir en unik mulighet til å studere dette fordi koblingen med solvinden på dagsiden er redusert. Dette gjør at vi kan isolere effektene fra magnetohaleaktivitet. Våre funn viser en forsterkning i ionosfærestrømmer på dagsiden ettersom nattsidens aktivitet øker, noe som tyder på at nattsideaktivitet påvirker dagsiden under substormer med nordoverrettet IMF. Vi observerer også at lobe-celler blir mer tydelige etter at substormer har startet. Dette tyder på at endringer i formen til magnetosfæren under substormer gjør koblingen mellom lobene og solvinden mer effektiv.

I tillegg utforsker vi interhemisfæriske asymmetrier i ionosfæredynamikk. Vi viser at interhemisfæriske asymmetrier i ionosærestrømmer, indusert av IMF B_y og sesongforskjeller, blir sterkt redusert på nattsiden under substormer, men ikke på dagsiden. Denne forskjellen i respons mellom ionosfærestrømmer på dagsiden og nattsiden understreker viktigheten av å inkludere nattsidedynamikk i klimatologiske modeller av ionosfærestrømmer, som tradisjonelt har fokusert på oppstrømsparametere. Videre viser vi at posisjonen til nordlysutbrudd under substormer avhenger av geomagnetisk aktivitetsnivå før utbruddet, indikert ved AL-indeksen. Dette tyder på at gradienter i ionosfærisk konduktans fører til en forskyvning av dynamikken i magnetohalen mot kveldssiden. Tilsammen gir denne avhandlingen nye innsikter i hvordan substormer endrer ionosfæriske strømmer, og fremhever den dynamiske responsen fra ionosfæren på magnetosfæriske prosesser, og legger et grunnlag for fremtidig modelleringsarbeid som mer nøyaktig fanger opp koblingen mellom magnetosfæren og ionosfæren.

List of publications

This thesis consists of an introductory section and three scientific papers. Two of these papers have been published in peer-reviewed journal, while the third is under review at the time of the thesis submission.

The three scientific papers that comprise the results of this thesis are

Paper I Elhawary, R., Laundal, K. M., Reistad, J. P., Hatch, S. M. (2022). *Possible ionospheric influence on substorm onset location.* Geophysical Research Letters, 49, e2021GL096691. https://doi.org/10.1029/2021GL096691.

Paper II Elhawary, R., Laundal, K. M., Reistad, J. P., Madelaire, M., Ohma, A. (2023). *Substorm impact on dayside ionospheric currents.* Geophysical Research Letters, 50, e2023GL104800. https://doi.org/10.1029/2023GL104800

Paper III Elhawary, R., Laundal, K. M., Reistad, J. P., Madelaire, M. *How do substorms influence hemispheric asymmetries in equivalent currents?*, In review.

Contents

Acknowledgements i

Abstract iii

Abstrakt (Norsk) v

List of publications vii

1 Introduction 1

2 Solar Wind and Interplanetary Magnetic Field Interaction with The Earth's Magnetic Field 3
- 2.1 Overview of Near-Earth space . . . 3
- 2.2 The Earth's Magnetic Field . . . 4
  - 2.2.1 The Earth's Internal Field . . . 5
  - 2.2.2 The Earth's External Field . . . 5
- 2.3 Dungey Cycle . . . 7
- 2.4 The Expanding Contracting Polar Cap Paradigm (ECPC) - Magnetospheric Perspective . . . 9

3 Ionospheric Convection and Current Systems as a Response to the Magnetosphere - Solar Wind Interactions 11
- 3.1 The Earth's Ionosphere . . . 11
- 3.2 Convection and Currents in The Polar Ionosphere . . . 12
  - 3.2.1 The Expanding Contracting Polar Cap Paradigm (ECPC) - Ionospheric Perspective . . . 12
  - 3.2.2 Convection During Different IMF Orientations . . . 14
  - 3.2.3 Ionospheric Current System . . . 17
- 3.3 High Latitudes Ionospheric Current Observations . . . 19

4 Substorm Dynamics: Modeling, Prediction, and Interhemispheric Asymmetries 21
- 4.1 Historical View of Substorms . . . 21
- 4.2 Substorm Current Wedge . . . 23
- 4.3 Models to Explain Substorms . . . 24
  - 4.3.1 Inside-Out Theory (Current Disruption Model) . . . 24
  - 4.3.2 Outside-In Theory (Bursty Bulk Flow Theory) . . . 25

4.4 Prediction of Substorms 28
4.4.1 Predicting Substorm Onset Timing 29
4.4.2 Predicting Substorm Onset Location 29
4.5 Substorms During Northward IMF 30
4.6 Substorm Influence on Interhemispheric Asymmetries 31

5 Data and Method **33**
5.1 Data 33
5.1.1 Ground-based Magnetometer Data 33
5.1.2 Geomagnetic Indices 33
5.1.3 Substorm Onset Detection 35
5.2 Method 36
5.2.1 Spherical Harmonic Analysis 36
5.2.2 The Inverse Problem 37
5.3 Uncertainties 38

6 Summary of the papers **43**

7 Conclusions **47**
7.1 Conclusions 47

8 Scientific results **61**

Chapter 1

Introduction

Geospace, the outer space surrounding our planet, is an energetic and dynamic environment where the Sun and Earth engage through energy and mass transfer. The magnetosphere, the region of space influenced by Earth's magnetic field, is subject to variations over a range of timescales, from minutes to days and years, mainly driven by the solar wind. These interactions also cause substantial variations in the ionized part of Earth's upper atmosphere, the ionosphere, which plays a critical role in space weather phenomena such as aurora and magnetic disturbances observed on ground.

When the Interplanetary Magnetic Field (IMF), transported by the solar wind, interacts with Earth's magnetic field at the dayside region of the magnetosphere, it leads to loading of energy to the nightside of the magnetosphere, the magnetotail. After some time, part of this stored magnetic energy can be released in explosive events called substorms. Substorms are short-lived phenomena that are highly unpredictable but happen on average several times daily. They can impact satellite operations, GPS accuracy, power grids, and communication systems. Understanding substorms helps predict space weather events and mitigate their effects on technology and infrastructure. Given their significance in magnetospheric dynamics, it is also an important research topic to understand planetary magnetic environments better.

The orientation of the IMF significantly influences the strength and shape of currents and plasma convection as observed from the ionosphere. The interaction between the magnetosphere and the the IMF occurs on the dayside, and therefore its influence is most important in the dayside ionosphere. Substorms, on the other hand, predominantly affect the nightside. However, the overall relative contribution of the dayside and the nightside to global plasma circulation remains uncertain. Furthermore, the unpredictability of the timing and location of substorm onsets poses a significant challenge, representing a crucial gap in our current prediction capabilities of ionospheric dynamics.

The objectives of this thesis are to

1. **Investigate the influence of substorms on ionospheric current systems, emphasizing the difference in response between the dayside and nightside.**

2. **Examine to what extent substorm onset location can be predicted.**

To achieve these objectives we analyzed magnetic field perturbations from the ground and the corresponding horizontal ionospheric current system. The thesis is

based on three papers, two of which are published in peer-reviewed journals, and a third which is in a peer review at the time of the thesis submission.

To fulfill the first objective of this thesis, In Paper II, we study global maps of the ionospheric currents during substorms that took place during northward IMF. During northward IMF conditions, the dynamics at the dayside magnetopause are minimal, presenting an opportunity to focus on the magnetotail dynamics. We employed a statistical approach, applying superposed epoch analysis of substorm events during this interval. Our approach highlighted the impact of the nightside dynamics on the dayside current system during such circumstances. In Paper III, we expand this approach to explore the influence of the nightside dynamics on both the dayside and nightside equivalent current during substorms that occur during a broader range of conditions. In these papers, we present global maps of the dayside and nightside ionospheric currents as well as maps of the changes in the currents during different conditions.

The second objective is explored in Paper I. In Paper I, we confirm earlier results that show that the substorm onset location is highly unpredictable. However, we also find that ionospheric dynamics can help determine the substorm onset location, suggesting that the ionosphere modulates magnetospheric dynamics. Since the first objective is investigated in papers II and III, we did not follow a chronological order when introducing the papers.

In the following chapters, we will present the background material needed to put the results of this thesis into context. In chapter 2, we introduce the theoretical framework that describes the magnetospheric system and briefly present relevant regions and physical processes in near-Earth space. In chapter 3, we connect the magnetospheric dynamics to the response of the ionospheric system. In chapter 4, we elaborate on the current understanding of substorms and set the stage for our results by discussing the role of substorms in influencing the magnetosphere-ionosphere coupling. In chapter 5, we present the data and methodology used throughout the analysis. In chapter 6, we summarize each of the three articles included in this thesis. In Chapter 7, we conclude the thesis. Paper I - III comprise chapter 8.

Chapter 2

Solar Wind and Interplanetary Magnetic Field Interaction with The Earth's Magnetic Field

In this chapter, we provide an overview of the fundamental interactions between the solar wind, the Interplanetary Magnetic Field (IMF), and Earth's magnetic field that shape the dynamic environment of geospace. Understanding these interactions is essential to comprehending the triggers and behavior of substorms, a key focus of this thesis. The solar wind and IMF are the primary external drivers of magnetospheric dynamics, exerting their influence through mechanisms such as magnetic reconnection, which can dramatically alter the configuration of Earth's magnetic field.

2.1 Overview of Near-Earth space

The solar wind, a plasma flow from the Solar upper atmosphere, moves radially away from the Sun. This movement gains speed, allowing the solar wind to become supersonic within a few solar radii from the Sun (*Parker*, 1958). As this rarefied plasma progresses, collisions become negligible. As a result, the Interplanetary Magnetic Field (IMF) becomes "frozen-in" to the solar wind, meaning that they move cohesively. The footpoints of the IMF remain anchored to the Sun as they are stretched into outer space. As the Sun rotates, the attached IMF attains a "Ballerina skirt" shape throughout the heliosphere. This phenomenon is called the Parker spiral. The motion of the solar wind and the IMF lines in the inner heliosphere are shown in Figure 2.1.

The solar wind undergoes fluctuations, changing in a wide spectrum of timescales. Typically, the solar wind takes 2 to 3 days to reach our planet, with speeds ranging from about 200 to 900 km/s near Earth.

Unlike the primarily radial movement of the solar wind, the orientation of the IMF can deviate from its typical Parker spiral pattern. Various coordinate systems are employed to categorize these directions, including the geocentric solar ecliptic system, the geocentric solar equatorial system, the solar magnetic coordinates, and the geocentric solar magnetic system (GSM) (*Fränz and Harper*, 2002; *Laundal and Richmond*, 2017). We utilize the GSM system to describe the three components of the IMF: B_x, B_y, and B_z. In the GSM system the x-axis points from Earth to the Sun, the y-axis is

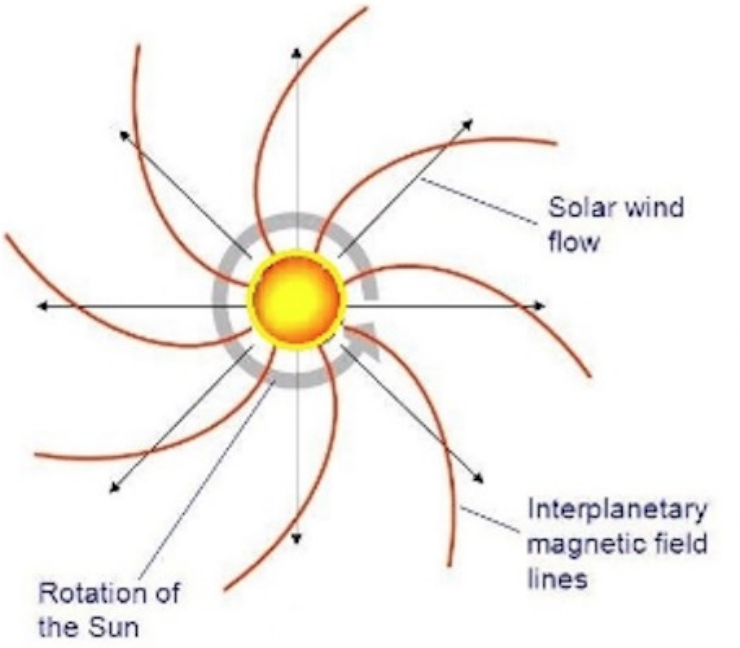

Figure 2.1: An overview of the Parker spiral, Figure by Ram Singh.

oriented perpendicularly to Earth's magnetic dipole, and the z-axis has the same direction as the projection of the magnetic dipole axis onto the plane where the x axis is the normal vector. In this system, the orientation of the IMF in the plane perpendicular to the x-axis is defined as the IMF clock angle, denoted as θ_{ca}, computed using

$$\theta_{ca} = \arctan 2(B_y, B_z). \tag{2.1}$$

IMF θ_{ca} is a useful tool to specify the IMF orientation. The IMF different orientations controls the reconnection geometry in the magnetosphere which we will discuss in the next chapter. The solar wind and IMF variations are key indicators for predicting space weather conditions. By closely monitoring the solar wind speed, its density, and the direction of the IMF, we can anticipate alterations in Earth's space environment. This understanding is crucial for taking early actions to modify potential space-related disturbances.

2.2 The Earth's Magnetic Field

Planet Earth is gifted with an impressive shield that protects life within this planet from the harmful galactic cosmic rays and dangerous solar wind (*Erdmann et al.*, 2021). This shield is the Earth's magnetic field, a feature that has not only been important for planetary protection against the solar wind and the cosmic rays, but also instrumental in human discovery and innovation. The use of magnetism began after the discovery

of the lodestone, a stone rich in magnetic iron oxide. The Chinese were the first to use lodestone to make the compass, several centuries before Christ. The compass arrived in Europe through Arab traders at the end of the 12th century (*Campbell*, 1997). Then the magnetic properties of the Earth were known when the Englishman William Gilbert published his book The Magnet in 1600, and after that, he began measuring changes in the geomagnetic field at the London Observatory.

Earth's magnetic field is a dipole-like field as shown in the upper panel of Figure 2.2. Our understanding of the Earth's magnetic field has changed since then and scientists developed mathematical models to help figure out its nature and behavior as will be described in the next sections. Careful analyses of rock magnetization from sites all over the world have established that the Earth's axial dipole polarity has undergone multiple reversals in the past. Each polarity interval typically lasts several thousand years. These geomagnetic reversals occur slowly and at irregular intervals. It is worth noting that the direction of the magnetic field around the Earth at present is from the south to the north pole (*Campbell*, 1997). The underlying mechanisms driving these reversals are still a subject of scientific inquiry, but they are likely related to complex processes within the Earth's core dynamo. During these reversals, the strength of the magnetic field weakens significantly, and the field configuration becomes complex with multiple poles.

2.2.1 The Earth's Internal Field

The Earth's magnetic field, as observed on the Earth's surface, is composed of external and internal components. The internal field originates mainly from a dynamo process inside the Earth's outer core. This process involves the movement of an electrically conductive fluid in the core, generating magnetic fields. The main dipole field of the Earth, a significant component of the inner field, is thought to arise from a single primary circulation within this fluid (*Campbell*, 1997). In contrast, non-dipole regional anomalies, which are deviations from the main field, are believed to be caused by various eddy motions in the outer layer of the liquid core, situated below the mantle (*Campbell*, 1997). Smaller geographical anomalies, known as surface anomalies, are field irregularities due to deposits of ferromagnetic materials in the Earth's crust (the largest is the Kursk anomaly, 400 km south of Moscow). Generally, Earth's inner magnetic field can be effectively represented as a dipole field up to approximately three Earth radii, as shown in the upper panel of Figure 2.2.

2.2.2 The Earth's External Field

On the other hand, the external field originates through the current systems in the ionosphere and the magnetosphere. The magnetic field on the dayside is compressed by the solar wind interactions, and the nightside is elongated and stretched as shown in the bottom panel of Figure2.2. The magnetosphere obtains its characteristic shape from its interactions with the solar wind and its embedded IMF. The bottom panel of Figure 2.2 illustrates the major regions of the magnetosphere where the **bow shock** represents the initial boundary the solar wind encounters, causing a dramatic reduction in speed and a transition to subsonic flow. Just beyond the Bow Shock lies the **magnetosheath**,

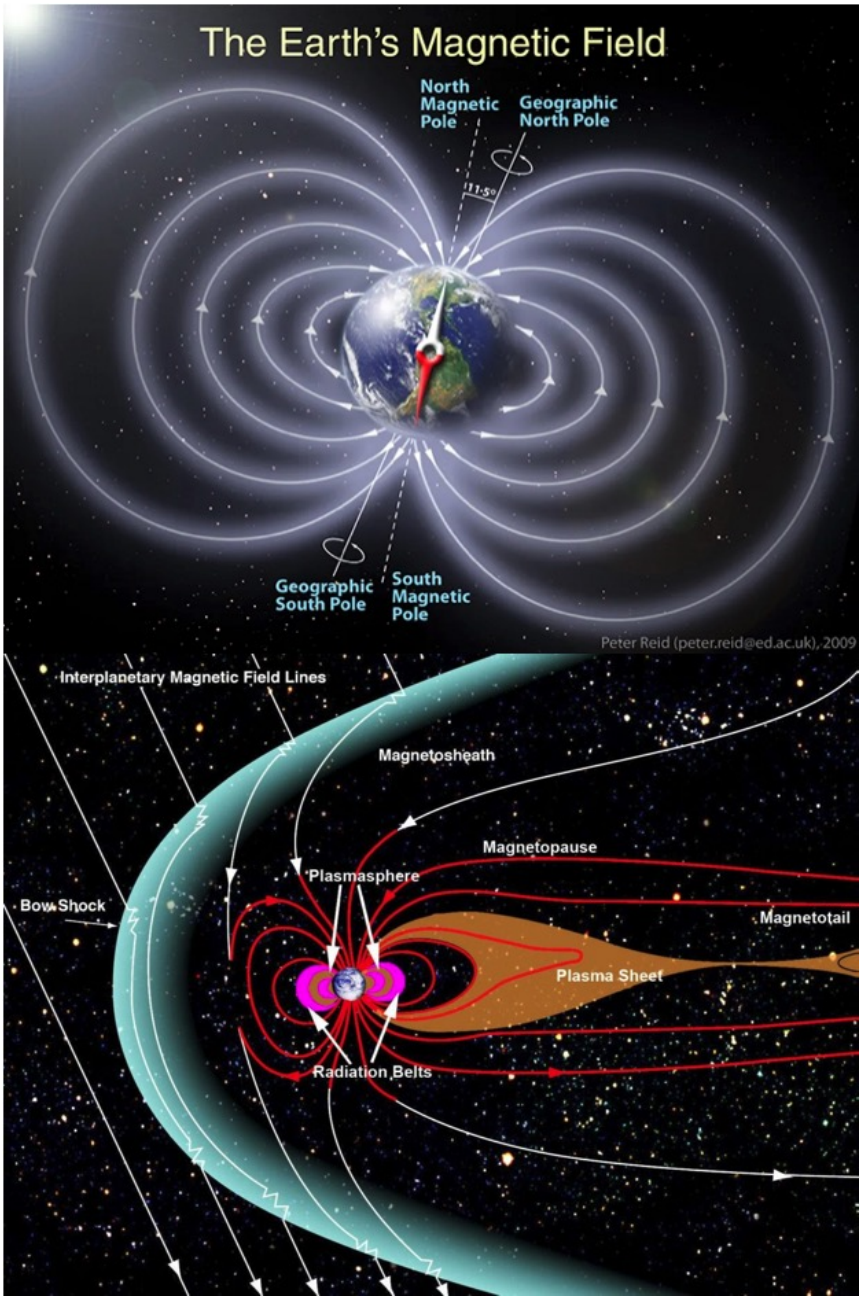

Figure 2.2: The main magnetic field is shown as a dipole-like field in the upper panel, Credit:NASA/Peter Reid. The lower panel shows the extension of the magnetic field away from the Earth and the main components of the magnetosphere, Credit: NASA/Goddard/Aaron Kaase

a region filled mainly with IMF and characterized by dynamic mixing with Earth's magnetic field, sandwiched between the bow shock and the magnetopause. The **magnetopause** itself is the definitive boundary that separates the magnetosphere from the solar wind. Within the inner section of the magnetosphere is the **plasmasphere**, containing cold low-energy ions and electrons. **The radiation belts**, or Van Allen Belts, comprise regions filled with charged particles trapped by Earth's magnetic field. In these middle and lower latitudes, the plasmasphere is abundant with dense ionospheric plasma that co-rotates with Earth. Beyond the plasmasphere, within the radiation belts, a more energetic plasma exists, consisting of particles trapped in Earth's magnetic field, contributing to the formation of the ring current. The **plasma sheet** is filled with highly energetic plasma, and it has a dynamic magnetic field structure and is the source of discrete nightside auroras. The **lobes** are situated on either side of the Plasma Sheet and extending to the magnetopause. They are filled with cold, low-density plasma connected to the IMF and not magnetically linked between the northern and southern hemispheres. Away from the Sun is the **magnetotail** that encompasses the plasma sheet and the lobes. The dayside ionosphere features polar cusps where magnetosheath plasma can directly access the magnetosphere and the ionosphere, leading to the formation of high-latitude dayside auroras. The ionosphere will be discussed in the next chapter.

2.3 Dungey Cycle

To explain the interaction of the solar wind with the magnetosphere and the subsequent global-scale plasma circulation, we need to explain how the magnetic reconnection plays a key role in facilitating the observed plasma dynamics.

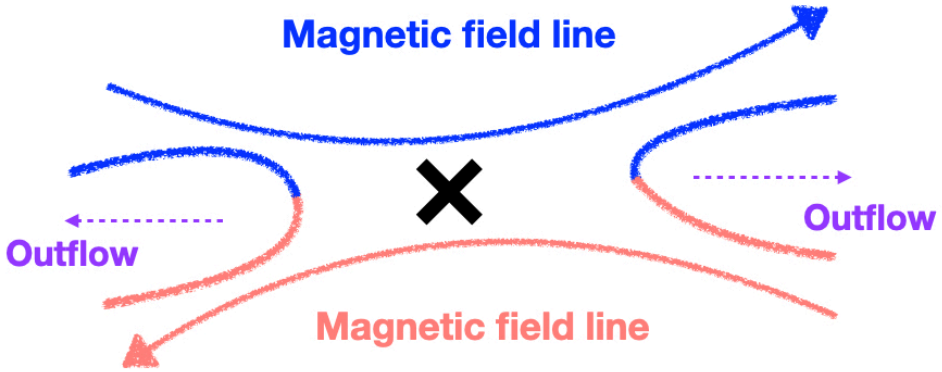

Figure 2.3: Illustration of magnetic reconnection between two magnetic field lines.

When the solar wind carrying the IMF reaches the Earth, the IMF interacts with the Earth's magnetic field. The mechanism facilitating this interaction is called reconnection. When the IMF orientation is southward, counter to the northward-pointing Earth's dipole field, they interact, and the magnetic topology is rearranged. The electrons move

from one field line and reconnect to another. This process converts magnetic field energy into kinetic and thermal energy in the plasma. Figure 2.3 illustrates a simplified explanation of the reconnection between two oppositely directed magnetic field lines. At point x, the upper and lower field lines reconnect, generating new interlinked field lines. On both the right and left are the outflow regions where the new field lines drift away from the reconnection point (extending to a line in 3D). Reconnection is most efficient when the encountering magnetic fields are entirely anti-parallel (*Dungey*, 1961; *Milan*, 2015). However, reconnection can still take place when there is an azimuthal component of the IMF, though this component introduces interhemispheric asymmetries, a topic we will discuss later.

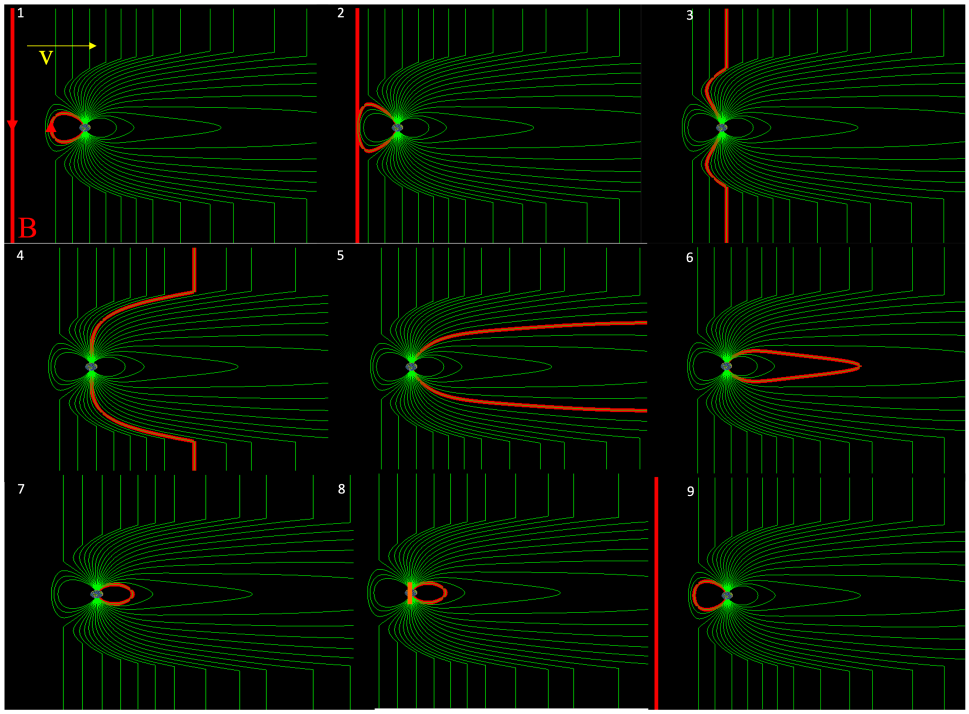

Figure 2.4: Overview of the magnetospheric circulation during Dungey cycle, credit to the COMET program at HAO.

Magnetic reconnection in the Earth's dayside magnetopause primarily takes place between the Earth's northward-oriented compressed dipole field and a southward-directed interplanetary magnetic field (IMF). This phenomenon sets off a plasma circulation, initially described by *Dungey* (1961). Figure 2.4 represents the Dungey cycle under conditions where the IMF is southward-oriented and absence of an azimuthal component. We here describe the Dungey cycle in stages based on Figure 2.4:

- Stage 1: The IMF near the dayside of the magnetopause is oriented southward, contrasting the northward alignment of the Earth's magnetic field.
- Stage 2: As the plasma of the solar wind and the accompanying magnetic field approach the Earth, the two magnetic fields reconnect at the dayside magnetopause.

- Stage 3: This reconnection led to creating newly opened magnetic field lines. One end of these lines remains anchored to the Earth's magnetic field, while the opposite end links to the IMF.
- Stage 4: The flow of the solar wind drags these open field lines tailward across the polar cap, adding them to the magnetotail lobes.
- Stage 5: These field lines are then further elongated towards the magnetotail.
- Stage 6: As the lobes amass more open field lines, increased magnetic pressure prompts another reconnection event within the magnetotail. Here, the field lines reconnect, anchoring themselves to both hemispheres.
- Stage 7: These elongated field lines experience a tension force that pushes them away from the reconnection site. As the stretched closed field lines approach Earth, they become more dipolar.
- Stage 8: Driven by pressure imbalances, these field lines migrate back to the dayside, potentially coming into contact with the IMF once again.
- Stage 9: The cycle repeats.

2.4 The Expanding Contracting Polar Cap Paradigm (ECPC) - Magnetospheric Perspective

Even though the Dungey cycle gives an overview of the large-scale interaction between the solar wind and the Earth's system through an open magnetosphere, the cycle does not provide an overview of the time dependence of the dynamics. *Freeman and Southwood* (1988); *Siscoe and Huang* (1985) recognized that the nightside reconnection does not necessarily follow the dayside reconnection immediately and that these two processes should be dealt with separately. This realization led to the two-stage description of the solar wind-magnetosphere-ionosphere coupling system by *Cowley and Lockwood* (1992) known as the expanding contracting polar cap paradigm (ECPC).

The first stage of ECPC, as shown in Figure 2.5, illustrates the magnetospheric response to a dayside reconnection pulse, as described by *Cowley and Lockwood* (1992). The left panel shows the equatorial plane, where the magnetospheric convection is excited due to a deformation of the magnetopause. This deformation results from the opening of magnetic flux through reconnection with the IMF. Meanwhile, the right panel presents a cross-sectional view from the nightside of the magnetotail, where magnetic flux is added to the lobes in the north and south, stimulating convection within these lobes. The dashed line in the figure represents the magnetospheric new configuration after achieving a new force balance or equilibrium with the solar wind.

The second stage takes place in the magnetotail, where the flux has been accumulated. Nightside reconnections start about 30 to 60 minutes after the first interaction between the IMF and the dayside magnetosphere. As a result, the size of the polar cap is reduced, and the flows are excited to have the circular shape of the polar cap again, creating a new smaller area than the initial size.

In reality, the size of the polar cap is very dynamic, and the flow from the dayside and nightside can vary greatly over time.

In the next chapter 3, we discuss the ECPC from the ionospheric perspective and the temporal evolution of the field lines in the ionosphere. We also discuss the current system related to the high-latitude dynamics.

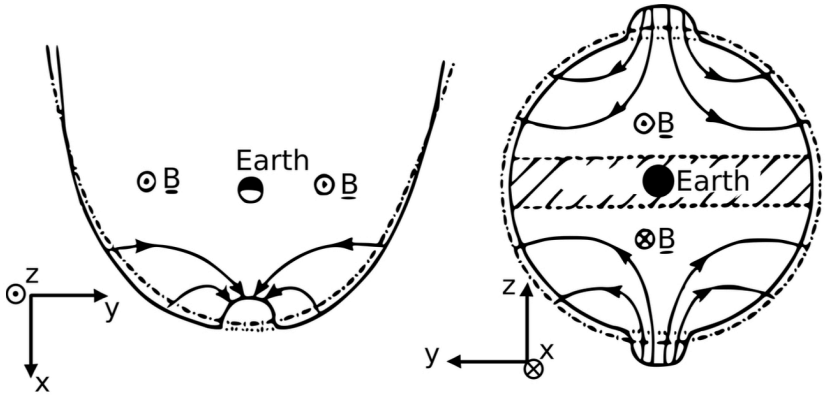

Figure 2.5: A schematic view of the magnetospheric convection due to dayside reconnection, from Cowley and Lockwood (1992).

Chapter 3

Ionospheric Convection and Current Systems as a Response to the Magnetosphere - Solar Wind Interactions

In this chapter, we explore how interactions between the Earth's magnetic field and the different orientations of the IMF influence ionospheric dynamics. We focus on the ECPC from the ionospheric perspective to show the influence of the reconnection on the ionospheric convection patterns at high latitudes. Additionally, we address the ionospheric current systems in relation to the magnetic field perturbations measured on the ground.

3.1 The Earth's Ionosphere

The Earth's ionosphere is a weakly ionized plasma region that extends vertically between $\sim$ 60 km and 1000 km or even higher. The ionosphere is composed of three regions: The D-region at 60-90 km, E-region at 90-150 km, and F-region at $\geq$150 km. The primary production mechanisms for the ionospheric plasma are solar radiation that ionizes particles in the atmosphere on the dayside, magnetospheric particle precipitation at high latitudes, mainly on the nightside, and a small contribution from cosmic rays. In the high altitude F-region the plasma is still considered frozen-in, while in the lower altitudes F-region, E-region, and D-region, the ions interact with the neutral atmosphere since the ion-neutral collision frequency becomes greater than or comparable to the gyro-frequency. The electrons, on the other hand, can be treated as frozen-in also in the E-region (*Kaeppler et al.*, 2015). The electric field in the ionosphere is a convection electric field, where the source is the magnetosphere that initiates the convection. We believe that the bases for qualitatively describing the large-scale dynamics of the system is that the magnetic stress and plasma pressure are the primary source of the dynamics whereas the currents and electric fields are derived quantities (*Parker*, 1996, 1997; *Vasyliūnas*, 2001, 2005a,b).

Collisions between neutral and charged particles significantly affect ionospheric dynamics. In the case of force balance between electromagnetic and collisional forces, the ionospheric current density $\mathbf{j}$ has a proportional relationship to the electric field, where the electrical conductivity describes the proportionality factor. This description

is known as the ionospheric Ohm's law (*Vasyliūnas*, 2012). We will discuss Ohm's law later in this chapter.

The plasma convection and the interaction between Earth's magnetic field and the solar wind in the magnetosphere lead to circulation in the ionosphere, given that the two systems are linked via the Earth's magnetic field. The Earth's magnetic field lines act as channels for Alfvén waves. These waves are a type of MHD waves that propagate along the magnetic field lines and can carry energy and momentum from the magnetosphere down to the ionosphere. Since the plasma in the magnetosphere is largely collisionless "frozen-in" plasma, it implies that the magnetic field and plasma are linked. As a result, changes in the magnetospheric field are effectively communicated to the ionosphere via Alfvén waves.

3.2 Convection and Currents in The Polar Ionosphere

3.2.1 The Expanding Contracting Polar Cap Paradigm (ECPC) - Ionospheric Perspective

The essence of the ECPC paradigm is that plasma flow within the system is governed by reconnection rather than the amount of open magnetic flux that is present. The convection acts to lead the system towards a new zero-flow equilibrium state in response to reconnection events. These reconnection events occur at the dayside magnetopause and in the magnetotail. Due to the dayside reconnection, the system is loaded with energy. This energy is transferred to the nightside magnetotail and can be stored for long periods of time. In the magnetotail, nightside reconnection occurs, which is considered a separate process from dayside reconnection. The two processes are uncorrelated on short time scales, but closely related on long time scales since the energy stored in the magnetotail must be released through nightside reconnection. Averaged over $\sim 3hrs$, the dayside and nightside reconnections balance (*Laundal et al.*, 2020).

Figure 3.1, akin to Figure 2.5 from Chapter 2, encapsulates the dynamic processes of the ECPC, highlighting the temporal evolution across three states in the magnetosphere/ionosphere before and after dayside reconnection. The initial state of the equatorial magnetosphere is depicted from above in the top row, showing total magnetic flux associated with Earth's main magnetic field, F_{tot}, minus the open magnetic flux, F. This difference is represented by a shaded gray area denoting all closed magnetic flux. The second row offers a magnetotail cross-sectional view, facing Earth, where the closed flux is the shaded gray region corresponding to the plasma sheet, with open flux positioned above and below. The polar ionospheric corresponding view is illustrated in the bottom row, showing the boundary between open and closed magnetic flux with a solid black line. The second column of the figure visualizes the magnetosphere immediately following a minor opening of magnetic flux, dF, due to dayside reconnection. Resultant flows from this reconnection are depicted as blue lines in the closed magnetosphere, the magnetospheric lobes, and the ionosphere. The third column demonstrates the new zero-flow equilibrium state, with solid black lines marking the updated new boundaries between open and closed magnetic flux.

In the magnetotail, reconnection reduces the open flux ratio, allowing closed field lines to travel towards the dayside magnetosphere via magnetic tension and subse-

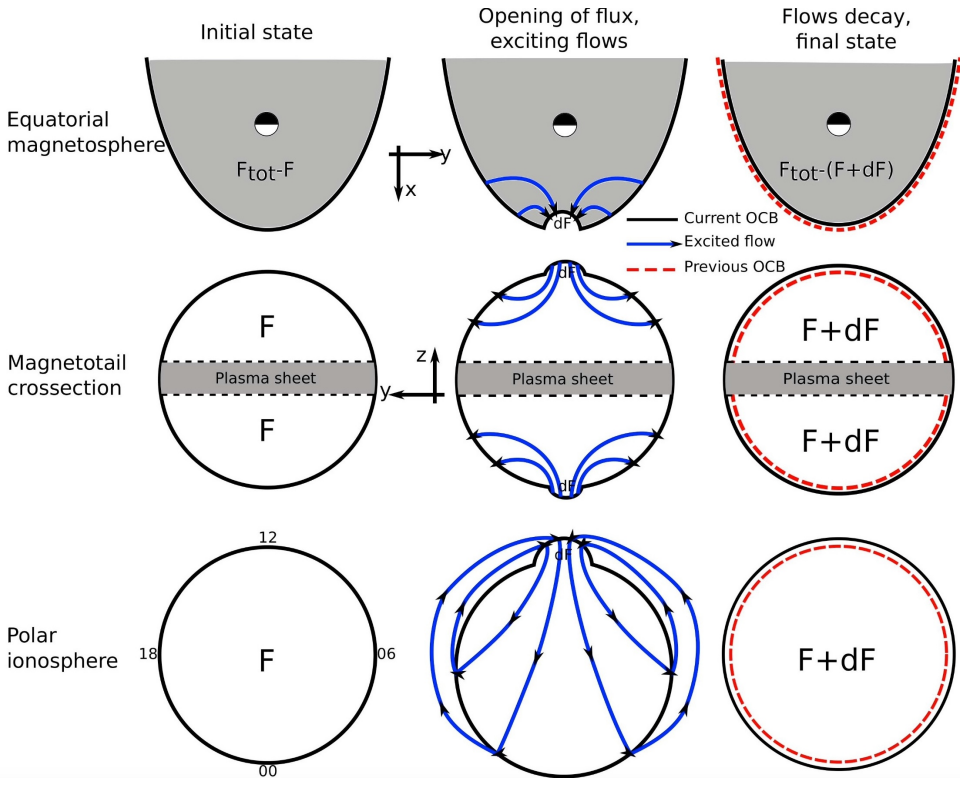

Figure 3.1: A schematic view of the different stages of the ECPC, from Reistad (2016) based on figures 5 and 6 of Cowley and Lockwood (1992).

quently through pressure imbalances induced by the flows, as illustrated in the left panel of Figure 3.2. The right panel displays the convection pattern observed according to the ECPC, showing the system transitioning towards a zero-flow equilibrium following balanced bursts of reconnection on the dayside and the nightside.

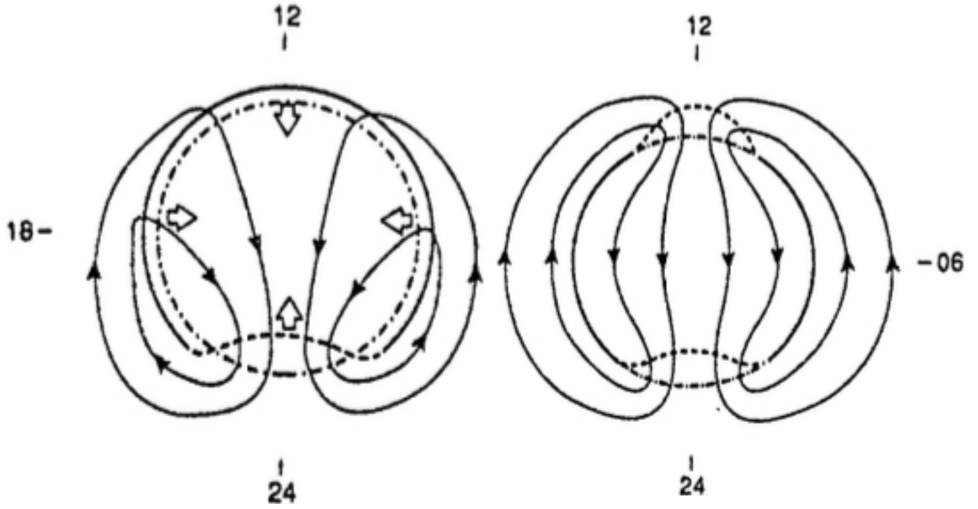

Figure 3.2: A schematic view of the nightside and the balance states, adopted from Cowley and Lockwood (1992).

The dayside reconnection rate Φ_D, affected by the orientation and strength of the IMF, can change rapidly, altering within minutes as solar wind conditions fluctuate. The nightside reconnection rate Φ_N in the magnetotail is bursty, and occurs with a delay relative to dayside reconnection. Variations in open flux are linked to reconnection rates through the relationship $dF/df = \Phi_D - \Phi_N$. Therefore, knowing the temporal development of the open flux content informs us of the balance between dayside and nightside reconnection. Empirical coupling functions can incorporate solar wind and IMF data to approximate the average dayside reconnection rate, as detailed by *Milan* (2015); *Milan et al.* (2012); *Newell et al.* (2007). Examining auroral boundaries, which reflect changes in the open magnetic flux, allows for the deduction of the nightside reconnection rate, as elucidated by *Ohma et al.* (2018).

3.2.2 Convection During Different IMF Orientations

The convection patterns at high latitudes are directly linked to the orientation of the IMF. During southward IMF ($B_z < 0$), we typically observe a two-cell convection pattern characterized by polar cap antisunward flow and sunward return flow on lower latitudes. However, the IMF does not usually approach Earth's magnetosphere with a purely southward orientation due to the helical nature of Parker spirals.

Periods of dominating IMF B_y introduce inter-hemispheric asymmetries to the magnetosphere and the ionosphere (*Walsh et al.*, 2014). As shown in panel b of Figure 3.3, the location of the reconnection in the dayside magnetopause is shifted towards higher latitudes due to the presence of IMF B_y. The flow in the lobes and the plasma sheet are

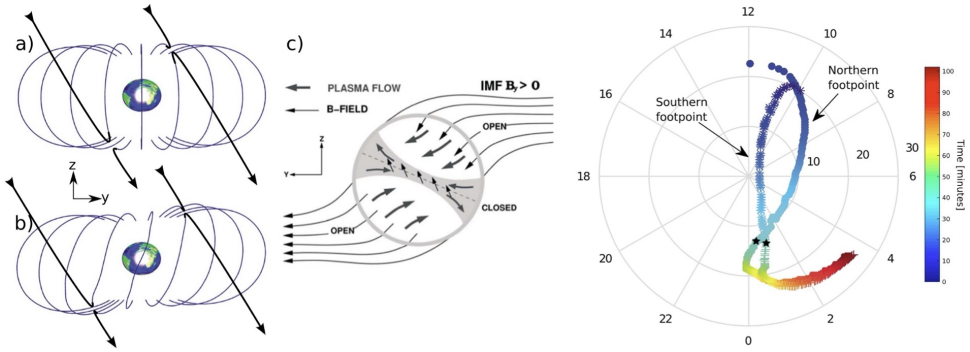

Figure 3.3: A schematic view of the ionospheric convection during southward IMF and in the presence of IMF B_y, from Tenfjord et al. (2015).

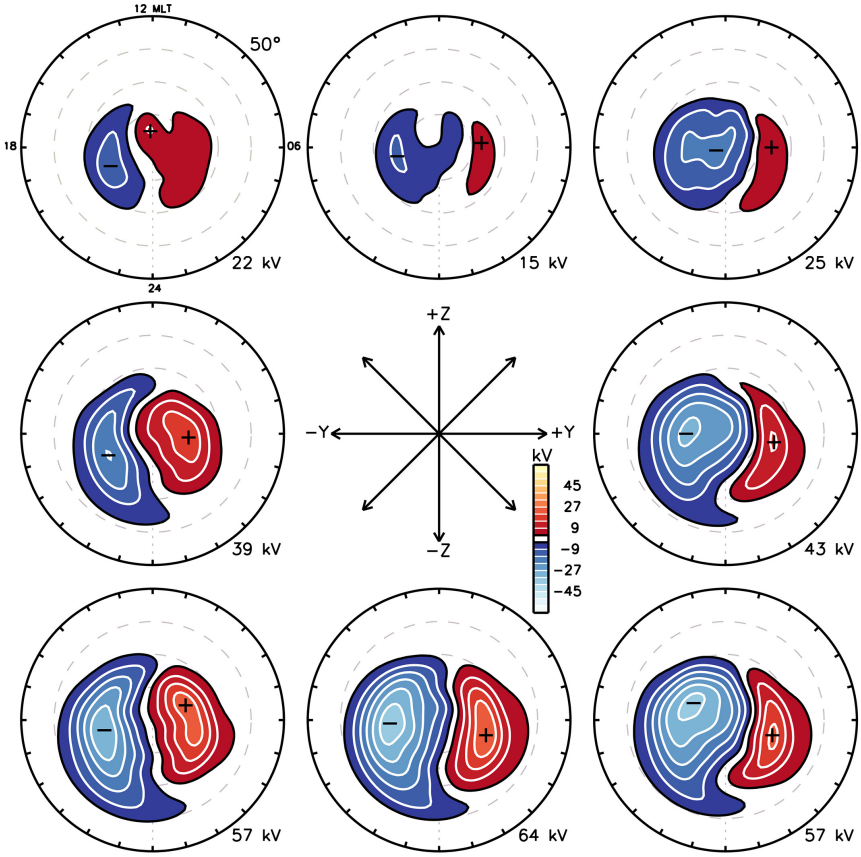

Figure 3.4: Statistical convection patterns sorted by IMF clock angle, from Thomas and Shepherd (2018)

shown in panel c of Figure 3.3. The asymmetry first introduced in the magnetosphere has an impact on the magnetic field and the plasma motion all the way down to the ionosphere, leading to asymmetric convection cells as shown in the right panel of Figure 3.3. *Tenfjord et al.* (2015) plotted the projected footpoints of magnetic field lines based on an MHD simulation with positive IMF B_y. The footpoints in the northern hemisphere marked with filled circles, and those in the southern hemisphere marked with an asterisk in the right panel of Figure 3.3.

These footpoints are plotted as time steps indicated by its color. Initially, these footpoints originate from the same field line in the solar wind and, after dayside magnetic reconnection, are found at asymmetric positions in the two hemispheres ($\sim$ 2 hours apart in MLT). This asymmetry, with the northern hemisphere footpoint moving dawnward and the southern hemisphere footpoint moving duskward immediately after reconnection, highlights the influence of the oppositely directed tension forces in the two hemispheres (*Tenfjord et al.*, 2015). Around 25 minutes later, this movement changes direction; the northern hemisphere footpoint shifts duskward, with a reverse movement in the Southern hemisphere. This is due to the influence of the asymmetric magnetic pressure forces in the two lobes, set up by the asymmetric forcing on the dayside. As field lines approach the neutral sheet and undergo reconnection, they exhibit asymmetric footpoints. As the flux tubes approach Earth they must return towards the dayside on either the dawn or dusk side due to pressure by the surrounding plasma and magnetic field. Initially, the northern hemisphere footpoint in the simulation was at 0 MLT, and the Southern hemisphere footpoint at 1 MLT, but over time, they tend to become more symmetric. This process implies that asymmetric azimuthal flows, and the twisting of the flux tube, are closely linked to asymmetric Birkeland currents in the two hemispheres (*Reistad et al.*, 2016; *Tenfjord et al.*, 2015).

For positive B_y, a banana-shaped convection cell is observed in the dawn region, and an orange cell is observed in the dusk side in the northern hemisphere as demonstrated in the middle right panel of Figure 3.4. The situation is opposite in the southern hemisphere. A negative B_y incurs a reverse longitudinal displacement, creating an opposite asymmetry in the convection cells in the northern hemisphere, as displayed in the corresponding panel to the left of Figure 3.4.

The influence of IMF orientations on high-latitude ionospheric convection patterns has been extensively studied through various observational techniques. Based on data from SuperDARN *Pettigrew et al.* (2010); *Thomas and Shepherd* (2018) applied spherical cap harmonic analysis to represent the convection patterns. Complementing this approach, *Reistad et al.* (2019) also demonstrated the dependency of convection patterns on IMF orientation, utilizing the spherical elementary current system method on similar radar data. Further supporting these findings, *Förster and Haaland* (2015) constructed convection patterns from Cluster spacecraft data in the magnetosphere. A consensus across these studies reveals the presence of typically two high-latitude ionospheric convection cells, which display a mirror symmetry between the northern and southern hemispheres.

When the IMF orientation is strictly northward ($B_z > 0, B_y \approx 0$), convection velocities in the central polar cap exhibit a distinct sunward flow, consistent with two lobe cells. This is believed to be caused by lobe reconnection (*Milan et al.*, 2000; *Reiff and Burch*, 1985). During pure northward IMF conditions, we observe a symmetrical four-cell convection pattern with two cells on either side of the noon-midnight merid-

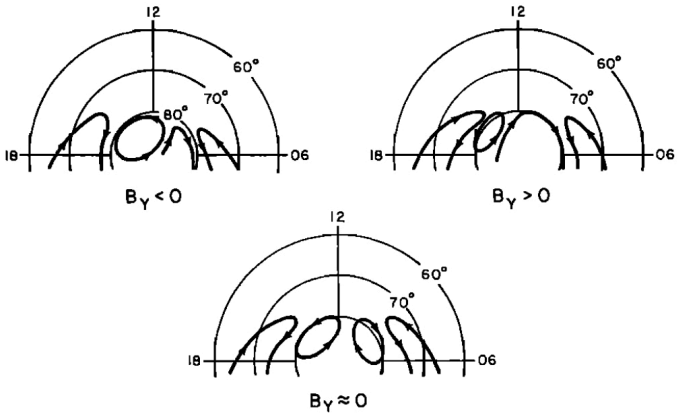

Figure 3.5: A schematic view of the ionospheric convection of the dayside during northward IMF and in the presence of IMF B_y, from Kelly (2009).

ian. The origin of the two outer convection cells is debatable. These cells could be created due to a delayed response to opening of flux on the dayside, or they could be due to a circulation forced by the viscous type interaction. During northward IMF conditions, the magnetosphere is often quieter, and the Dungey-type reconnection rate is thought to be negligible, suggesting that viscous interactions are the driving force behind the observed convection pattern rather than reconnection (*Kelly*, 2009; *Wilder et al.*, 2009). We think both processes might be involved in creating these cells, and they are not mutually exclusive. The bottom panel of Figure 3.5 illustrates the dayside convection patterns, while the top middle panel of Figure 3.4 presents statistical average maps of northward IMF conditions based upon SuperDARN radar data of F-region plasma drifts.

The upper panels of Figure 3.5 show that during $B_z 0$ and B_y conditions, the strength and shape of the inner convection cells change based on the polarity of the B_y component. When $B_z and B_y > 0$, the dawn cell with the sunward circulation expands, and the duck cell almost disappears. It is the opposite in the case of $B_z > 0, and B_y < 0$, where the dusk cell expands and the dawn cell disappears.

3.2.3 Ionospheric Current System

In this thesis, we estimate the ionospheric current based on ground magnetic field perturbations. The use of ground measurements limits the ability to model the full 3D ionospheric current system. In this section, we discuss this limitation and the standard methods used to retrieve the ionospheric currents.

The ionospheric currents can be decomposed to Hall and Pedersen currents. This decomposition is based on the physical relationship between the current density and the electric field. In steady state, the ionospheric Ohm's law relates the current density $\mathbf{j}$ to the electric field in the neutral frame of reference $\mathbf{E}'$ as:

$$\mathbf{j} = \sigma_P \mathbf{E'}_{\perp} + \sigma_H (\hat{\mathbf{b}} \times \mathbf{E'}_{\perp}) + \sigma_{\parallel} \mathbf{E}_{\parallel}. \tag{3.1}$$

Here $\mathbf{E}' = \mathbf{E} + \mathbf{u} \times \mathbf{B}$ where $\mathbf{u}$ is the neutral wind velocity. $\hat{\mathbf{b}}$ is a unit vector along the main geomagnetic field $\mathbf{B}$. $\sigma_{\parallel}$ is the conductivity in a direction parallel to the magnetic field. σ_P is Pedersen conductivity, and σ_H is Hall conductivity. This equation is derived from the ion and electron momentum equations assuming steady-state conditions, thermal equilibrium, and isotropic pressure(*Vasyliūnas*, 2012). We assume that $\mathbf{u} = 0$.

The integration of Ohm's law over altitudes enables the representation of the current as a surface sheet current density. The height integrated Ohm's law is given by:

$$\mathbf{J}_{\perp} = \Sigma_P \mathbf{E}'_{\perp} + \Sigma_H (\hat{\mathbf{b}} \times \mathbf{E}'), \tag{3.2}$$

where Σ_P and Σ_H are height-integrated Pedersen and Hall conductivities (conductances). In this equation the ionospheric currents depend on Hall and Pedersen conductances and the electric field. However, these quantities cannot be estimated using ground measurements alone. To further understand how the magnetic field perturbations relate to these quantities, we use another approach to decompose the current, the Helmholtz decomposition.

In this decomposition, the horizontal sheet current is decomposed into a sum of divergence-free J_{Df} and curl-free J_{Cf} currents, $\mathbf{J} = \mathbf{J}_{Df} + \mathbf{J}_{Cf}$. In the case of radial field lines, which is a good approximation at high latitudes, the sum of curl-free currents and field-aligned currents have no magnetic field signature on the ground. In this case, the divergence-free part of the horizontal current is the only component that is related to the magnetic field perturbations on the ground.

The question now is how to physically interpret the divergence-free component, which we can estimate using ground magnetic field perturbations with techniques described in Chapter 5, in terms of Hall, Pedersen, and field-aligned currents. As discussed by *Laundal et al.* (2015) the high-latitude divergence-free current is equivalent to the Hall current and the curl-free current is equivalent to the Pedersen currents if the gradient of the Hall and Pedersen conductances are parallel to E'. In other words, for certain conditions, the magnetic field of Pedersen currents and field-aligned currents cancel on ground. This is the Fukushima theorem (*Fukushima*, 1976, 1994).

Taking the divergence of the ionospheric horizontal current as stated in equation 3.2, we get an expression for the radial (assumed field-aligned) current:

$$\nabla \cdot \mathbf{J}_{\perp} = \mathbf{J}_{\parallel} = \Sigma_P \nabla \cdot \mathbf{E} + \hat{\mathbf{r}} \cdot (\mathbf{E} \times \nabla \Sigma_H) + \mathbf{E} \cdot \nabla \Sigma_H. \tag{3.3}$$

Similarly, we can take the curl of the divergence-free current to get the equivalent field-aligned current (J_{EFAC}) as:

$$\hat{\mathbf{r}} \cdot (\nabla \times \mathbf{J}) = J_{\mathrm{EFAC}} = -\nabla \Sigma_H \cdot \mathbf{E} - \nabla \Sigma_H \nabla \cdot \mathbf{E} - \hat{\mathbf{r}} \cdot (\mathbf{E} \times \nabla \Sigma_P) \tag{3.4}$$

The J_{EFAC}, which we can estimate with ground magnetometers, is equal to the FACs if the the last terms of equation 3.3 and equation 3.4 are zero. In that case

$$J_{\parallel} = \frac{1}{\alpha} J_{\mathrm{EFAC}} \tag{3.5}$$

where $\alpha = \frac{\Sigma_H}{\Sigma_P}$. This relation gives a physical interpretation for J_{EFAC}, although the assumptions involved are quite severe and often invalid. For example, during active periods such as the expansion phase of substorms, the J_{EFAC} fails to represent the actual FAC accurately (*Walker et al.*, 2024).

3.3 High Latitudes Ionospheric Current Observations

In this section, we describe the large-scale characteristics of ionospheric current patterns.

Figure 3.6 illustrates the large-scale average system of Hall, Pedersen, and Field-Aligned Currents (FACs) in the northern hemisphere. Hall currents flow in the direction of $\mathbf{E} \times \mathbf{B}$, flowing anti-sunward at the dawn and dusk edges of the auroral zone and sunward across the polar cap. Pedersen currents, aligning parallel to $\mathbf{E}$ and perpendicular to $\mathbf{B}$, close FACs when the conductance is uniform. The FACs consist of region 1 (R1) and region 2 (R2) currents. R1 and R2 flow in opposite directions at any given local time. R1 current are at high latitudes, while R2 currents are equatorward of R1. There are also smaller-scale structures of FACs known as region 0 (R0) currents that are more dynamic and flow within the auroral zone; R0 current is not presented in the previous figure.

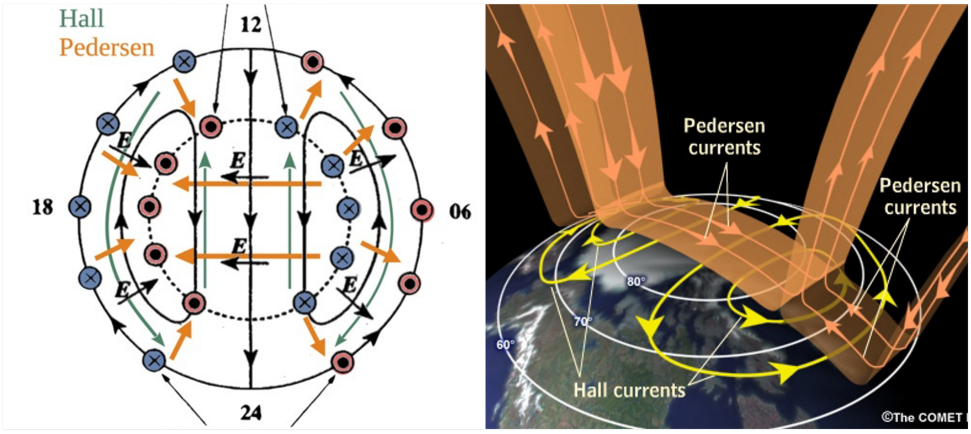

Figure 3.6: A schematic view of the ionospheric currents at high latitudes. The right panel is adapted from the COMET program at HAO, and the left panel is adapted from Cowley (2000)

The solar wind conditions and IMF orientation significantly influence the ionospheric convection pattern, as elaborated in the previous section. southward IMF leads to a two-cell convection pattern, while northward IMF can result in a more complex configuration, including lobe reconnection and the presence of the northward B_z (NBZ) current system in the polar cap (*Iijima*, 1984). The NBZ current system, prominent during northward IMF conditions, shows an increase in magnitude with the IMF B_z component and is also influenced by the IMF B_y component, as shown in Figure 3.7 and our study (*Elhawary et al.*, 2023). In this figure we plotted J_{EFAC} as we use observations from the ground magnetic field observations. Observations from low Earth orbit satellites have been instrumental in mapping these large-scale FACs and in understanding their relationship with the ionospheric convection and solar wind conditions (*Anderson et al.*, 2008; *Iijima and Potemra*, 1976).

The ionospheric horizontal currents estimated from the magnetic field perturbations on the ground are also called the equivalent ionospheric current. This equivalent ionospheric current is called auroral electrojets at high latitudes. This equivalent current

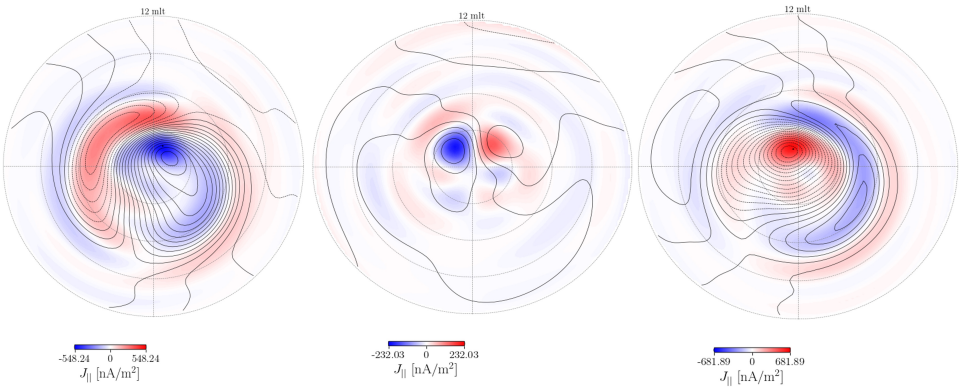

Figure 3.7: Map of the equivalent field-aligned current in red and blue and the equivalent horizontal ionospheric current showing the presence of the NBZ cells during northward IMF conditions.

observed at high latitudes is sometimes divided in two primary patterns: the Disturbed polar systems DP1 and DP2. The DP2 system consists of twin vortices at high latitudes, one in the morning sector and the other in the evening sector (*Clauer and Kamide*, 1985; *Obayashi*, 1967). The primary driving force of the DP2 current is the interaction of the solar wind with the magnetosphere, and its behavior is largely predictable based on solar wind characteristics, often increasing in magnitude and spatial extent during intense disturbances.

The DP1 system, on the other hand, is closely associated with substorms and is driven by energy release in the magnetotail (*Clauer et al.*, 1981, 1983). The DP1 system intensifies during the substorm expansion phase, predominantly featuring a westward current in the midnight sector, with return currents observed across the polar cap and sub-auroral ionosphere (*Clauer and Kamide*, 1985). The behavior of the DP1 system is less predictable compared to the DP2 system. DPY occurs in the dayside auroral and polar cap regions, and its current pattern depends on the IMF B_y component (*Svalgaard*, 1973).

Chapter 4

Substorm Dynamics: Modeling, Prediction, and Interhemispheric Asymmetries

4.1 Historical View of Substorms

Substorms have long been a subject of intense debate, with controversy surrounding their definition, phases, onset, and underlying mechanisms. The study of this phenomenon dates back to 1741 when Celsius and Graham observed magnetic disturbances at two different locations occured simultaneously. They concluded that such disturbances are not localized but are global phenomena. In the same year, Celsius made a groundbreaking correlation between auroras and magnetic disturbances (*Campbell*, 1997).

In 1770, Wilcke noted that the rays of the aurora align with the Earth's magnetic field lines. This early work laid the foundation for a more formalized study of substorms. *Chapman* (1962) defined them as phenomena related to magnetic storms, calling them "polar substorms." Two years later, his student (*Akasofu*, 1964) refined this phenomenon as "auroral substorms". According to Akasofu, a substorm commences with a sudden localized brightening of the aurora at the equatorward boundary of the nightside auroral oval, referred to as substorm onset as shown in the top row of Figure 4.1 at 03:12:19 UT. The aurora then expands poleward, eastward, and westward, leading to the first phase in Akasofu's description - the expansion phase as seen in the following panels of Figure 4.1. This phase concludes as the aurora reverts to its pre-onset levels, which Akasofu termed the recovery phase.

To encompass the magnetospheric processes linked to substorms, *Coroniti et al.* (1968) introduced the concept of "magnetospheric substorms." Further contributing to this, *McPherron* (1970) expanded on the phases to include the growth phase, during which the kinetic energy of the solar wind is converted into magnetic energy within the magnetotail. This phase typically lasts for 30-60 minutes (*Li et al.*, 2013; *Lui*, 1991). The expansion phase usually endures for 10-30 minutes (*Lui*, 1991), initiated by substorm onset and characterized by the aurora's brightening and expansion. Lastly, the recovery phase can last for over two hours, leading to a gradual re-establishment of quiet conditions (*McPherron and Chu*, 2016).

The signature of these phases observed on the ground is shown in Figure 4.2 using the SML index. The magnetic indices will be discussed in chapter 5. The substorm onset marks a sharp enhancement of the magnetic field perturbations at around 06:00

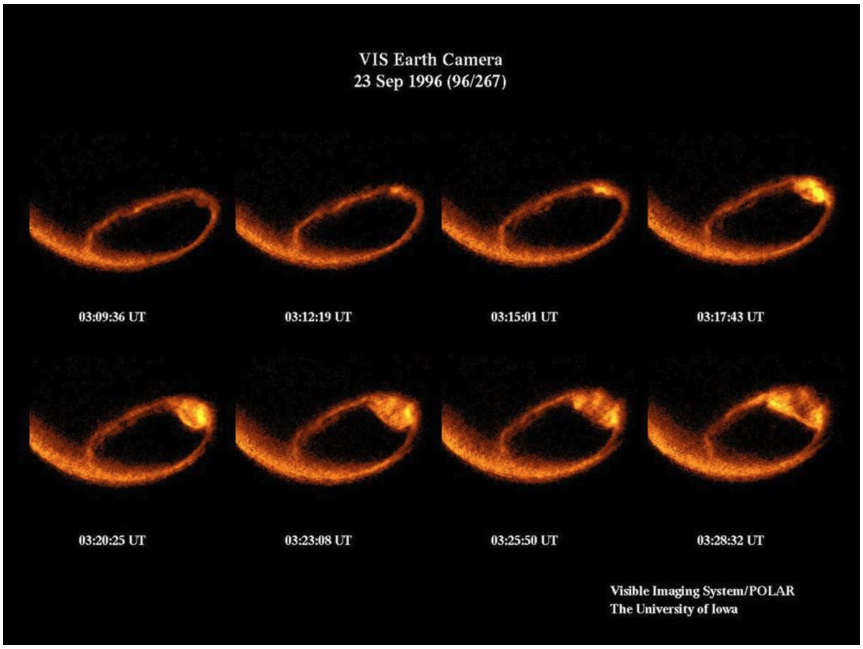

Figure 4.1: EUV images of the auroral oval from space showing how the aurora is developing during the cycle of the substorm. credit: NASA and University of Iowa

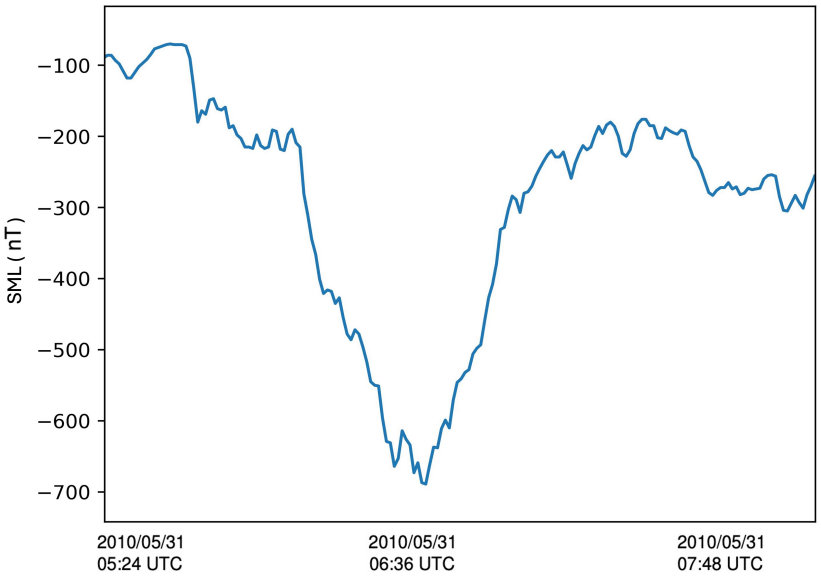

Figure 4.2: SML index during substorm cycle occurred in May 31st, 2010. The onset of the substorm expansion phase took place around 06:00 UT, while the recovery phase started around 06:30 UT which lasted for more than 1 hour.

UT. The expansion phase follows the onset and shows the increase of the magnetic perturbations at around 06:30 UT. After this increase reaches the maximum, the recovery phase starts. The ground signature of the recovery phase is a reduction of the magnetic field perturbations, as seen in Figure 4.2.

In August 1979, physicists involved in substorm research convened to produce a comprehensive report (*Rostoker et al.*, 1980). They critiqued existing methods for identifying substorm signatures and reached a consensus on its definition. According to this collective agreement, a substorm is a transient process initiated on Earth's night side. It serves as a mechanism through which a significant amount of energy derived from solar wind-magnetosphere interactions is deposited into the auroral ionosphere and magnetosphere.

4.2 Substorm Current Wedge

The substorm current wedge (SCW) is a strong current system that develops in the Earth's magnetosphere during the expansion phase of a magnetic substorm. This system comprises field-aligned currents (FACs) that take on a wedge shape, forming a vital link between the magnetosphere, and the ionosphere. Observations from ground-based magnetometers in both the auroral oval and at mid-latitudes, as well as data from geosynchronous orbit, align well with the established model of the SCW (*Gjerloev and Hoffman*, 2014; *Kepko et al.*, 2015; *McPherron et al.*, 1973).

McPherron et al. (1973) introduced the classic SCW description as a current system composed of one current loop comprised of four segments as presented in Figure 4.3a. This model describes how the interruption of the cross-tail current connects to the ionosphere through FACs. A downward FAC exits the magnetosphere on the dawnside into the ionosphere, and an upward FAC moves from the ionosphere back into the equatorial plane on the duskside. These FACs are linked within the ionosphere by a westward electrojet traversing the auroral bulge. At higher latitudes in the auroral oval, ground magnetic perturbations are dominated by the westward electrojet resulting in a negative bay signature.

The interpretation in terms of Hall, Pedersen, and field-aligned currents at mid-latitudes is complicated because the Fukushima theorem requires radial field lines, which are not present at mid-latitudes. Perturbations at mid-latitudes that occur concurrently as the substorm expansion phase are usually interpreted as a direct signature of the FACs. However, due to the geometry and distances involved, it is difficult to determine the details of the SCW structure from such observations. At mid-latitudes, the observed FAC widths vary - the dawnward FAC is broader, while the duskward FAC is narrower. There are also other currents, such as the ring current and partial ring currents, besides other fine structures within the FACs.

At geosynchronous orbit, the FACs and the decrease in cross-tail current predominantly influence magnetic disturbances. This disturbance pattern resembles the positive bay signature typically recorded at mid-latitude observation stations. The northward component increases (dipolarization), and the eastward component has an anti-asymmetric pattern dependent on local times. The dipolarization and positive bay signature observed by midlatitude ground magnetometers and by geosynchronous magnetometers are consistent in local time (*Chu*, 2015; *Nagai*, 1982).

The variability in FAC widths at mid-latitudes, along with the observations from the geosynchronous orbit, lead us to consider the three-dimensional insights provided by simulations, which offer a more comprehensive understanding of the structure and dynamics of the SCW response during substorms. Simulations have provided valuable insights into the three-dimensional structure of the SCW, particularly the buildup of current loops involving both region-1 and region-2 type FACs and localized loops within the tail, as illustrated by Figure 4.3b. The buildup of the SCW is driven by flow bursts that transport magnetic flux from the reconnection site to the near-Earth region, thereby altering the magnetic field from a stretched tail configuration to a more dipolar shape (*Kepko et al.*, 2015). This dipolarization is accompanied by magnetic shear at the dipolarized region's boundaries, leading to the formation of region-1 type FACs that flow into the ionosphere after midnight and exit it before midnight.

Figure 4.3b, adapted from *Birn and Hesse* (2013) illustrates the scenario closer to Earth showing that the magnetic field shear intensifies as the flow is decelerated and deflected by the inner dipole field's magnetic pressure. The resulting azimuthal flows that bend the field lines create earthward FACs at dawn and tailward FACs at dusk, which are also of region-1 type. These flows contribute to the twisting of the magnetic field, visualized through the concept of flux ropes. The degree of twist and thus the strength of the FACs depends on ionospheric boundary conditions and the ionospheric conductivity, which can influence how the magnetosphere develops due to its ionosphere connection (*Kepko et al.*, 2015).

While magnetic perturbations observed at different latitudes on the ground and in geosynchronous orbit supported the classical SCW view, this picture is debatable. Recent propositions suggest the SCW may consist of a double loop system (*Gjerloev and Hoffman*, 2014) or a collection of smaller loops, known as 'wedgelets,' rather than a singular loop (*Liu et al.*, 2015). Figure 4.3c, following modifications from (*Kepko et al.*, 2015), includes both region-1 and region-2 type FACs and local loops confined to the tail, indicating that region-2 type currents may close within the magnetotail through a westward partial ring current instead of radial currents. *Sergeev et al.* (2014) affirmed the need for a second region-2 type current to align with distributed in situ measurements within the dipolarized region. The variability in the relative strengths of region-1 and region-2 type currents from one substorm event to another suggests that current closure in the magnetotail is variable and contingent on how the total current is partitioned among various loops.

4.3 Models to Explain Substorms

Two primary theories dominate the discourse on the initiation and evolution of substorms: the Inside-Out theory and the Outside-In theory.

4.3.1 Inside-Out Theory (Current Disruption Model)

The inside-out theory postulates that substorms are initiated by disruptions in the near-Earth magnetotail, which then propagate earthward to trigger substorm onset. *Lui* (1996) proposed that these disruptions initially occur in the near-Earth magnetotail, situated at 8-10 Earth radii (RE), eventually progressing tailward to induce a phenomenon

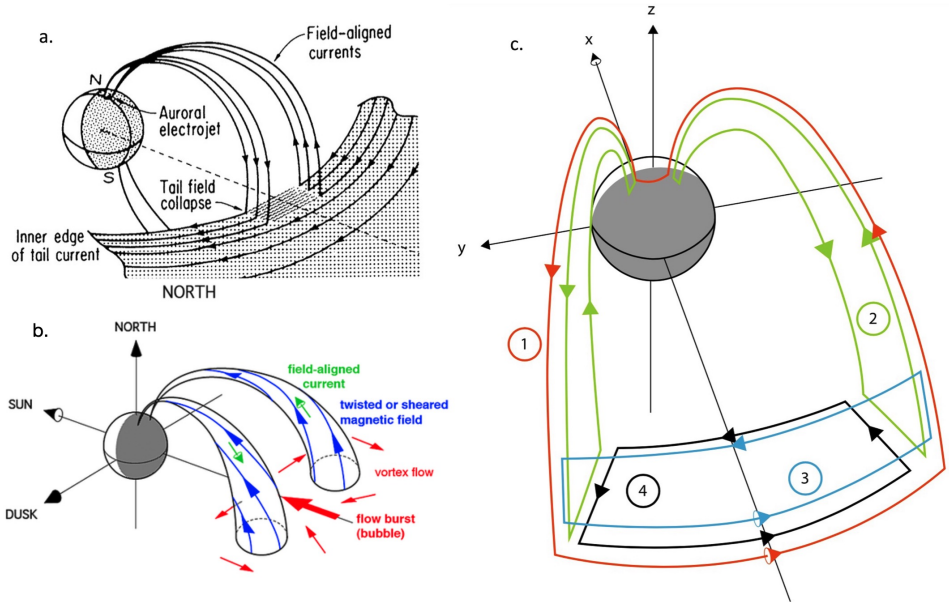

Figure 4.3: The Substorm Current Wedge and its components. Panel a. is adopted from the classical view of McPherron et al. (1973). Panel b. is adopted from Birn and Hesse (2013). Panel c. is adopted from Kepko et al. (2015).

called mid-tail reconnection. Based on one single event concluded that the disruptions initiate in the inner magnetosphere (*Henderson*, 2009). This model, sometimes referred to as the near-Earth current disruption model, aligns conceptually with the Inside-Out theory. It extends the understanding of how fast flows are injected and decelerated, contributing to substorm expansion. While this theory offers a framework for describing substorm growth phases, it may lack a comprehensive view of onset mechanisms. In the growth phase, an intense cross-tail current mainly supported by a duskward anisotropy in thermal ions provides a significant free energy source at $\sim$10 RE. At substorm onset, a feature known as the current wedge forms, consistent with changes in current-carrying particle distributions (*Mitchell et al.*, 1990). Several phenomena, such as magnetic reconnection further downtail, support this theory (*Nagai et al.*, 1998). As shown in Figure 4.4, the model starts with an intense cross-tail current primarily supported by a duskward anisotropy in thermal ions. Then a current wedge forms at the substorm onset. In the end, morphological changes in the magnetic field are consistent with current-carrying particle distribution changes.

4.3.2 Outside-In Theory (Bursty Bulk Flow Theory)

The outside-in theory asserts that magnetic reconnection events in the mid-tail (20 - 30 RE) is the main driver of the energy release and the substorms in the magnetotail. This model suggest that instabilities in the thin current sheet drives near Earth reconnection as the first step of the process which creates the bursty bulk flows to the inner edge of

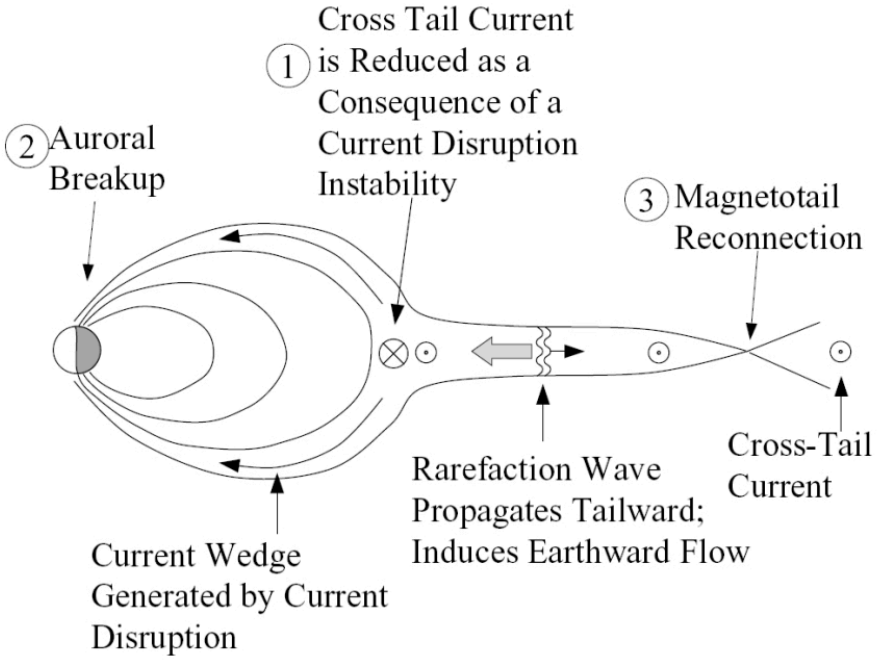

Figure 4.4: A schematic figure shows the sequence where the current wedge formation is in the second stage of the inside-out (current disruption) model. Adopted from NASA/TM-2001-209985.

the magnetotail and subsequently a reduction of the cross tail current due to the pileup of the flux and depolarization of the magnetic field and generating earthward flows that lead to near-Earth substorm onset (*Baker et al.*, 1996). This model emphasizes the importance of stored energy in the magnetotail and its subsequent release during substorms.

Notice that the sequence of the outside-in theory is different from the sequence of the inside-out theory as shown in Figure 4.5. In the outside-in theory magnetic reconnection initially occurs in the distant tail, creating earthward flow and eventually causing near-Earth substorm onset, while it comes as the third and last stage of the inside-out theory. Then, Earthward flows (Bursty Bulk Flows) and localized brightening in the auroral region support this theory, that is assumed to initiate the instabilities in the inside-out theory. The Last stage is the generation of the substorm current wedges and breakup of the aurora which comes in the second stage in the current disruption model.

Several other models have been proposed to explain the triggering mechanisms of the substorm onset for example, *Kan* (1998) proposed the Magnetosphere-Ionosphere (MI) coupling model. The model suggested that a substorm initiates begins when the convection of the plasma sheet braking exceeds a specific rate, leading to rapid dipolarization of the magnetic field. Then a dipolarization-induced electric field launches Alfvén wave which is responsible for transporting the disrupted tail current away from the dipolarization region. shortly after that, the substorm expansion onset occurs in the

ionosphere, marked by a sudden brightening of the equatorward-most pre-onset auroral arc. During the expansion phase, new tail reconnection is necessary to sustain the phase. This model aligns with the current disruption scenario in most respects, except assuming that Earthward flows originated from mid-tail or distant tail processes. *Machida et al.* (2009) proposed another model, the Catapult Current-Sheet Relaxation Model. This model explained the triggering of the substorm as a process combining the inside-out and the outside-in theories. It proposed an earthward flow caused by the relaxation of the stressed current sheet and a duskward flow near Earth intensified due to the braking of these flows just before substorm onset. This process triggers instabilities, leading to the disruption observed in current systems. The model also suggests that the relaxation of the current sheet naturally forms a thin current at its edge, surrounded by strong magnetic fields, which help initiate magnetic reconnection. Once reconnection begins, it significantly contributes to driving the substorm. Another suggestion by *Lyons et al.* (2022) based on SuperDARN data suggests that substorms start with plasma in the dayside, that crosses over the polar cap to the open/closed boundary where it triggers localized magnetic reconnections. Then, as this plasma moves closer to Earth, it triggers substorms expansion. The concept can be seen as a sequence of event trying to reconciles the inside-out and outside-in models rather than being a model itself.

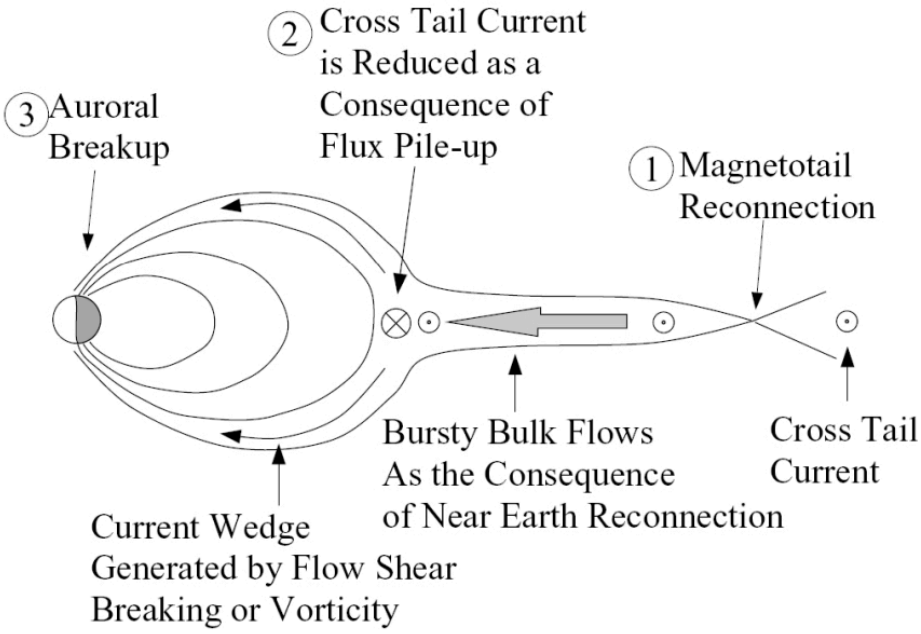

Figure 4.5: A schematic figure shows the sequence where the current wedge formation is in the last stage of the outside-in theory. Adopted from Shiokawa et al. (1998).

Each model can explain certain characteristics of substorms, and they are not necessarily mutually exclusive. Some contemporary research is focused on a synthesis of these models or considering them under specific solar wind conditions, geometries, or

types of substorms.

The best approach may be to consider the various models as complementary, with each providing insights into different aspects of substorms. By combining the strengths of the different models and continuing to gather observational evidence, scientists can build a more complete model that can help better understanding of these complex space weather events.

4.4 Prediction of Substorms

While the dayside dynamics are relatively predictable being influenced by the solar wind dynamics, substorm onset location and timing remain highly unpredictable. Figure 4.6 provides a visual summary of these dynamics. The top panel shows the predictable nature of the dayside reconnection process, while the right side of the figure illustrates the less predictable nightside reconnection events, marked by bursts of energy that lead to substorm activity and the dazzling auroras observed near the poles. While the cumulative effect of dayside and nightside reconnection over time may be equivalent, the predictability of individual substorm events on the nightside is remarkably challenging.

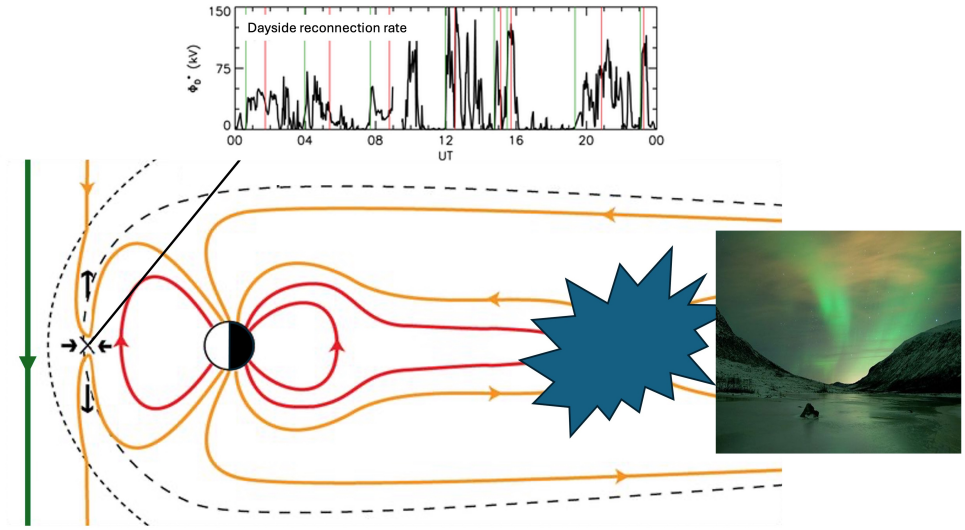

Figure 4.6: Diagram illustrating the magnetospheric dynamics during substorm events. The top panel shows the predictable nature of dayside magnetic reconnection influenced by solar wind conditions, adopted from (Milan et al., 2021). The schematic representation of the magnetosphere highlights the structured dayside reconnection points, adopted from (Eastwood et al., 2017). The right side shows the nightside of the magnetosphere, where reconnection is less predictable, leading to sporadic substorm activity and the resulting auroral displays, credit to NASA.

4.4.1 Predicting Substorm Onset Timing

To Predict the timing of when a substorm would occur in the magnetotail, *Uritsky et al.* (2001) discussed the substorms as perturbed self-organized critical (SOC) dynamics of the magnetosphere. The study suggested that localized current sheet instabilities and subsequent magnetic reconnection in the magnetotail can be modeled as SOC avalanches. The authors examined how changes in solar wind energy input and critical current density in the magnetotail influence large-scale perturbations comparable to substorms. The results revealed that the large-scale disturbances generated by the model, which mimic magnetospheric substorms, depend on the energy accumulated in the system and how this energy dissipates internally. Also, *Valliéres-Nollet et al.* (2010) presented substorms as a self-organized critical phenomenon. The study focused on the central plasma sheet of the magnetotail, where substorms originate. It examined the behavior of this region as a (SOC) system under the influence of solar wind energy input. The research utilized a 2-D SOC model to reproduce observed dual scaling regimes of substorms, revealing that small and large events follow different power laws. The results of both researches led to the conclusion that it is a challenge to be able to predict when and where substorm onset would occur. From another perspective, employing machine learning, *Sado et al.* (2023) predicted geomagnetic substorm onset timing through analyzing auroral images. By classifying these images and transforming the results into time-series data, the study develops a classifier that predicts substorm onset within a 15-minute interval after analyzing 30 minutes of auroral images. The classifier on average, correctly identifies 59% of both substorm and non-substorm events with a 39% correctly predicted and a 20% of non-substorm events were wrongly predicted as substorms (false positive rate), highlighting the challenges and potential of using machine learning for space weather prediction. Machine learning and SOC served as a theoretical framework for assist predicting the unpredictable substorms.

4.4.2 Predicting Substorm Onset Location

From an observational perspective, scientists used global ultraviolet (UV) imaging observations of the substorms onsets to predict where substorms take place. Global ultraviolet (UV) imaging has illuminated the temporal and spatial dynamics of substorm onsets, revealing a concentration around pre-midnight sectors in Magnetic Local Time (MLT) (*Frey et al.*, 2004; *Liou*, 2010). This moment of the substorm onset is the moment when the dynamics of the magnetosphere and the ionosphere are coupled, and the influence of the magnetotail dynamics is translated into energy and plasma exchange. This distribution aligns with theoretical expectations linking upward currents at the duskward edge of the SCW with downward electron flows. However, it's argued that these onset events precede the SCW formation (*Kepko et al.*, 2015), suggesting that the SCW structure might not fully explain the observed duskward shift in onset locations. Furthermore, the initial aurora of a substorm may not directly correlate with field-aligned currents (FACs) but may instead be connected to the transition between dipolar and stretched magnetic field lines, as suggested by studies such as (*Mende et al.*, 2003).

The precise determination of substorm onset locations has long been challenging to predict. Earlier works hinted at a lower latitude occurrence of substorms under neg-

ative IMF B_z conditions (*Liou et al.*, 2001). *Gérard et al.* (2004) investigated auroral substorm onset locations using IMAGE-FUV imagers, analyzing the influence of solar wind conditions. They showed that substorm onsets are primarily concentrated between 2000 and 0200 MLT, occurring in regions of preexisting proton precipitation, which suggests initiation in areas with stretched but dipole-like magnetic field lines near Earth. The study found a correlation between substorm onset latitudes and the solar wind dynamic pressure. This correlation possibly indicates an equatorward shift of the auroral oval due to increased open magnetic flux in the magnetosphere (*Milan et al.*, 2009). *Østgaard et al.* (2011) analyzed over 6600 substorms to investigate the interhemispheric asymmetry of substorm onset locations in relation to the interplanetary magnetic field (IMF). It confirms that the IMF clock angle significantly organizes average substorm onset locations in both hemispheres, suggesting that the onset location can be affected by the dayside and lobe reconnection geometries, along with magnetic tension on open field lines before tail reconnection. They also show that the IMF B_y has a non-linear correlation with the onset local time.

Elhawary et al. (2022) reveals that substorm onsets tend to manifest at earlier local times during geomagnetically active periods compared to quieter intervals. Through regression analyses, we showed that the correlation between the AL index and onset MLT is comparable to that of the IMF B_y, which was previously reported in studies conducted by *Liou and Newell* (2010); *Østgaard et al.* (2011); *Wang et al.* (2007). The influence of the AL index on onset MLT is the same in both hemispheres, unlike the hemisphere-specific effects of IMF B_y. The small and hemisphere-specific effect suggests that B_y alters the magnetospheric projection of substorm onsets on the ionosphere, without affecting the onset location in the magnetotail locations. *Gabrielse et al.* (2014) revealed a dawn-dusk asymmetry in injection occurrence rates, favoring the pre-midnight sector. These rates increase with geomagnetic activity, which might be related to substorm occurrence, however not every injection is followed by a substorm. In paper I, we discuss the ionospheric feedback on magnetotail reconnection sites, potentially guiding the placement of substorm onsets.

Despite this progress, the predictability of substorm onset locations remains limited. We performed a linear regression model integrating IMF B_y, the AL index, aberration angles, and dipole tilt. Our comprehensive model explains merely 11% of the observed MLT variation in substorm onsets. This highlights the high unpredictability of substorm onset locations, emphasizing the need for further exploration into this phenomenon.

4.5 Substorms During Northward IMF

Though substorms are known to occur more frequently under southward IMF B_z conditions, they can also occur under northward IMF B_z (*Lee et al.*, 2010a,b; *Miyashita et al.*, 2011; *Peng et al.*, 2013). *Crooker* (1992); *Song et al.* (2000) discussed the possibility of the nightside reconnection under northward IMF B_z. *Wu et al.* (2002) identified two substorms occurring after more than 15 hours of continuous northward IMF. *Lee et al.* (2010a,b) found several substorms under northward IMF conditions during the recovery stages of intense storms, with these substorms being as strong as typical ones seen with moderately southward IMF. *Miyashita et al.* (2011) reported a sequence of 11 substorms, from very weak to moderate intensity, happening during a prolonged pe-

riod of northward IMF, lasting about 19 hours. *Tanaka et al.* (2010) showed through global MHD simulation that a sudden collapse of the plasma sheet as a high-pressure region in the inner magnetosphere could trigger substorm onset under northward IMF B_z. Although the energy source for the northward IMF B_z substorms is still ambiguous, *Akasofu* (1975) suggested that the energy –in the magnetotail during northward IMF B_z– might be stored from former southward IMF B_z conditions. Also, *Peng et al.* (2013) suggested that the main source for the northward IMF B_z substorms is the energy stored in the magnetotail during an earlier interval of southward IMF B_z. *Peng et al.* (2013) implied that the energy released in the magnetotail during substorms occurs during northward or southward IMF conditions. On the other hand, for the prolonged intervals of northward IMF conditions, *Miyashita et al.* (2011) suggested that the presence of large IMF B_y might play an important role in the dayside reconnection that leads to energy piling in the magnetotail. While during storm time, *Li et al.* (2012) suggested that the energy stored in the magnetotail is not fully released during intense storms.

Northward IMF substorms experience the minimum dayside reconnection effect allowing us to distinguish between the influence of the nightside dynamics on the dayside dynamics. Under conditions of northward IMF, an intense and localized current system forms within the dayside polar cap, as identified in studies by *Iijima* (1984); *Laundal et al.* (2018); *Milan* (2015). This current system, known as the northward-directed B_z (NBZ) or lobe cells, arises from lobe reconnection processes. The NBZ current system consists of a pair of convection cells: a positive, upward-flowing current in the pre-noon sector and a negative, downward-flowing current in the post-noon sector, both situated poleward of the region-1 currents on the dayside. These lobe cells indicates a reversed convection pattern on the dayside, influenced by variations in ionospheric conductance, as described by *Reistad et al.* (2019). *Elhawary et al.* (2023) demonstrated that during northward IMF substorms, these lobe cells are modulated by nightside magnetospheric dynamics, exhibiting reduced strength in the growth phase compared to the expansion phase. We discuss in paper II three possible mechanisms that could be the reason behind this behavior. Substorms occurring during northward conditions should attract more attention to untie the dayside and nightside dynamics to identify the important nightside factors influencing the ionospheric current systems.

4.6 Substorm Influence on Interhemispheric Asymmetries

The orientation of IMF B_y influences the tension forces that act on magnetic flux in the magnetosphere. The effects of IMF B_y are not limited to the magnetosphere but extend to the ionosphere, introducing asymmetries to the coupled system. In the previous chapter 3, we have discussed how this asymmetry influenced the convection and ionospheric current system. In this section, we will discuss how it is added to the magnetosphere and how the substorms have a role in reducing these asymmetries. *Cowley* (1981) originally described the impact of the IMF B_y component causing asymmetric addition of field lines to the magnetotail. When B_y is positive, the tension in the reconnected field lines draws them toward dawn in the northern hemisphere and dusk in the southern hemisphere, leading to magnetic flux accumulation and increased pressure in these areas. This accumulation could also be influenced by lobe reconnection, where

the IMF tension supports the flux buildup. The resulting higher pressure drives plasma and field line convection, shifting the plasma in the northern hemisphere toward dusk and dawn in the southern hemisphere, thereby adjusting the footpoints of the field lines accordingly. *Cowley* (1981) suggested this asymmetry extends into the magnetosphere upon these field lines' reconnection in the magnetotail. *Khurana et al.* (1996) offered an alternative view, attributing the asymmetric pressure distribution from uneven flux loading to directly influence magnetospheric behavior via fast-mode MHD pressure waves. This mechanism induces duskward flows in both hemispheres, contributing to the *By* component observed in the magnetotail. They highlight the significance of the timescale on which the magnetosphere can adapt to IMF changes, suggesting rapid reconfiguration is possible through pressure wave propagation. One major contrast between the description presented by *Khurana et al.* (1996) and the one proposed by *Cowley* (1981) lies in the time frames over which the magnetospheric system can react and adjust to the conditions of the IMF because the travel time of pressure waves is longer than the convection velocity. *Tenfjord et al.* (2018) corroborated this rapid magnetospheric response to IMF *By* shifts through Lyon-Fedder-Mobarry (LFM) global MHD simulations, finding immediate adjustments that suggest lobe pressure as a key factor in asymmetry induction. Studies by *Petrukovich* (2011) and *Tenfjord et al.* (2015) highlighted a correlation between magnetospheric B_y amplitude and polarity with IMF B_y, affecting magnetic field line footpoint displacement across hemispheres. Can nightside dynamics impact this asymmetry?

Substorms can modify nightside convection, affecting the overall adjustment of IMF- and dipole tilt-induced asymmetries in the magnetosphere-ionosphere system. They tend to diminish asymmetries in nightside magnetic field mapping across hemispheres. *Ohma et al.* (2018, 2022) observed that substorms lessen the longitudinal displacement asymmetry of magnetic field line footpoints during their expansion phase, using conjugate auroral features and geosynchronous magnetic field data. *Grocott et al.* (2010) found through superposed epoch analysis that substorms eliminate IMF B_y's control over nightside ionospheric convection, suggesting substorms modulate the impact of IMF B_y on interhemispheric asymmetries.

Chapter 5

Data and Method

5.1 Data

5.1.1 Ground-based Magnetometer Data

The research in this thesis is based on analyzing the magnetic field perturbations measured by the extensive network of ground magnetometers within the SuperMAG collaboration. SuperMAG collects data from over 600 stations globally. These stations could belong to different institutes or organizations, for example, MAGDAS http://magdas2.serc.kyushu-u.ac.jp/. They could also overlap with other observational networks such as INTERMAGNET https://intermagnet.org/. SuperMAG offers magnetic field data in both 1-minute and 1-second resolution. For our study, the 1-minute resolution proved adequate. *Gjerloev* (2009, 2012) use a technique to make a standard version of the data from all the different projects to ensure uniformity in units and coordinates. The data we have incorporated into our thesis is the version with baseline subtraction to eliminate long-term trends and any residual offsets.

We use stations located above 50° in magnetic latitude within the northern hemisphere. Figure 5.1 illustrates their geographical distribution on a polar projection. The number of stations with data availability fluctuates from time to time. We verify the presence of a sufficient number of stations available at the time of analysis. Our investigation spanned data collected from 1990 to 2019.

Our initial plan was to analyze data from both the northern and southern hemispheres. However, the sparse coverage of magnetometer data in the southern hemisphere presents significant challenges for examining the ionospheric equivalent current in that region. Later in this chapter, we will discuss how we derived the equivalent ionospheric currents from the magnetic field perturbations.

5.1.2 Geomagnetic Indices

Geomagnetic indices based on ground magnetometer data represent global geomagnetic activity. In our analysis, we rely on indices such as the AL index and SML index, which are defined below.

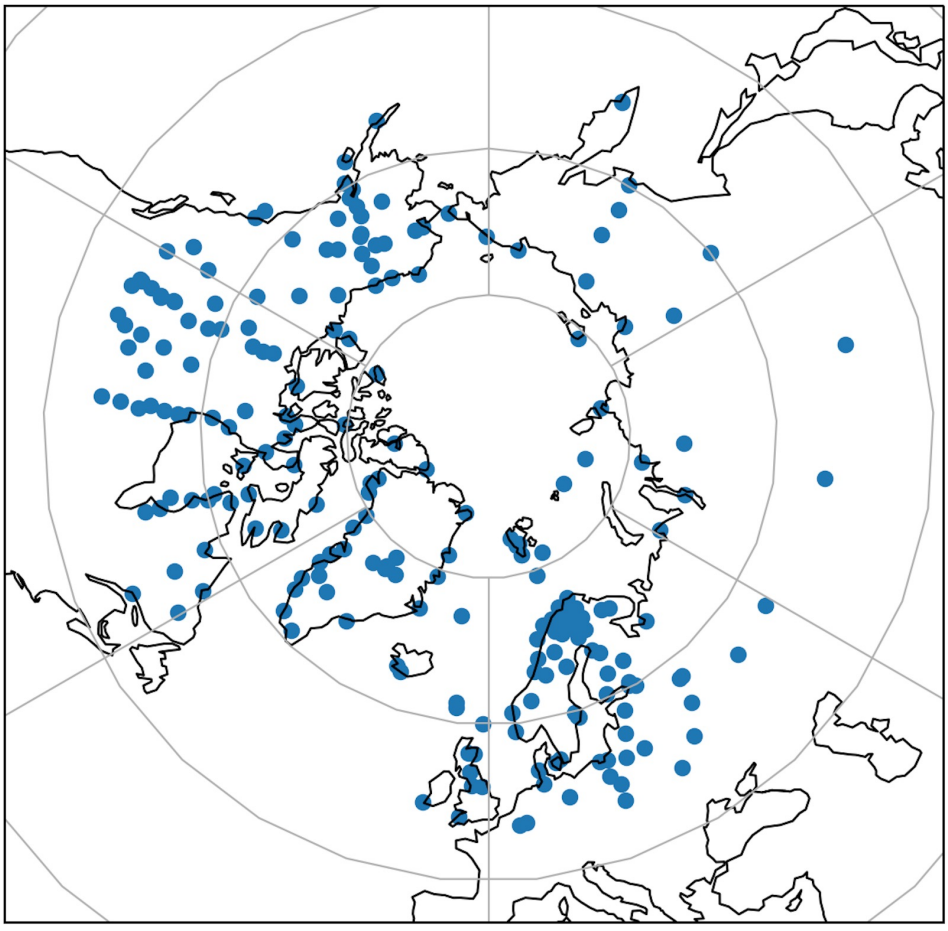

Figure 5.1: Map of the northern hemisphere stations with geomagnetic latitude $\geq 50^{\circ}$ listed in SuperMAG, we used in our study the stations based on the data availability.

AL Index

The Auroral Electrojet indices AE, AL, AU, and AO were introduced by *Davis and Sugiura* (1966). These indices quantify the electric currents flowing in the ionospheric auroral region. To capture the latitudinal extent of these auroral electrojets, a series of magnetometers are positioned within the band of the auroral oval in the northern hemisphere. This distribution ensures that at least one station is near the peak activity of both the westward and eastward auroral electrojets at all times. There is a lack of a complete and evenly spaced longitudinal network in the southern hemisphere.

The World Data Centre for Geomagnetism in Kyoto provides these indices today, known as AE(12), reflecting data from 12 magnetometers. Recorded at 1-minute intervals, the AU and AL indices are determined by the highest and lowest background-adjusted horizontal field components from these stations. AU is typically associated with the directly driven current system linked to the dayside reconnection events and shows an increase during the substorm growth phase. Conversely, the AL index is closely related to the auroral electrojet within the substorm current wedge, displaying more negative values during the substorm expansion phase.

SML Index

Newell and Gjerloev (2011) proposed a new generalized SuperMAG AL index (SML). The new index is defined through the perturbations of 100 stations on average, while AL is defined through 12 stations only. The aim of this new index is to ensure that the observed enhancement is on a global scale and, therefore, to better define the timing of events such as substorm onsets.

Midlatitude Positive Bay

The midlatitude positive bay (MPB) is a high positive pulse in the northward component of the magnetic field perturbations observed at mid-latitude stations near midnight. It generally rises in about 20 min and decays more slowly, the same behavior as the expansion and recovery phases of substorms. The MPB index is a measure used to quantify the impact of these perturbations caused by the SCW at mid-latitudes. It is calculated as $X^2 + Y^2$, where X is the northward and Y is the eastward components of the magnetic field, respectively (*Chu*, 2015; *McPherron and Chu*, 2016). The data is collected from stations between 20° and 50° in magnetic latitude. Since X and Y are measured in nT, the MPB index is in nT^2.

5.1.3 Substorm Onset Detection

Substorm onsets can be detected using geomagnetic indices, and several substorm lists exist based on this approach. *Newell and Gjerloev* (2011) and *Forsyth et al.* (2015) identify substorms using indices derived from ground magnetometer data in the auroral zone, while *McPherron and Chu* (2018) use the magnetic response of the influence of substorms on mid-latitude perturbations. In the case of the substorm lists identified at high latitude, the drop of the SML index should be more than 100 nT below the initial level before the substorm according to the definition by *Newell and Gjerloev* (2011). It is characterized by a sharp decrease of about 45 nT in less than 3 minutes. Then

this decrease should last around 30 minutes and reach at least 100 nT as shown in Figure 4.2. On the other hand, the mid-latitude substorm list requires the MPB index to rise more than 25 nT^2, and an interval of 30 minutes should separate the MPB identified onsets.

Although the geomagnetic indices are useful in identifying substorm onsets, we believe that the identification through the examination of a sequence of ultraviolet (FUV or UVI) images taken from satellites is a better method to identify substorms as detailed in *Frey et al.* (2004); *Liou and Newell* (2010). Substorm onsets identified through the FUV and UVI images must first show a distinct local brightening of the aurora, followed by a poleward and azimuthal expansion. A candidate onset is discarded if it happens less than 30 minutes after the previously defined onset. Images associated with substorm events are transformed into the geomagnetic coordinate system to determine the onset MLT and MLat. We refer to this list as the FL list.

5.2 Method

5.2.1 Spherical Harmonic Analysis

Considering that the atmosphere is a non-conductive layer, $\mathbf{j} = 0$, leading to $\nabla \times \mathbf{B} = 0$ based on Ampere's law. Consequently, the magnetic field detected at ground level can be represented using a scalar potential, expressed as $\mathbf{B} = -\nabla V$, a concept introduced by *Gauss* (1877) as detailed in (*Glassmeier and Tsurutani*, 2014). Furthermore, since $\nabla \cdot \mathbf{B} = 0$, V obeys the Laplace equation $\nabla^2 V = 0$ (*Chapman and Bartels*, 1940).

In spherical coordinates, the Laplace equation is

$$\frac{\partial}{\partial r}\left(r^2 \frac{\partial V}{\partial r}\right) + \frac{1}{\sin\theta}\frac{\partial}{\partial \theta}\left(\sin\theta \frac{\partial V}{\partial \theta}\right) + \frac{1}{\sin^2\theta}\frac{\partial^2 V}{\partial \phi^2} = 0 \tag{5.1}$$

where θ, ϕ, and r are the colatitude, longitude, and radius. We can write the solution in terms of spherical harmonics:

$$\begin{aligned} V = a \sum_{n=1}^{\infty} \sum_{m=0}^{n} \Big(&(\frac{a}{r})^{n+1} [g_n^m \cos(m\phi) + h_n^m \sin(m\phi)] + \\ &(\frac{r}{a})^n [q_n^m \cos(m\phi) + s_n^m \sin(m\phi)] \Big) P_n^m(\cos(\theta)) \end{aligned} \tag{5.2}$$

where $a = 6371.2$ km is the radius of the Earth. g_n^m and h_n^m are the coefficients of the spherical harmonics of the internal sources, called Gauss coefficients, while q_n^m and s_n^m describe external sources. P_n^m are Schmidt semi-normalized Legendre functions dependent only on the colatitude (θ). The integers n and m are the degree and order, respectively. It should be noted that m can only be less than or equal to n. By calculating the gradient of V, we find relationships between the spherical harmonic coefficients and the observed magnetic field components.

The main magnetic field is modeled mathematically using a set of spherical harmonic coefficients. A commonly used model is The International Geomagnetic Reference Field (IGRF) (*Alken et al.*, 2021). The Earth's core magnetic field is in a state of continuous and unpredictable change, with variations occurring over long time scales

(years). To accurately reflect these temporal changes, particularly those occurring over relatively few years, the International Geomagnetic Reference Field (IGRF) is regularly revised. These revisions are typically made every five years to ensure the model remains up-to-date with the current state of the Earth's magnetic field. IGRF uses a maximum degree n of 13 for epochs after 1995.

In the following we discuss how we use spherical harmonic analysis to analyze magnetic field perturbations from ground magnetometer data. We start by transforming SuperMAG data to the quasi-dipole (QD) coordinate system, adopting the method explained in (*Laundal and Richmond*, 2017; *Laundal et al.*, 2016). We treat this system as an orthogonal spherical coordinate system, using the QD components to solve for the spherical harmonic coefficients q_n^m and s_n^m. We also estimate the coefficients g_n^m and h_n^m, which in our case represent induced currents, given that the main magnetic field has been subtracted in the SuperMAG pre-processing. The coefficients are estimated using the linear set of equations that appear by calculating the gradient of V and relating it to the observed coefficients. The inversion of this set of equations is explained in the next section. In this procedure, θ is the magnetic colatitude, and ϕ is the magnetic local time in radians.

Following *Laundal et al.* (2016), we represent the equivalent horizontal ionospheric current (EHIC) measured from the ground as a scalar potential in terms of the external coefficients of the magnetic field q_n^m and s_n^m:

$$\Psi = \frac{a}{\mu_0} \sum_{n=1}^{\infty} \sum_{m=0}^{n} \left(\frac{2n+1}{n+1} \right) \left(\frac{a+h}{a} \right)^n [q_n^m \cos(m\phi) + s_n^m \sin(m\phi)] P_n^m(\cos(\theta)). \quad (5.3)$$

Here h is the height with respect to the reference radius a. We choose $h = 110$ km. μ_0 is the permeability. Figure 3.7 shows the contours of the EHIC during northward conditions derived utilizing spherical harmonics. We also derived the J_{EFAC} applying the spherical harmonics as shown in Figure 3.7. To express J_{EFAC} in terms of the spherical harmonics we recall that $J_{\text{EFAC}} = \frac{1}{\alpha}[\nabla \times j_\perp]_r$. Then, replacing $[\nabla \times j_\perp]_r$ with $\nabla\Psi$, we obtain an equation containing $\nabla^2\Psi$. Utilizing spherical harmonics allows for the computation of this term, as demonstrated in (*Sabaka et al.*, 2010) and allows us to express the equivalent field-aligned current as:

$$J_{\text{EFAC}} = \sum_{n=1}^{\infty} \sum_{m=0}^{n} \frac{n(2n+1)}{a\alpha\mu_0} \left(\frac{a+h}{a} \right)^{n-2} [q_n^m \cos(m\phi) + s_n^m \sin(m\phi)] P_n^m(\cos(\theta)). \quad (5.4)$$

5.2.2 The Inverse Problem

With the spherical harmonic representation of the magnetic field, we obtain a linear system of equations $\mathbf{d} = \mathbf{G}\mathbf{m}$ where $\mathbf{d}$ is the magnetic field measurements in a column vector form, $\mathbf{m}$ is the spherical harmonic coefficients, and $\mathbf{G}$ is the matrix that characterizes the linear relation between the observations and the parameters given by taking the gradient of equation 5.2.

To find $\mathbf{m}$ we used a technique called regularized iteratively re-weighted least squares. Most real inverse problems are ill-posed problems without a unique solution, and minor measurement errors may lead to significant changes to the solution.

To overcome this problem, we use techniques to "smooth out" the solutions. This process is known as regularization. It helps make the solution more stable and physically meaningful by incorporating additional information or assumptions about what the solution should be. We use the technique of *Madelaire et al.* (2022), which is based on zeroth-order Tikhonov regularization (*Tikhonov et al.*, 1998). Our regularization, or smoothing, limits the total magnetic energy in the model magnetic field integrated over the surface of the ionosphere. The extent to which this is prioritized over model-data fit is determined by a regularization parameter λ. Choosing λ is equivalent to finding the right balance between goodness of fit and minimum magnetic energy (smoothness). We use the method of *Madelaire et al.* (2022) to find λ based on Generalized Cross-Validation. In our study, we also applied iterative re-weighted least-squares with Huber weights (also following the method of *Madelaire et al.* (2022)) to reduce the influence of outliers on the final solution. Huber weights are beneficial when the data contains a few extreme values that would skew the results *Huber* (1964), reducing the impact of these outliers. Huber weights help ensure that the model's parameters are more representative of typical data. In our analysis, more constraints were applied to the method to find the simplest model to explain the data. We enforced hemispheric symmetry using only the $n-m$ odd terms, since we anyway only use data from the northern hemisphere. The spherical harmonic series is truncated at $n = 35$ and $m = 3$. The low truncation for m is based on the assumption that the gradient of the east/west is smoother than the north/south as explained in (*Laundal et al.*, 2016) and used in several empirical models of ionospheric electrodynamics.

5.3 Uncertainties

There are sources of uncertainty in this study that could be related to the collected data or the methodology applied. It is almost impossible to avoid or quantify all the uncertainties, but in this section, we will discuss the uncertainties we are aware of and how we dealt with them.

Magnetometer data is the primary data source on which we base our results. The uncertainty in the measurements is very low, ranging between 1 and 5 nT (*Curto*, 2019). However, the error may effectively be larger since, as discussed earlier in this chapter, the data obtained from SuperMAG are baseline subtracted . The subtraction technique, described in *Gjerloev* (2012), has assumptions that may lead to potential systematic measurement errors. For example, in determining the slowly varying component and the diurnal component, the approach relies on a choice of a window size, which may lead to either over-smoothing or under-smoothing the data. Another source of error in the baseline subtraction can be related to the cubic convolution interpolation used to resample the data. This interpolation technique has assumptions related to the smoothing and continuity of the data. If these assumptions are unsatisfied, the baseline can be wrong (*Gjerloev*, 2012). Assuming the typical value is zero during quiet days can also be a source of error, and it needs to be modified as it can neglect unrecognized currents present during these quiet times. Subtracted baselines should be accurately determined; otherwise, it can lead to underestimating or overestimating the magnetic field perturbations used to create our ionospheric current maps.

Another source of data uncertainties is related to defining substorm onsets using

magnetometer data. Some substorm lists based on geomagnetic indices identify substorm onsets at unrealistic MLTs. For example, we found that more than 18 % of the substorms defined in the *Forsyth et al.* (2015) SOPHIE list are detected by magnetometers on the dayside. Figure 5.2 shows a histogram of the number of events in the SOPHIE list as a function of MLT in hours. 10% of the *Newell and Gjerloev* (2011) NG events were identified on the dayside. In our papers we include substorms only if the onset MLT is between 18 and 6. We also analyzed different substorm lists to ensure that the results does not strongly rely on the substorm definition used in a single list, since this is debatable.

Defining the substorm onsets between 18 and 6 MLT is subjective and it is interesting to investigate how the choice impacts the results. In paper II, we analyzed substorms during northward conditions. In that paper, we plot the maximum value of the NBZ current positive cells (called P-cell) and the minimum value negative cell (called N-cell) to represent the intensity of the NBZ current. Based on the SOPHIE list, we chose the substorm onsets to be defined only on the night side and our results show that the magnitude of the cells increases around substorm onset. Using the complete list without filtering the substorms detected on the dayside leads to different conclusions, as shown in Figure 5.3. In the top panel of this figure, the magnitude of the P-cell for the whole list decreases after substorm onset, while the nightside onset list shows the opposite behavior. In the bottom panel, the behavior of the N-cell for the nightside onsets list follows that of the substorm, with changing magnitude during the expansion and recovery phases. The curve based on the whole list does not follow the same trend. The results of the nightside SOPHIE and NG lists agree well with the results of the FL list. From our point of view, selecting the nightside substorms in the other lists is, therefore, the correct choice.

Another issue is that the distribution of the magnetometers is not uniform, as shown in figure 5.1. Also, the data availability from the magnetometers varies over time, introducing high uncertainties in the spatial resolution of the ionospheric current maps. With such datasets, studying single substorm events is challenging since obtaining reliable global maps of the current becomes problematic. Consequently, we have adopted a statistical approach to analyze substorm events, utilizing a superposed epoch analysis merging different substorms. Due to the variation of the magnitude of substorms, some events may lead to outliers. To reduce the influence of these outliers, we employed Huber weights, as discussed in the previous section, which help reduce the impact of these extreme events and facilitate generating average maps of the current systems. To quantify the uncertainty related to variations between events, we employed the bootstrap technique.

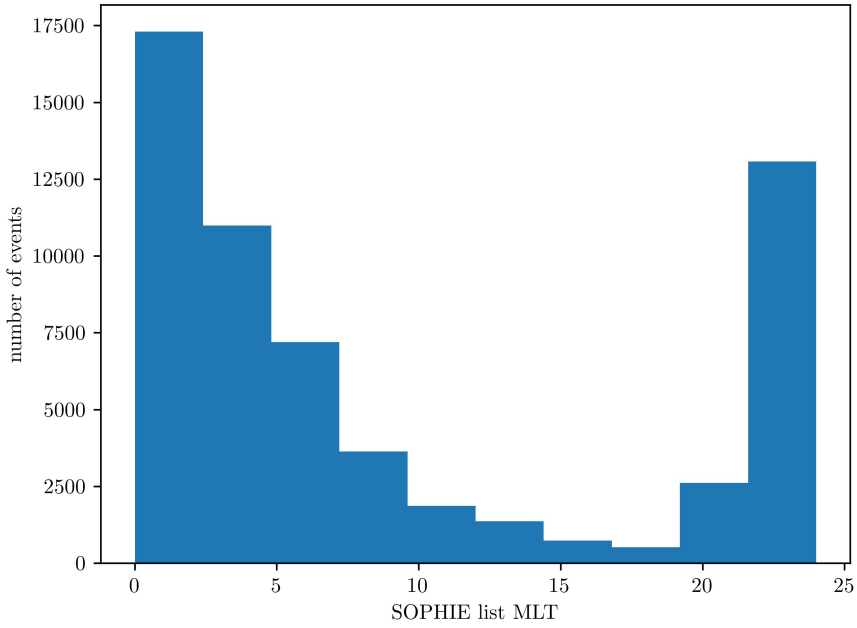

Figure 5.2: Histogram of the number of events in the SOPHIE list between 1995 and 2018 versus the magnetic local time provided with this events list.

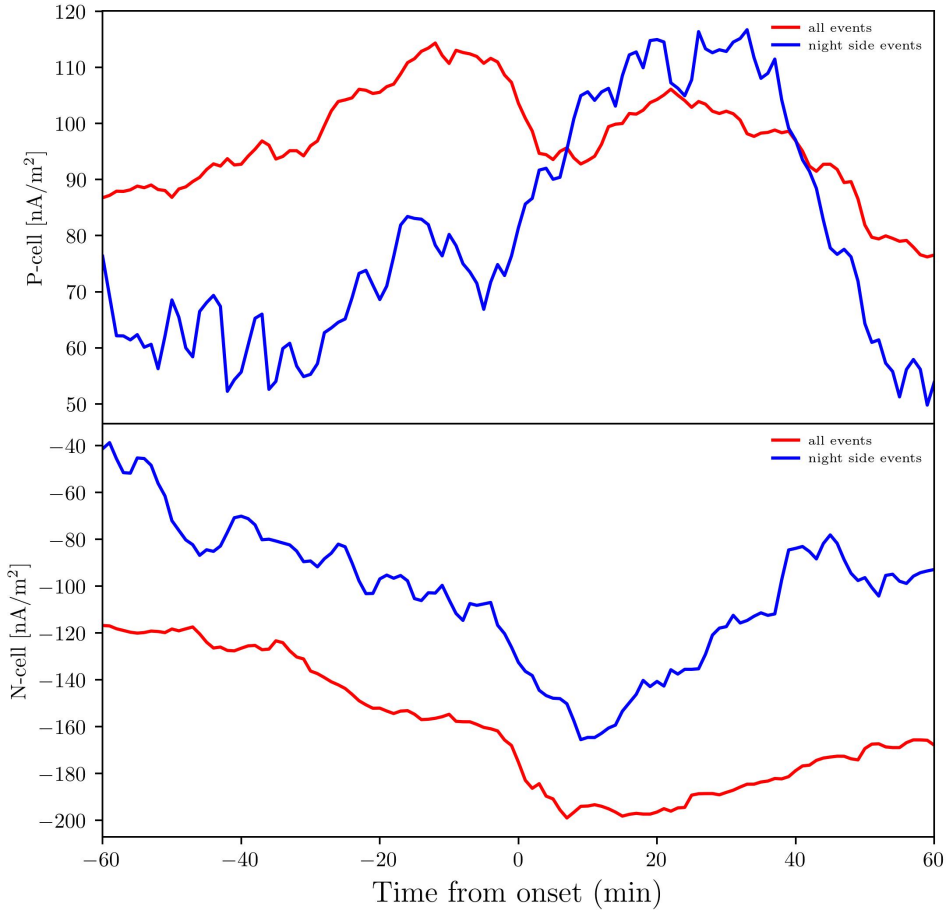

Figure 5.3: Comparison of the P-cell between the whole SOPHIE list (red color) and the night side selected SOPHIE list (blue color) in the top panel. Furthermore, the N-cell comparison is shown in the bottom panel with the same color scheme.

Chapter 6

Summary of the papers

In this chapter, we will discuss the results of the three papers that comprise the essence of this thesis.

Paper I: Possible Ionospheric Influence on Substorm Onset Location

Keypoints

- Prior to the onset of a substorm, the ionospheric state differs based on whether the substorm initiates early or late in local time.
- During high geomagnetic activity periods, substorm onsets typically shift to earlier local times.
- We propose that duskward shift in magnetospheric substorm activity may be caused by a higher ionospheric conductance.

In paper I, we analyzed 6192 substorm events from 1996 to 2005. We investigated how different factors can be used to predict the substorm onset location. We showed that the level of geomagnetic activity before substorm onset, represented by the AL index, explains $\sim$5% of the variation in onset MLT. Previous studies show that about $\sim$5% of the variation in onset MLT can be explained by variations in the interplanetary magnetic field B_y component. If IMF B_y is negative (positive), the substorm onsets tend to be observed at later (earlier) local times in the northern (southern) hemisphere. Our paper shows that during geomagnetically active (quiet) times, substorms tend to begin at earlier (later) local times. A critical difference between the effect of IMF B_y and the effect of the geomagnetic activity is that the onset MLT dependence is the same in the two hemispheres with respect to the AL index.

We refer to this similar MLT dependence in both hemispheres as a real shift, and the inter-hemispheric asymmetry with respect to IMF B_y as a mapping effect. We employed a linear regression model that combines IMF B_y, the AL index, the aberration angle, and the dipole tilt angle. This model explained about $\sim$11% of the observed variation in substorm onset MLT.

The aim of this paper was to address the second objective of the thesis. Our results show how unpredictable the substorm onset location is and that further investigation is needed.

Paper II: Substorm impact on dayside ionospheric currents

Keypoints

- Substorms occur during northward conditions may impact the NBZ dayside ionospheric currents.
- Before the onset of northward IMF substorms, lobe cells exhibit unusual weakness, becoming more pronounced after onset.
- We propose three possible mechanisms to understand how magnetotail activities may affect ionospheric currents on the dayside during northward conditions.

In paper II, we investigate the dayside and nightside ionospheric currents response influenced by substorm activities. In this paper, we explore the first objective of the thesis. We performed superposed epoch analyses of ground magnetic field data during substorms under northward IMF conditions. To ensure a precise analysis, we selected substorms that maintained a northward IMF orientation from 45 minutes before to 20 minutes after onset. Given the ambiguity of defining a substorm onset, the study examined responses across three different substorm lists derived from various observation methods, each had specific criteria to refine the data set. We confirm the increase in the westward electroject currents during nightside after substorm onset takes place. A new finding of this analysis is that the lobe cells increase just before the substorm onset. This enhancement is consistently observed over all substorm lists, indicating an impact of the nightside dynamics on dayside ionospheric currents during northward conditions.

We discuss three possible mechanisms that could explain the observations: The first possible mechanism accounts for the remote nightside current contribution and the initiation of the SCW. This mechanism can explain the observed dayside NBZ cells increase after onset but can not explain the increase before onset. The second mechanism explains the increase in the NBZ cells in terms of compressive and shear Alfvénic waves communicating between the magnetosphere and the ionosphere. The compressive waves could reach the ionosphere earlier than the establishment of a substorm current wedge, and be responsible for the observed dayside enhancement prior to the substorm onset. This is followed by shear Alfvénic waves sustaining the increase during the substorm expansion phase. The third mechanism proposes that changes in flaring angle could enhance the lobe reconnection efficiency, maintaining the elevated NBZ cells throughout the substorm.

Paper III: How do substorms influence hemispheric asymmetries in equivalent currents?

Keypoints

- Substorms can reduce interhemispheric asymmetries induced by IMF B_y and dipole tilt in the nightside ionospheric currents.
- The IMF and dipole tilt has little impact on substorm currents, while Substorms have no impact on dayside currents.
- This study provides insights into the development of future climatological models of ionospheric currents that currently depend solely on upstream parameters.

Paper III shows how substorms influence ionospheric currents, with a specific focus on the differential impacts on the dayside and nightside currents and the roles of dipole tilt and IMF B_y. We show that the seasonal variations and IMF B_y orientations have minimal impact on the enhancement in current associated with the substorms (the DP1 current). We show that substorms can diminish inter-hemispheric asymmetries in the nightside equivalent current caused by variations in the Interplanetary Magnetic Field (IMF) B_y component and Earth's dipole tilt. However, the substorm dynamics have minimal impact on the dayside currents. Our results highlight the need for the existing climatological models to include parameters that can account for nightside dynamics. Through our investigation, we have observed that during substorms, the equivalent current predominantly forms a single cell in the post-midnight sector. This phenomenon occurs irrespective of the IMF B_y orientation and dipole tilt, emphasizing that the nightside dynamics is independent of these variables. The aim of this paper was to meet the first objective of the thesis that we started working on in paper II. In this paper, we expand on exploring the influence of substorms on the current system under various conditions.

The results of papers II and III cover the first objective of the thesis, which shows a difference in the dayside current response to substorms occurring during northward conditions and all the other different orientations. The results of both papers show that the substorm influences on the nightside dynamics is the same regardless of the IMF orientation or seasonal variation.

Chapter 7

Conclusions

7.1 Conclusions

In this thesis, we aim to investigate the impact of substorms on the ionospheric currents under different conditions. Additionally, we have assessed the impact of pre-substorm ionospheric conditions on predicting the location of substorm onsets.

In Paper II, we investigated substorms under special conditions of northward IMF. We discovered that these substorms had an impact on both the dayside and nightside ionospheric equivalent current. These results led us to investigate the influence of substorms on currents during other IMF orientations and seasons in Paper III. We found that these substorms have limited impact on the dayside current. Interestingly, we observed no IMF or dipole tilt influence on the nightside currents after the substorm onsets, which implies a reduction in interhemispheric asymmetries there. Both studies emphasize the significant impact of substorms on nightside currents. The current patterns estimated in Papers II and III can be used to inform choices of parameterization in future empirical models of ionospheric currents that aim to include substorm dynamics. The research conducted in these two papers aimed to fulfill the first objective of the thesis: Investigate the influence of substorms on ionospheric current systems, emphasizing the difference in response between the dayside and nightside.

Papers II and III illustrate the great impact of substorms on ionospheric currents. Despite their importance, the timing and location of substorm onsets remain highly unpredictable. This motivated us to investigate the onset location of the substorms, in Paper I. We found that geomagnetic activity is as important as IMF conditions in predicting the substorm onset location, and it suggests that ionospheric feedback plays a role in modifying magnetospheric dynamics.

Despite our efforts to enhance the prediction of substorm onset locations, the additional variables considered in Paper I only explain an additional 5 to 6 % in substorm onset location variation compared to earlier studies. In total, we explain about 11%. These small numbers emphasize the current limitations in our understanding of the factors influencing substorm onset locations. This research, therefore, should not be viewed merely in the context of its immediate outcomes but as a step toward better exploring the factors affecting the substorm onsets. The results of Paper I addressed the second objective of this thesis: Examine to what extent substorm onset location can be predicted.

Bibliography

Akasofu, S. I. (1964), The development of the auroral substorm, *Planetary and Space Science*, *12*(4), 273–282, doi:10.1016/0032-0633(64)90151-5. 4.1

Akasofu, S.-I. (1975), The roles of the north-south component of the interplanetary magnetic field on large-scale auroral dynamics observed by the dmsp satellite, *Planetary and Space Science*, *23*(10), 1349–1354, doi:https://doi.org/10.1016/0032-0633(75)90030-6. 4.5

Alken, P., E. Thébault, C. D. Beggan, H. Amit, J. Aubert, J. Baerenzung, T. N. Bondar, W. J. Brown, S. Califf, A. Chambodut, A. Chulliat, G. A. Cox, C. C. Finlay, A. Fournier, N. Gillet, A. Grayver, M. D. Hammer, M. Holschneider, L. Huder, G. Hulot, T. Jager, C. Kloss, M. Korte, W. Kuang, A. Kuvshinov, B. Langlais, J. M. Léger, V. Lesur, P. W. Livermore, F. J. Lowes, S. Macmillan, W. Magnes, M. Mandea, S. Marsal, J. Matzka, M. C. Metman, T. Minami, A. Morschhauser, J. E. Mound, M. Nair, S. Nakano, N. Olsen, F. J. Pavón-Carrasco, V. G. Petrov, G. Ropp, M. Rother, T. J. Sabaka, S. Sanchez, D. Saturnino, N. R. Schnepf, X. Shen, C. Stolle, A. Tangborn, L. Tøffner-Clausen, H. Toh, J. M. Torta, J. Varner, F. Vervelidou, P. Vigneron, I. Wardinski, J. Wicht, A. Woods, Y. Yang, Z. Zeren, and B. Zhou (2021), International geomagnetic reference field: the thirteenth generation, *Earth, Planets and Space*, *73*(1), 49, doi:10.1186/s40623-020-01288-x. 5.2.1

Anderson, B. J., H. Korth, C. L. Waters, D. L. Green, and P. Stauning (2008), Statistical birkeland current distributions from magnetic field observations by the iridium constellation, *Annales Geophysicae*, *26*(3), 671–687, doi:10.5194/angeo-26-671-2008. 3.3

Baker, D. N., T. I. Pulkkinen, V. Angelopoulos, W. Baumjohann, and R. L. McPherron (1996), Neutral line model of substorms: Past results and present view, *Journal of Geophysical Research: Space Physics*, *101*(A6), 12,975–13,010, doi:https://doi.org/10.1029/95JA03753. 4.3.2

Birn, J., and M. Hesse (2013), The substorm current wedge in mhd simulations, *Journal of Geophysical Research: Space Physics*, *118*(6), 3364–3376, doi:https://doi.org/10.1002/jgra.50187. 4.2, 4.3

Campbell, W. H. (1997), *Introduction to geomagnetic fields*, Cambridge University Press. 2.2, 2.2, 2.2.1, 4.1

Chapman, S. (1962), Earth storms: Retrospect and prospect, *Journal of the Physical Society of Japan*, *17*, 6–15. 4.1

Chapman, S., and J. Bartels (1940), *Analysis of the Data, and Physical Theories,*, vol. 2, Oxford University Press, doi:10.2307/3606494. 5.2.1

Chu, X. (2015), *Configuration and generation of substorm current wedge*, University of California, Los Angeles. 4.2, 5.1.2

Clauer, C. R., and Y. Kamide (1985), Dp 1 and dp 2 current systems for the march 22, 1979 substorms, *Journal of Geophysical Research: Space Physics*, *90*(A2), 1343–1354, doi:https://doi.org/10.1029/JA090iA02p01343. 3.3

Clauer, C. R., R. L. McPherron, C. Searls, and M. G. Kivelson (1981), Solar wind control of auroral zone geomagnetic activity, *Geophysical Research Letters*, *8*(8), 915–918, doi:https://doi.org/10.1029/GL008i008p00915. 3.3

Clauer, C. R., R. L. McPherron, and C. Searls (1983), Solar wind control of the low-latitude asymmetric magnetic disturbance field, *Journal of Geophysical Research: Space Physics*, *88*(A3), 2123–2130, doi:https://doi.org/10.1029/JA088iA03p02123. 3.3

Coroniti, F. V., R. L. McPherron, and G. K. Parks (1968), Studies of the magnetospheric substorm: 3. concept of the magnetospheric substorm and its relation to electron precipitation and micropulsations, *Journal of Geophysical Research (1896-1977)*, *73*(5), 1715–1722, doi:https://doi.org/10.1029/JA073i005p01715. 4.1

Cowley, S. (1981), Magnetospheric asymmetries associated with the y-component of the imf, *Planetary and Space Science*, *29*(1), 79–96, doi:https://doi.org/10.1016/0032-0633(81)90141-0. 4.6

Cowley, S., and M. Lockwood (1992), Excitation and decay of solar-wind driven flows in the magnetosphere-ionosphere system, *Annales Geophysicae*, *10*, 103–115. 2.4, 2.5, 3.1, 3.2

Cowley, S. W. H. (2000), *Magnetosphere-Ionosphere Interactions: A Tutorial Review*, pp. 91–106, American Geophysical Union (AGU), doi:https://doi.org/10.1029/GM118p0091. 3.6

Crooker, N. U. (1992), Reverse convection, *Journal of Geophysical Research: Space Physics*, *97*(A12), 19,363–19,372, doi:https://doi.org/10.1029/92JA01532. 4.5

Curto, J. J. (2019), Uncertainty in hourly mean data from classical magnetometers, *Earth, Planets and Space*, *71*(1), 139, doi:10.1186/s40623-019-1119-2. 5.3

Davis, T. N., and M. Sugiura (1966), Auroral electrojet activity index ae and its universal time variations, *Journal of Geophysical Research (1896-1977)*, *71*(3), 785–801, doi:https://doi.org/10.1029/JZ071i003p00785. 5.1.2

Dungey, J. W. (1961), Interplanetary magnetic field and the auroral zones, *Phys. Rev. Lett.*, *6*, 47–48, doi:10.1103/PhysRevLett.6.47. 2.3, 2.3

Eastwood, J. P., R. Nakamura, L. Turc, L. Mejnertsen, and M. Hesse (2017), The scientific foundations of forecasting magnetospheric space weather, *Space Science Reviews*, *212*(3), 1221–1252, doi:10.1007/s11214-017-0399-8. 4.6

Elhawary, R., K. M. Laundal, J. P. Reistad, and S. M. Hatch (2022), Possible ionospheric influence on substorm onset location, *Geophysical Research Letters*, *49*(4), e2021GL096,691, doi:https://doi.org/10.1029/2021GL096691. 4.4.2

Elhawary, R., K. M. Laundal, J. P. Reistad, M. Madelaire, and A. Ohma (2023), Substorm impact on dayside ionospheric currents, *Geophysical Research Letters*, *50*(14), e2023GL104,800, doi:https://doi.org/10.1029/2023GL104800. 3.3, 4.5

Erdmann, W., H. Kmita, J. Z. Kosicki, and Ł. Kaczmarek (2021), How the geomagnetic field influences life on earth –an integrated approach to geomagnetobiology, *Origins of Life and Evolution of Biospheres*, *51*(3), 231–257, doi:10.1007/s11084-021-09612-5. 2.2

Forsyth, C., I. J. Rae, J. C. Coxon, M. P. Freeman, C. M. Jackman, J. Gjerloev, and A. N. Fazakerley (2015), A new technique for determining substorm onsets and phases from indices of the electrojet (sophie), *Journal of Geophysical Research: Space Physics*, *120*(12), 10,592–10,606, doi:https://doi.org/10.1002/2015JA021343. 5.1.3, 5.3

Fränz, M., and D. Harper (2002), Heliospheric coordinate systems, *Planetary and Space Science*, *50*(2), 217–233, doi:10.1016/S0032-0633(01)00119-2. 2.1

Freeman, M., and D. Southwood (1988), The effect of magnetospheric erosion on mid- and high-latitude ionospheric flows, *Planetary and Space Science*, *36*(5), 509–522, doi:https://doi.org/10.1016/0032-0633(88)90110-9. 2.4

Frey, H. U., S. B. Mende, V. Angelopoulos, and E. F. Donovan (2004), Substorm onset observations by IMAGE-FUV, *Journal of Geophysical Research: Space Physics*, *109*(A10), 2, doi:10.1029/2004JA010607. 4.4.2, 5.1.3

Fukushima, N. (1976), Generalized theorem for no ground magnetic effect of vertical currents connected with pedersen currents in the uniform-conductivity ionosphere, in *Report of Ionosphere and Space Research in Japan*. 3.2.3

Fukushima, N. (1994), Some topics and historical episodes in geomagnetism and aeronomy, *Journal of Geophysical Research: Space Physics*, *99*(A10), 19,113–19,142, doi:https://doi.org/10.1029/94JA00102. 3.2.3

Förster, M., and S. Haaland (2015), Interhemispheric differences in ionospheric convection: Cluster edi observations revisited, *Journal of Geophysical Research: Space Physics*, *120*(7), 5805–5823, doi:https://doi.org/10.1002/2014JA020774. 3.2.2

Gabrielse, C., V. Angelopoulos, A. Runov, and D. L. Turner (2014), Statistical characteristics of particle injections throughout the equatorial magnetotail, *Journal of Geophysical Research: Space Physics*, *119*(4), 2512–2535, doi:https://doi.org/10.1002/2013JA019638. 4.4.2

Gauss, C. F. (1877), *Allgemeine Theorie des Erdmagnetismus*, pp. 119–193, Springer Berlin Heidelberg, Berlin, Heidelberg, doi:10.1007/978-3-642-49319-5{_}5. 5.2.1

Gérard, J. C., B. Hubert, A. Grard, M. Meurant, and S. B. Mende (2004), Solar wind control of auroral substorm onset locations observed with the IMAGE-FUV imagers, *Journal of Geophysical Research: Space Physics*, *109*(A3), 1–13, doi: 10.1029/2003JA010129. 4.4.2

Gjerloev, J. W. (2009), A global ground-based magnetometer initiative, *Eos, Transactions American Geophysical Union*, *90*(27), 230–231, doi:https://doi.org/10.1029/2009EO270002. 5.1.1

Gjerloev, J. W. (2012), The SuperMAG data processing technique, *Journal of Geophysical Research: Space Physics*, *117*(9), 1–19, doi:10.1029/2012JA017683. 5.1.1, 5.3

Gjerloev, J. W., and R. A. Hoffman (2014), The large-scale current system during auroral substorms, *Journal of Geophysical Research: Space Physics*, *119*(6), 4591–4606, doi:https://doi.org/10.1002/2013JA019176. 4.2

Glassmeier, K.-H., and B. T. Tsurutani (2014), Carl friedrich gauss; general theory of terrestrial magnetism; a revised translation of the german text, *History of Geo- and Space Sciences*, *5*(1), 11–62, doi:10.5194/hgss-5-11-2014. 5.2.1

Grocott, A., S. E. Milan, T. K. Yeoman, N. Sato, A. S. Yukimatu, and J. A. Wild (2010), Superposed epoch analysis of the ionospheric convection evolution during substorms: Imf by dependence, *Journal of Geophysical Research: Space Physics*, *115*(A5), doi:https://doi.org/10.1029/2010JA015728. 4.6

Henderson, M. G. (2009), Observational evidence for an inside-out substorm onset scenario, *Annales Geophysicae*, *27*(5), 2129–2140, doi:10.5194/angeo-27-2129-2009. 4.3.1

Huber, P. J. (1964), Robust Estimation of a Location Parameter, *The Annals of Mathematical Statistics*, *35*(1), 73 – 101, doi:10.1214/aoms/1177703732. 5.2.2

Iijima, T. (1984), *Field-Aligned Currents During Northward IMF*, pp. 115–122, American Geophysical Union (AGU), doi:https://doi.org/10.1029/GM028p0115. 3.3, 4.5

Iijima, T., and T. A. Potemra (1976), The amplitude distribution of field-aligned currents at northern high latitudes observed by triad, *Journal of Geophysical Research (1896-1977)*, *81*(13), 2165–2174, doi:https://doi.org/10.1029/JA081i013p02165. 3.3

Kaeppler, S. R., D. L. Hampton, M. J. Nicolls, A. Strømme, S. C. Solomon, J. H. Hecht, and M. G. Conde (2015), An investigation comparing ground-based techniques that quantify auroral electron flux and conductance, *Journal of Geophysical Research: Space Physics*, *120*(10), 9038–9056, doi:https://doi.org/10.1002/2015JA021396. 3.1

Kan, J. R. (1998), A globally integrated substorm model: Tail reconnection and magnetosphere-ionosphere coupling, *Journal of Geophysical Research: Space Physics*, *103*(A6), 11,787–11,795, doi:https://doi.org/10.1029/98JA00361. 4.3.2

Kelly, M. C. (2009), *The Earth's Ionosphere: Plasma Physics and Electrodynamics, Second Edition*, vol. 96, 2 ed., Academic Press. 3.5, 3.2.2

Kepko, L., R. McPherron, S. Apatenkov, W. Baumjohann, J. Birn, M. Lester, R. Nakamura, T. Pulkkinen, and V. Sergeev (2015), The Substorm Current Wedge Revisited, in *AAS/AGU Triennial Earth-Sun Summit*, *AAS/AGU Triennial Earth-Sun Summit*, vol. 1, p. 206.03. 4.2, 4.3, 4.4.2

Khurana, K. K., R. J. Walker, and T. Ogino (1996), Magnetospheric convection in the presence of interplanetary magnetic field by : A conceptual model and simulations, *Journal of Geophysical Research: Space Physics*, *101*(A3), 4907–4916, doi:https://doi.org/10.1029/95JA03673. 4.6

Laundal, K. M., and A. D. Richmond (2017), Magnetic Coordinate Systems, *Space Science Reviews*, *206*(1-4), 27–59, doi:10.1007/s11214-016-0275-y. 2.1, 5.2.1

Laundal, K. M., S. E. Haaland, N. Lehtinen, J. W. Gjerloev, N. Østgaard, P. Tenfjord, J. P. Reistad, K. Snekvik, S. E. Milan, S. Ohtani, and B. J. Anderson (2015), Birkeland current effects on high-latitude ground magnetic field perturbations, *Geophysical Research Letters*, *42*(18), 7248–7254, doi:https://doi.org/10.1002/2015GL065776. 3.2.3

Laundal, K. M., J. W. Gjerloev, N. Østgaard, J. P. Reistad, S. Haaland, K. Snekvik, P. Tenfjord, S. Ohtani, and S. E. Milan (2016), The impact of sunlight on high-latitude equivalent currents, *Journal of Geophysical Research: Space Physics*, *121*(3), 2715–2726, doi:https://doi.org/10.1002/2015JA022236. 5.2.1, 5.2.2

Laundal, K. M., C. C. Finlay, N. Olsen, and J. P. Reistad (2018), Solar wind and seasonal influence on ionospheric currents from swarm and champ measurements, *Journal of Geophysical Research: Space Physics*, *123*(5), 4402–4429, doi:https://doi.org/10.1029/2018JA025387. 4.5

Laundal, K. M., J. P. Reistad, S. M. Hatch, T. Moretto, A. Ohma, N. Østgaard, P. A. R. Tenfjord, C. C. Finlay, and C. Kloss (2020), Time-scale dependence of solar wind-based regression models of ionospheric electrodynamics, *Scientific Reports*, *10*(1), 16,406, doi:10.1038/s41598-020-73532-z. 3.2.1

Lee, D., K. Choi, S. Ohtani, J. H. Lee, K. C. Kim, K. S. Park, and K. H. Kim (2010a), Can intense substorms occur under northward imf conditions?, *Journal of Geophysical Research: Space Physics*, *115*(A1), doi:https://doi.org/10.1029/2009JA014480. 4.5

Lee, D., S. Ohtani, and J. H. Lee (2010b), On the poleward boundary of the nightside auroral oval under northward interplanetary magnetic field conditions, *Journal of Geophysical Research: Space Physics*, *115*(A8), doi:https://doi.org/10.1029/2009JA014906. 4.5

Li, H., C. Wang, W. Y. Xu, and J. R. Kan (2012), Characteristics of magnetospheric energetics during geomagnetic storms, *Journal of Geophysical Research: Space Physics*, *117*(A4), doi:https://doi.org/10.1029/2012JA017584. 4.5

Li, H., C. Wang, and Z. Peng (2013), Solar wind impacts on growth phase duration and substorm intensity: A statistical approach, *Journal of Geophysical Research: Space Physics*, *118*(7), 4270–4278, doi:https://doi.org/10.1002/jgra.50399. 4.1

Liou, K. (2010), Polar Ultraviolet Imager observation of auroral breakup, *Journal of Geophysical Research: Space Physics*, *115*(12), 1–7, doi:10.1029/2010JA015578. 4.4.2

Liou, K., and P. T. Newell (2010), On the azimuthal location of auroral breakup: Hemispheric asymmetry, *Geophysical Research Letters*, *37*(23), 1–5, doi:10.1029/2010GL045537. 4.4.2, 5.1.3

Liou, K., P. T. Newell, D. G. Sibeck, C. I. Meng, M. Brittnacher, and G. Parks (2001), Observation of IMF and seasonal effects in the location of auroral substorm onset, *Journal of Geophysical Research: Space Physics*, *106*(4), 5799–5810, doi:10.1029/2000ja003001. 4.4.2

Liu, J., V. Angelopoulos, X. Chu, X.-Z. Zhou, and C. Yue (2015), Substorm current wedge composition by wedgelets, *Geophysical Research Letters*, *42*(6), 1669–1676, doi:https://doi.org/10.1002/2015GL063289. 4.2

Lui, A. T. Y. (1991), A synthesis of magnetospheric substorm models, *Journal of Geophysical Research: Space Physics*, *96*(A2), 1849–1856, doi:https://doi.org/10.1029/90JA02430. 4.1

Lui, A. T. Y. (1996), Current disruption in the earth's magnetosphere: Observations and models, *Journal of Geophysical Research: Space Physics*, *101*(A6), 13,067–13,088, doi:https://doi.org/10.1029/96JA00079. 4.3.1

Lyons, L. R., Y. Nishimura, J. Liu, W. A. Bristow, Y. Zou, and E. F. Donovan (2022), Verification of substorm onset from intruding flow channels with high-resolution superdarn radar flow maps, *Journal of Geophysical Research: Space Physics*, *127*(8), e2022JA030,723, doi:https://doi.org/10.1029/2022JA030723, e2022JA030723 2022JA030723. 4.3.2

Machida, S., Y. Miyashita, A. Ieda, M. Nosé, D. Nagata, K. Liou, T. Obara, A. Nishida, Y. Saito, and T. Mukai (2009), Statistical visualization of the earth's magnetotail based on geotail data and the implied substorm model, *Annales Geophysicae*, *27*(3), 1035–1046, doi:10.5194/angeo-27-1035-2009. 4.3.2

Madelaire, K. M., M.and Laundal, S. M. Reistad, J. P.and Hatch, and O. A. (2022), Transient high latitude geomagnetic response to rapid increases in solar wind dynamic pressure, *Frontiers in Astronomy and Space Sciences 9*, doi:10.3389/fspas.2022.953954. 5.2.2

McPherron, R. L. (1970), Growth phase of magnetospheric substorms, *Journal of Geophysical Research*, *75*(28), 5592–5599, doi:10.1029/ja075i028p05592. 4.1

McPherron, R. L., and X. Chu (2016), Relation of the auroral substorm to the substorm current wedge, *Geoscience Letters*, *3*(1), doi:10.1186/s40562-016-0044-5. 4.1, 5.1.2

McPherron, R. L., and X. Chu (2018), The midlatitude positive bay index and the statistics of substorm occurrence, *Journal of Geophysical Research: Space Physics*, *123*(4), 2831–2850, doi:https://doi.org/10.1002/2017JA024766. 5.1.3

McPherron, R. L., C. T. Russell, M. G. Kivelson, and P. J. Coleman Jr. (1973), Substorms in space: The correlation between ground and satellite observations of the magnetic field, *Radio Science*, *8*(11), 1059–1076, doi:https://doi.org/10.1029/RS008i011p01059. 4.2, 4.3

Mende, S. B., C. W. Carlson, H. U. Frey, L. M. Peticolas, and N. Østgaard (2003), Fast and image-fuv observations of a substorm onset, *Journal of Geophysical Research: Space Physics*, *108*(A9), doi:https://doi.org/10.1029/2002JA009787. 4.4.2

Milan, S. (2015), Sun et lumière: Solar wind-magnetosphere coupling as deduced from ionospheric flows and polar auroras, in *Astrophysics and Space Science Proceedings, Springer International Publishing*, vol. 41, p. 3364. 2.3, 3.2.1, 4.5

Milan, S. E., M. Lester, S. W. H. Cowley, and M. Brittnacher (2000), Dayside convection and auroral morphology during an interval of northward interplanetary magnetic field, *Annales Geophysicae*, *18*(4), 436–444, doi:10.1007/s00585-000-0436-9. 3.2.2

Milan, S. E., J. Hutchinson, P. D. Boakes, and B. Hubert (2009), Influences on the radius of the auroral oval, *Annales Geophysicae*, *27*(7), 2913–2924, doi:10.5194/angeo-27-2913-2009. 4.4.2

Milan, S. E., J. S. Gosling, and B. Hubert (2012), Relationship between interplanetary parameters and the magnetopause reconnection rate quantified from observations of the expanding polar cap, *Journal of Geophysical Research: Space Physics*, *117*(A3), doi:https://doi.org/10.1029/2011JA017082. 3.2.1

Milan, S. E., J. A. Carter, H. Sangha, G. E. Bower, and B. J. Anderson (2021), Magnetospheric flux throughput in the dungey cycle: Identification of convection state during 2010, *Journal of Geophysical Research: Space Physics*, *126*(2), e2020JA028,437, doi:https://doi.org/10.1029/2020JA028437, e2020JA028437 2020JA028437. 4.6

Mitchell, D. G., D. J. Williams, C. Y. Huang, L. A. Frank, and C. T. Russell (1990), Current carriers in the near-earth cross-tail current sheet during substorm growth phase, *Geophysical Research Letters*, *17*(5), 583–586, doi:https://doi.org/10.1029/GL017i005p00583. 4.3.1

Miyashita, Y., Y. Kamide, K. Liou, C.-C. Wu, A. Ieda, N. Nishitani, S. Machida, Y. Saito, and T. Mukai (2011), Successive substorm expansions during a period of prolonged northward interplanetary magnetic field, *Journal of Geophysical Research: Space Physics*, *116*(A9), doi:https://doi.org/10.1029/2011JA016719. 4.5

Nagai, T. (1982), Observed magnetic substorm signatures at synchronous altitude, *Journal of Geophysical Research: Space Physics*, *87*(A6), 4405–4417, doi:https://doi.org/10.1029/JA087iA06p04405. 4.2

Nagai, T., M. Fujimoto, Y. Saito, S. Machida, T. Terasawa, R. Nakamura, T. Yamamoto, T. Mukai, A. Nishida, and S. Kokubun (1998), Structure and dynamics of magnetic reconnection for substorm onsets with geotail observations, *Journal of Geophysical Research: Space Physics*, *103*(A3), 4419–4440, doi:https://doi.org/10.1029/97JA02190. 4.3.1

Newell, P. T., and J. W. Gjerloev (2011), Evaluation of supermag auroral electrojet indices as indicators of substorms and auroral power, *Journal of Geophysical Research: Space Physics*, *116*(A12), doi:https://doi.org/10.1029/2011JA016779. 5.1.2, 5.1.3, 5.3

Newell, P. T., T. Sotirelis, K. Liou, C.-I. Meng, and F. J. Rich (2007), A nearly universal solar wind-magnetosphere coupling function inferred from 10 magnetospheric state variables, *Journal of Geophysical Research: Space Physics*, *112*(A1), doi:https://doi.org/10.1029/2006JA012015. 3.2.1

Obayashi, T. (1967), The interaction of solar plasma with geomagnetic field in disturbed condition, *In: King JW, Newman WS (eds) Solar terrestrial physics. N.Y.* 3.3

Ohma, A., N. Østgaard, J. P. Reistad, P. Tenfjord, K. M. Laundal, K. Snekvik, S. E. Haaland, and M. O. Fillingim (2018), Evolution of asymmetrically displaced footpoints during substorms, *Journal of Geophysical Research: Space Physics*, *123*(12), 10,030–10,063, doi:https://doi.org/10.1029/2018JA025869. 3.2.1, 4.6

Ohma, A., K. M. Laundal, J. P. Reistad, and N. Østgaard (2022), Evolution of imf by induced asymmetries during substorms: Superposed epoch analysis at geosynchronous orbit, *Frontiers in Astronomy and Space Sciences*, *9*, doi:10.3389/fspas.2022.958749. 4.6

Østgaard, N., K. M. Laundal, L. Juusola, A. Åsnes, S. E. Håland, and J. M. Weygand (2011), Interhemispherical asymmetry of substorm onset locations and the interplanetary magnetic field, *Geophysical Research Letters*, *38*(8), 1–5, doi:10.1029/2011GL046767. 4.4.2

Parker, E. N. (1958), Suprathermal Particle Generation in the Solar Corona., *Astrophysical Journal*, *128*, 677, doi:10.1086/146580. 2.1

Parker, E. N. (1996), The alternative paradigm for magnetospheric physics, *Journal of Geophysical Research: Space Physics*, *101*(A5), 10,587–10,625, doi:https://doi.org/10.1029/95JA02866. 3.1

Parker, E. N. (1997), Reply, *Journal Of Geophysical Research*, *102*(A5), 9657–9568. 3.1

Peng, Z., C. Wang, Y. F. Yang, H. L. Y. Q. Hu, and J. Du (2013), Substorms under northward interplanetary magnetic field: Statistical study, *Journal of Geophysical Research: Space Physics*, *118*, 364374, doi:doi:10.1029/2012JA018065. 4.5

Petrukovich, A. A. (2011), Origins of plasma sheet by, *Journal of Geophysical Research: Space Physics*, *116*(A7), doi:https://doi.org/10.1029/2010JA016386. 4.6

Pettigrew, E. D., S. G. Shepherd, and J. M. Ruohoniemi (2010), Climatological patterns of high-latitude convection in the northern and southern hemispheres: Dipole tilt dependencies and interhemispheric comparisons, *Journal of Geophysical Research: Space Physics*, *115*(A7), doi:https://doi.org/10.1029/2009JA014956. 3.2.2

Reiff, P. H., and J. L. Burch (1985), Imf by-dependent plasma flow and birkeland currents in the dayside magnetosphere: 2. a global model for northward and southward imf, *Journal of Geophysical Research: Space Physics*, *90*(A2), 1595–1609, doi:https://doi.org/10.1029/JA090iA02p01595. 3.2.2

Reistad, J. P. (2016), Mechanisms responsible for asymmetric aurora between the conjugate hemispheres. 3.1

Reistad, J. P., N. Østgaard, P. Tenfjord, K. M. Laundal, K. Snekvik, S. Haaland, S. E. Milan, K. Oksavik, H. U. Frey, and A. Grocott (2016), Dynamic effects of restoring footpoint symmetry on closed magnetic field lines, *Journal of Geophysical Research: Space Physics*, *121*(5), 3963–3977, doi:https://doi.org/10.1002/2015JA022058. 3.2.2

Reistad, J. P., K. M. Laundal, N. Østgaard, A. Ohma, E. G. Thomas, S. Haaland, K. Oksavik, and S. E. Milan (2019), Separation and quantification of ionospheric convection sources: 2. the dipole tilt angle influence on reverse convection cells during northward imf, *Journal of Geophysical Research: Space Physics*, *124*(7), 6182–6194, doi:https://doi.org/10.1029/2019JA026641. 3.2.2, 4.5

Rostoker, G., S.-I. Akasofu, J. Foster, R. Greenwald, Y. Kamide, K. Kawasaki, A. Lui, R. McPherron, and C. Russell (1980), Magnetospheric substorms definition and signatures, *Journal of Geophysical Research: Space Physics*, *85*(A4), 1663–1668, doi:https://doi.org/10.1029/JA085iA04p01663. 4.1

Sabaka, T. J., G. Hulot, and N. Olsen (2010), *Mathematical Properties Relevant to Geomagnetic Field Modeling*, pp. 503–538, Springer Berlin Heidelberg, Berlin, Heidelberg, doi:10.1007/978-3-642-01546-5_17. 5.2.1

Sado, P., L. B. N. Clausen, W. J. Miloch, and H. Nickisch (2023), Substorm onset prediction using machine learning classified auroral images, *Space Weather*, *21*(2), e2022SW003,300, doi:https://doi.org/10.1029/2022SW003300, e2022SW003300 2022SW003300. 4.4.1

Sergeev, V. A., A. V. Nikolaev, N. A. Tsyganenko, V. Angelopoulos, A. V. Runov, H. J. Singer, and J. Yang (2014), Testing a two-loop pattern of the substorm current wedge (scw2l), *Journal of Geophysical Research: Space Physics*, *119*(2), 947–963, doi:https://doi.org/10.1002/2013JA019629. 4.2

Shiokawa, K., W. Baumjohann, G. Haerendel, G. Paschmann, J. F. Fennell, E. Friis-Christensen, H. Lühr, G. D. Reeves, C. T. Russell, P. R. Sutcliffe, and K. Takahashi (1998), High-speed ion flow, substorm current wedge, and multiple pi 2 pulsations, *Journal of Geophysical Research: Space Physics*, *103*(A3), 4491–4507, doi:https://doi.org/10.1029/97JA01680. 4.5

Siscoe, G. L., and T. S. Huang (1985), Polar cap inflation and deflation, *Journal of Geophysical Research: Space Physics*, *90*(A1), 543–547, doi:https://doi.org/10.1029/JA090iA01p00543. 2.4

Song, P., T. Gombosi, D. DeZeeuw, K. Powell, and C. Groth (2000), A model of solar windmagnetosphereionosphere coupling for due northward imf, *Planetary and Space Science*, *48*(1), 29–39, doi:https://doi.org/10.1016/S0032-0633(99)00065-3. 4.5

Svalgaard, L. (1973), Polar cap magnetic variations and their relationship with the interplanetary magnetic sector structure, *Journal of Geophysical Research (1896-1977)*, *78*(13), 2064–2078, doi:https://doi.org/10.1029/JA078i013p02064. 3.3

Tanaka, T., A. Nakamizo, A. Yoshikawa, S. Fujita, H. Shinagawa, H. Shimazu, T. Kikuchi, and K. K. Hashimoto (2010), Substorm convection and current system deduced from the global simulation, *Journal of Geophysical Research: Space Physics*, *115*(A5), doi:https://doi.org/10.1029/2009JA014676. 4.5

Tenfjord, P., N. Østgaard, K. Snekvik, K. M. Laundal, J. P. Reistad, S. Haaland, and S. E. Milan (2015), How the imf by induces a by component in the closed magnetosphere and how it leads to asymmetric currents and convection patterns in the two hemispheres, *Journal of Geophysical Research: Space Physics*, *120*(11), 9368–9384, doi:https://doi.org/10.1002/2015JA021579. 3.3, 3.2.2, 4.6

Tenfjord, P., N. Østgaard, S. Haaland, K. Snekvik, K. M. Laundal, J. P. Reistad, R. Strangeway, S. E. Milan, M. Hesse, and A. Ohma (2018), How the imf by induces a local by component during northward imf bz and characteristic timescales, *Journal of Geophysical Research: Space Physics*, *123*(5), 3333–3348, doi:https://doi.org/10.1002/2018JA025186. 4.6

Thomas, E. G., and S. G. Shepherd (2018), Statistical patterns of ionospheric convection derived from mid-latitude, high-latitude, and polar superdarn hf radar observations, *Journal of Geophysical Research: Space Physics*, *123*(4), 3196–3216, doi:https://doi.org/10.1002/2018JA025280. 3.4, 3.2.2

Tikhonov, A., A. Leonov, and A. IAgola (1998), *Nonlinear Ill-posed Problems*, no. v. 2 in Applied mathematics and mathematical computation, Chapman & Hall. 5.2.2

Uritsky, V., M. Pudovkin, and A. Steen (2001), Geomagnetic substorms as perturbed self-organized critical dynamics of the magnetosphere, *Journal of Atmospheric and Solar-Terrestrial Physics*, *63*(13), 1415–1424, doi:https://doi.org/10.1016/S1364-6826(00)00243-1, forced and/or Self-Organized Criticality (FSOC) in Space Plasmas. 4.4.1

Valliéres-Nollet, M.-A., P. Charbonneau, V. Uritsky, E. Donovan, and W. Liu (2010), Dual scaling for self-organized critical models of the magnetosphere, *Journal of Geophysical Research: Space Physics*, *115*(A12), doi:https://doi.org/10.1029/2010JA015641. 4.4.1

Vasyliūnas, V. M. (2001), Electric field and plasma flow: What drives what?, *Geophysical research letters*, *28*(11), 2177–2180, doi:10.1029/2001GL013014. 3.1

Vasyliūnas, V. M. (2005a), Relation between magnetic fields and electric currents in plasmas, *Annales Geophysicae*, *23*(7), 2589–2597, doi:10.5194/angeo-23-2589-2005. 3.1

Vasyliūnas, V. M. (2005b), Time evolution of electric fields and currents and the generalized ohm's law, *Annales Geophysicae*, *23*(4), 1347–1354, doi:10.5194/angeo-23-1347-2005. 3.1

Vasyliūnas, V. M. (2012), The physical basis of ionospheric electrodynamics, *Ann. Geophys.*, *30*, doi:10.5194/angeo-30-357-2012. 3.1, 3.2.3

Walker, S. J., K. M. Laundal, J. P. Reistad, S. M. Hatch, A. Ohma, and J. Gjerloev (2024), The ionospheric leg of the substorm current wedge: Combining iridium and ground magnetometers, *ESS Open Archive*, doi:10.22541/essoar.170542196.62700911/v1. 3.2.3

Walsh, A. P., S. Haaland, C. Forsyth, A. M. Keesee, J. Kissinger, K. Li, A. Runov, J. Soucek, B. M. Walsh, S. Wing, et al. (2014), Dawn–dusk asymmetries in the coupled solar wind–magnetosphere–ionosphere system: A review, in *Annales Geophysicae*, pp. 705–737, Copernicus GmbH. 3.2.2

Wang, H., H. Lühr, S. Y. Ma, and H. U. Frey (2007), Interhemispheric comparison of average substorm onset locations: Evidence for deviation from conjugacy, *Annales Geophysicae*, *25*(4), 989–999, doi:10.5194/angeo-25-989-2007. 4.4.2

Wilder, F. D., C. R. Clauer, and J. B. H. Baker (2009), Reverse convection potential saturation during northward imf under various driving conditions, *Journal of Geophysical Research: Space Physics*, *114*(A8), doi:https://doi.org/10.1029/2009JA014266. 3.2.2

Wu, C., K. Liou, R. Lepping, and C. Meng (2002), Observations of substorms during prolonged northward imf conditions, in *Sixth International Conference on Substorms*, vol. 10, Univ of Wash Press, Seattle. 4.5

Chapter 8

Scientific results

Paper I

Possible ionospheric influence on substorm onset location.

Elhawary, R. Laundal, K. M. Reistad, J. P. and Hatch, S. M.
Geophysical Research Letters, **49/e2021GL096691.** (2022)

Geophysical Research Letters

RESEARCH LETTER
10.1029/2021GL096691

Possible Ionospheric Influence on Substorm Onset Location

R. Elhawary[1], K. M. Laundal[1], J. P. Reistad[1], and S. M. Hatch[1]

[1]Birkeland Centre for Space Science, University of Bergen, Bergen, Norway

Key Points:

- Ionospheric conditions before substorm onset are different for substorms with an early local time onset versus late local time onset
- Substorm onsets tend to move to earlier local times with increasing geomagnetic activity
- We suggest that higher ionospheric conductance leads to a duskward shift in magnetospheric substorm activity

Correspondence to:

R. Elhawary,
reham.elhawary@uib.no

Citation:

Elhawary, R., Laundal, K. M., Reistad, J. P., & Hatch, S. M. (2022). Possible ionospheric influence on substorm onset location. *Geophysical Research Letters*, *49*, e2021GL096691. https://doi.org/10.1029/2021GL096691

Received 22 OCT 2021
Accepted 9 FEB 2022

Author Contributions:

Supervision: K. M. Laundal, J. P. Reistad
Writing – review & editing: K. M. Laundal, J. P. Reistad, S. M. Hatch

Abstract Auroral substorm onset locations are highly unpredictable. Previous studies have shown that the B_y component of the interplanetary magnetic field (IMF) explains ∼5% of the variation in onset magnetic local time (MLT), while solar wind conditions and the other IMF components have even less explanatory power. In this study, we show that the level of geomagnetic activity before substorm onset, as indicated by the AL index, explains an additional ∼5% of the variation in onset MLT. We discuss our results with regard to recent modeling studies, which show that gradients in the ionospheric Hall conductance can lead to a duskward shift of the magnetotail dynamics. Our findings suggest that this magnetosphere-ionosphere coupling effect may also influence the location of substorm onsets.

Plain Language Summary Substorms are explosive disturbances in our magnetotail that impact the earth's ionosphere. They happen on average several times per day and as a result of this phenomenon, we can see the marvelous aurora. Substorms happen on the nightside of the earth and can take place over a wide range of latitudes and longitudes. In this study, we show that substorms tend to begin at earlier local times during geomagnetically active times than during quiet times. We interpret this tendency as a sign that ionospheric conditions may play a role in determining where substorms occur.

1. Introduction

Substorms are abrupt global-scale changes in the magnetotail that release the energy stored in the nightside magnetosphere into the two nightside polar ionospheres via field-aligned currents and particle precipitation. Akasofu (1964) defined the substorm in terms of two phases, the expansion phase, and the recovery phase. Later McPherron (1970) defined a third phase of the substorm, the growth phase. The growth phase of the substorm is the period before the onset of the expansion phase, typically lasting for 30–60 min (Lui, 1991), when kinetic energy in the solar wind is transferred to magnetic energy in the magnetotail and then thermal energy in the plasma sheet. During the expansion phase, the aurora suddenly becomes bright and evolves into a global distribution in typically 10–30 min. Finally, a recovery phase can last for more than 2 hr. See, for example, McPherron and Chu (2016) for a detailed review about the development of the definition of substorms.

The substorm cycle is an integral component of solar wind-magnetosphere-ionosphere coupling: Substorms are the central process by which the magnetosphere releases magnetic flux opened on the dayside back into the solar wind through reconnection in the neutral sheet of the magnetotail (Milan et al., 2010). Substorms also release energy in the magnetotail that reorganizes ionospheric flows (Grocott et al., 2017).

Global UV images of the aurora have shown that 80% of substorm onsets (i.e., between the 10th and 90th percentile) happen in a ∼3.2 hr wide range of magnetic local time (MLT), centered pre-midnight (Frey et al., 2004; Liou, 2010). It may not be surprising that substorm auroras take place at pre-midnight, given that the upward current at the duskward edge of the substorm current wedge (SCW) should be associated with downward electrons. However, we believe that the onsets listed by Frey et al. (2004); Liou (2010) occur before the SCW is developed (Kepko et al., 2015) and the structure of the SCW probably does not explain the duskward shift. Furthermore, the onset aurora may not be closely associated with FACs at all (Mende et al., 2003), but instead, map to the transition between the dipolar and the stretched field lines. Beyond this statistical distribution, the location of substorm onsets remains largely unpredictable. Previous studies have attempted to predict the location of the substorm onset by correlating the MLT and magnetic latitude (MLat) of the substorm onset with different parameters. For instance, Liou et al. (2001) found that substorms occur at lower latitudes when the interplanetary magnetic field (IMF) B_z component is negative, compared to positive. Gérard et al. (2004) also found a correlation between MLat of the substorm onset and solar wind dynamic pressure. Both effects may be the result of relatively more open flux in the magnetosphere, which moves the auroral oval equatorward (Milan et al., 2009).

Many other studies have shown that the substorm onset MLT depends on the polarity of IMF B_y rather than IMF B_z (Liou & Newell, 2010; Østgaard et al., 2004, 2005, 2011; Wang et al., 2007). Using the lists of substorm onsets based on global UV imaging by Frey et al. (2004) and Liou (2010), Østgaard et al. (2011) showed that the substorm onset MLT and IMF B_y are correlated. Though the relationship between IMF B_y and substorm onset MLT is statistically significant, IMF B_y only explains 5% of the variation of the substorm onset MLT. Tenfjord et al. (2015) argued that the asymmetric addition of open flux during IMF B_y periods leads to an induced B_y in the magnetosphere, which in turn can lead to changes in the observed projection of the substorm onset on the ionosphere. This projection effect may explain the observed variation of onset location versus IMF B_y. Furthermore, simultaneous observations of substorm onsets in the two hemispheres show that the correlation of the relative shift in MLT with IMF B_y is much higher (Østgaard et al., 2005), consistent with our interpretation that the IMF B_y effect is due to a relative shift of the onset MLT in each hemisphere (i.e., an effect of field line mapping), and not a real shift of the onset location in the magnetosphere. In addition to IMF B_y, the dipole tilt angle may also have a similar effect on the observed onset location in the ionosphere: Due to tail warping associated with nonzero dipole tilt (e.g., Tsyganenko, 1998), a positive dipole tilt angle will lead to an added positive B_y component on closed field-lines in the magnetotail at dusk, and an added negative B_y component at dawn (e.g., Liou & Newell, 2010; Figure 3). This perturbation field would project phenomena in the dusk magnetotail to earlier (later) local times in the northern (southern) ionosphere. Substorm onset statistics presented by Liou and Newell (2010) and Østgaard et al. (2011) are consistent with this idea, assuming that most onsets happen at dusk in the magnetotail.

The results presented in these previous studies may be completely explained by mapping effects, while the location of the onset in the magnetotail remains unpredictable. The observed shift toward dusk of the typical onset location is similar to the observed distribution of tail reconnection (e.g., Angelopoulos et al., 1994; Kiehas et al., 2018). One potential explanation of this shift is related to the Hall effect in a thin current sheet. This was investigated by Lu et al. (2016) and Lu et al. (2018), who conducted a hybrid 3D global simulation and a particle in a cell simulation, respectively, with uniform ionospheric conductances to exclude the ionospheric effects. They found that the Hall effect is stronger on the dusk side due to higher ion perpendicular temperature, and a smaller B_z. Another potential explanation that includes the ionospheric contribution to the observed shift was presented in Lotko et al. (2014). They performed three MHD simulations: In the first simulation, they introduced uniform ionospheric conductance and observed symmetric magnetotail activity. In the second simulation, they introduced high Hall conductance in the auroral oval and monitored the magnetotail activity which shifted toward dusk. In the third simulation, they introduced an unrealistic depression in Hall conductance in the auroral oval and monitored the magnetotail activity which shifted toward dawn. The results of Lotko et al. (2014) suggest that ionospheric feedback influences the duskward shift of tail reconnection and, possibly, substorm onsets. In the current paper, we test this idea using observations of substorm onsets, ground magnetic field perturbations, and solar wind conditions.

2. Observations

We use the Frey et al. (2004) and Liou (2010) lists to investigate substorm onsets in this study. The two lists combined have 6,192 substorms in the period 1996–2005, with 4,762 substorms observed in the Northern hemisphere and 1,430 substorms observed in the Southern hemisphere. The substorm onsets identified in Frey et al. (2004) as "a clear local brightening of the aurora." Two additional criteria have been applied to identify the substorm onset in this list: After observing the clear local brightening, they require (a) that the expansion of the aurora lasts for at least 20 min, (b) that the poleward expansion goes over the poleward boundary of the oval, and (c) that the onset occurs at least 30 min after a previously identified onset. In the list provided by Liou (2010), the substorm onset is identified as "a sudden brightening of the aurora." The author then uses the same criteria as Frey et al. (2004) except that in the second step, he does not require the poleward expansion to go beyond the poleward boundary of the oval. Afterward, the identified images related to substorm events are transformed to geomagnetic coordinate system to provide the onset MLT and MLat.

To investigate whether the ionospheric state may possibly influence substorm onset location, we used the magnitude of the horizontal geomagnetic data from the northern hemisphere (ground B) $= \sqrt{< E_{qd}^2 + N_{qd}^2 >}$ where E_{qd} and N_{qd} are the eastward and northward component of the magnetic field in quasi-dipole coordinates. The ground magnetic field perturbations were obtained from the SuperMAG database in geographic

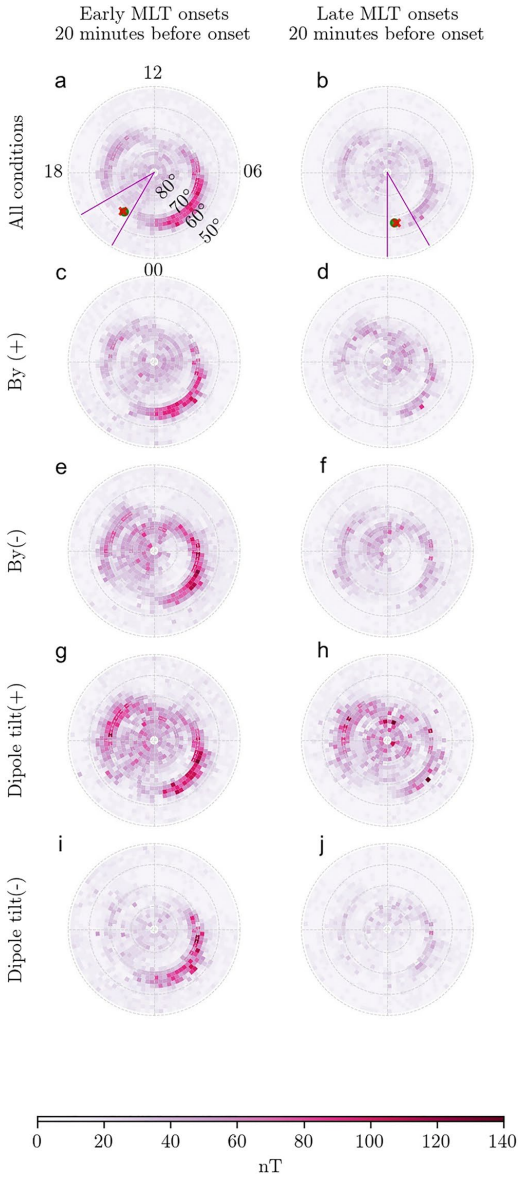

Figure 1. Maps of the magnitude of the average horizontal magnetic field perturbations (ground B) 20 min before the substorm onset. The left column shows onsets observed between 20 and 22 MLT (early) and the right column shows onsets observed between 24 and 02 MLT (late). Panels a and b show maps of early and late onsets based on all the available data. Panels c and d (e and f) show early and late onsets that occurred when IMF B_y was positive (negative). Panels g and h (i and j) show maps for positive (negative) dipole tilt angle. Each panel uses an equal-area grid with 2° MLat resolution.

coordinates with the baseline subtracted as described in Gjerloev (2012). The data is then converted to quasi-dipole coordinates following Laundal et al. (2016). Figure 1 shows maps of the magnitude of (ground B). The colors represent the median ground B perturbations magnitude 20 min before substorm onsets for different conditions of IMF B_y and dipole tilt angle.

The left column shows onsets observed between 20 and 22 MLT (hereafter "early onsets") and the right column shows onsets observed between 24 and 02 MLT (late onsets), as the distribution of the substorm onsets is centered around 23 MLT (Gérard et al., 2004; Liou & Newell, 2010). Figures 1a and 1b show the median magnetic field perturbations 20 min before early and late substorm onsets, respectively. The magenta lines are the boundaries of the onset locations. The red cross × is the location of the mean onset location while the green circle • is the median. The median MLT of the early (late) subset is 21.47 (0.54). We find that the magnitude of ground B is generally higher during the 20 min preceding early substorm onsets than during the 20 min preceding late substorm onsets.

The separation into early and late onsets biases the distributions of IMF B_y and dipole tilt angle since we know that these parameters influence the onset location. To ensure that this bias is not the reason for the different ground B magnitudes, we further separate the onsets by the sign of IMF B_y and dipole tilt angle. Panels (c–f) of Figure 1 show maps of ground B for early and late onsets with the different polarity of IMF B_y, and $|B_y| > 1$ nT. We used measurements of IMF B_y with a 1-min resolution provided from the OMNI data set, time shifted to the bow shock. We use the median during the 20 min before the substorm onset. For both polarities of IMF B_y, the magnitude of ground B for early onset substorms is higher than the magnitude for late-onset substorms. Panels (g–j) of Figure 1 show maps of ground B for substorms that occurred at times with different dipole tilt angle Ψ (Laundal & Richmond, 2017). For both signs of the dipole tilt angle, the magnitude of ground B is higher for early substorms than late substorms. These panels show that the bias in B_y and Ψ is not the reason for the different B magnitudes in the two columns.

Motivated by our results showing profound differences in the ionospheric state before early and late substorm onsets, we have examined the relationship between substorm onset MLT and four different parameters: The auroral lower (AL) index, the solar wind aberration angle, the dipole tilt angle, and IMF B_y. For all variables except for dipole tilt angle, we use the mean value during the 60 min before onset. Figures 2a–2d show the results of a regression analysis of MLT and each of these variables separately. In each panel, the regressor is divided into 10 bins with an equal number of observations, and the median onset MLT is shown in blue (red) for substorms observed in the northern (southern) hemisphere. The vertical bars represent the standard error of the median (see, e.g., Greene, 2003, page 878; not the standard deviation). The dashed lines represent regression models to be discussed in more detail below. Figure 2e shows the result of a multivariable regression analysis where all four parameters are combined and will be explained below. We have also examined the relationship between the substorm onset MLT and IMF B_z. The median IMF B_z for early and late MLT onsets is −1.8 and −1.5 nT, respectively. This result is consistent with Liou et al. (2001), who found that there is no clear relationship between IMF B_z and variations of the MLT of the substorm onsets. That IMF B_z is not strongly related to the onset MLT, while the AL index is, is counter-intuitive because the IMF B_z and AL are

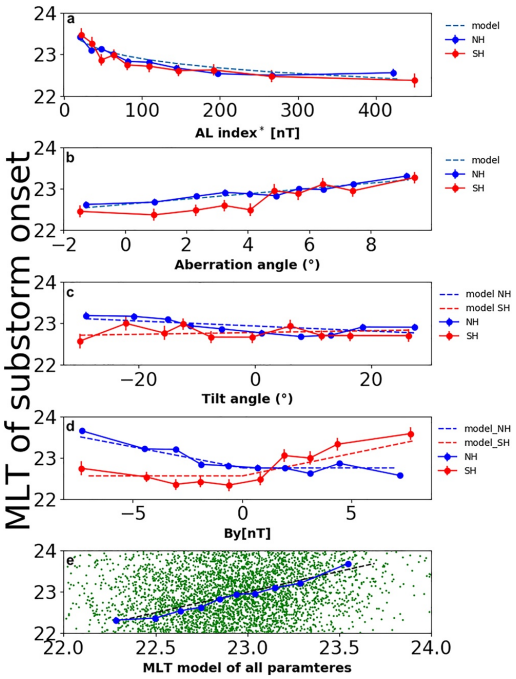

Figure 2. Panels (a–d) shows the relationship between the substorm onset MLT and the AL index, the aberration angle, the dipole tilt angle, and IMF B_y respectively, panel (e) shows the multivariable regression analysis with the four parameters. Each substorm onset from the combined lists is plotted against the model prediction as green dots. The black dashed line represents where the data would be in the ideal case that the model makes perfect predictions. Our model follows the dashed line closely.

correlated. However, the AL index is not a simple function of the simultaneous B_z, but also depends on the delayed response of the magnetotail to energy transfer from the solar wind to the magnetosphere (Laundal et al., 2020). Our results therefore indicate that the possible ionospheric influence on substorm onset location depends more on the time-delayed magnetotail component.

Figure 2a shows the relationship between the onset MLT and the AL index. The purpose of analyzing the variation between onset MLT and the AL index is to quantify the effect that is observed in Figure 1, that stronger magnetic field perturbations before a substorm are associated with earlier onset MLTs. The AL index measures the maximum strength of the westward electrojet from 12 magnetometers longitudinally distributed along the auroral oval, and is here taken as a proxy of geomagnetic activity. The x-axis of Figure 2a represents a modified AL, AL*, defined as max(AL) - AL, where max(AL) is the maximum value of AL = 7.85 nT. This ensures that AL* is always positive. We see from Figure 2a that the variation of substorm onset MLT as a function of AL is nonlinear. We therefore seek a regression model on the form $y = a - b\mathrm{AL}^{*\gamma}$, where y is the onset MLT and a, b, and γ are model parameters to be fitted. Since AL* is positive, y will be real for all γ. The model parameters are estimated using non-linear least squares, with all data points individually (not the median values). The resulting model parameters are a = 25.7 hr, b = 1.69 hr/nT, and γ = 0.1. The coefficient of determination (the square of the correlation coefficient) r^2 is 0.049, which means that the model explains about 4.9% of the variation of the substorm onset MLT, roughly the same as IMF B_y-based statistical models (see Østgaard et al., 2011, and below). In contrast to variation with IMF B_y, the variation with AL is in the same direction in both hemispheres.

Figure 2b shows the relationship between the aberration angle and the MLT of the substorm onset. The aberration angle α is the angle between the Sun-Earth line and the solar wind velocity as defined by (Hones et al., 1986). We calculate the aberration angle as $\alpha = \tan^{-1}(-V_y/V_x)$, where V_y is the solar wind velocity in the GSM y-direction. The V_y provided by OMNI is given in an inertial frame, but we have converted to an Earth fixed frame by adding Earth's orbital speed, 29.8 km/s. We expect that the onset MLT varies linearly with aberration angle, since the magnetosphere aligns with the solar wind velocity (a "windsock effect"). This is also supported by the medians in Figure 2b. We therefore seek a model on the form $y = a + b\alpha$. We estimated model parameters are a = 22.6 hr and b = 0.96, when the angle α is given in hours. The fact that b is so close to 1 is in agreement with the expected windsock effect. The coefficient of determination is 2.5%.

Figure 2c shows the relationship between the dipole tilt angle Ψ and the MLT of the substorm onset. We see that the onset MLT decreases (increases) with dipole tilt angle in the Northern (Southern) hemisphere. The figure indicates that the relationships are linear, so we seek models on the form $y_{n,s} = a_{n,s} + b_{n,s}\Psi$, where the subscripts refer to the Northern and Southern hemispheres. We find that $a_n(a_s)$ = 22.9(22.7) and $b_n(b_s)$ = − 0.006(0.002) hr/degree. In both cases, the models explain less than 1% of the substorm onset MLT variation. However, since the number of samples is so large, the probability that this would occur by chance is less than 10^{-8}. In the other regression models, the correlation is higher, and the p value is smaller.

Figure 2d shows the relationship between the IMF B_y component of the solar wind and the MLT of the substorm onset. Milan et al. (2010) suggested that for IMF B_y to impact the onset MLT, the polarity must be the same for a long time prior to the substorm onset. In our analysis, we used the mean of IMF B_y 1 hr before the substorm onset. We see that if IMF B_y is negative (positive), the substorm onsets tend to be observed at later (earlier) local times in the northern (southern) hemisphere. For the opposite sign, the variation is minimal. This is in agreement with the results by Østgaard et al. (2011). Because of this, we seek regression models of the form

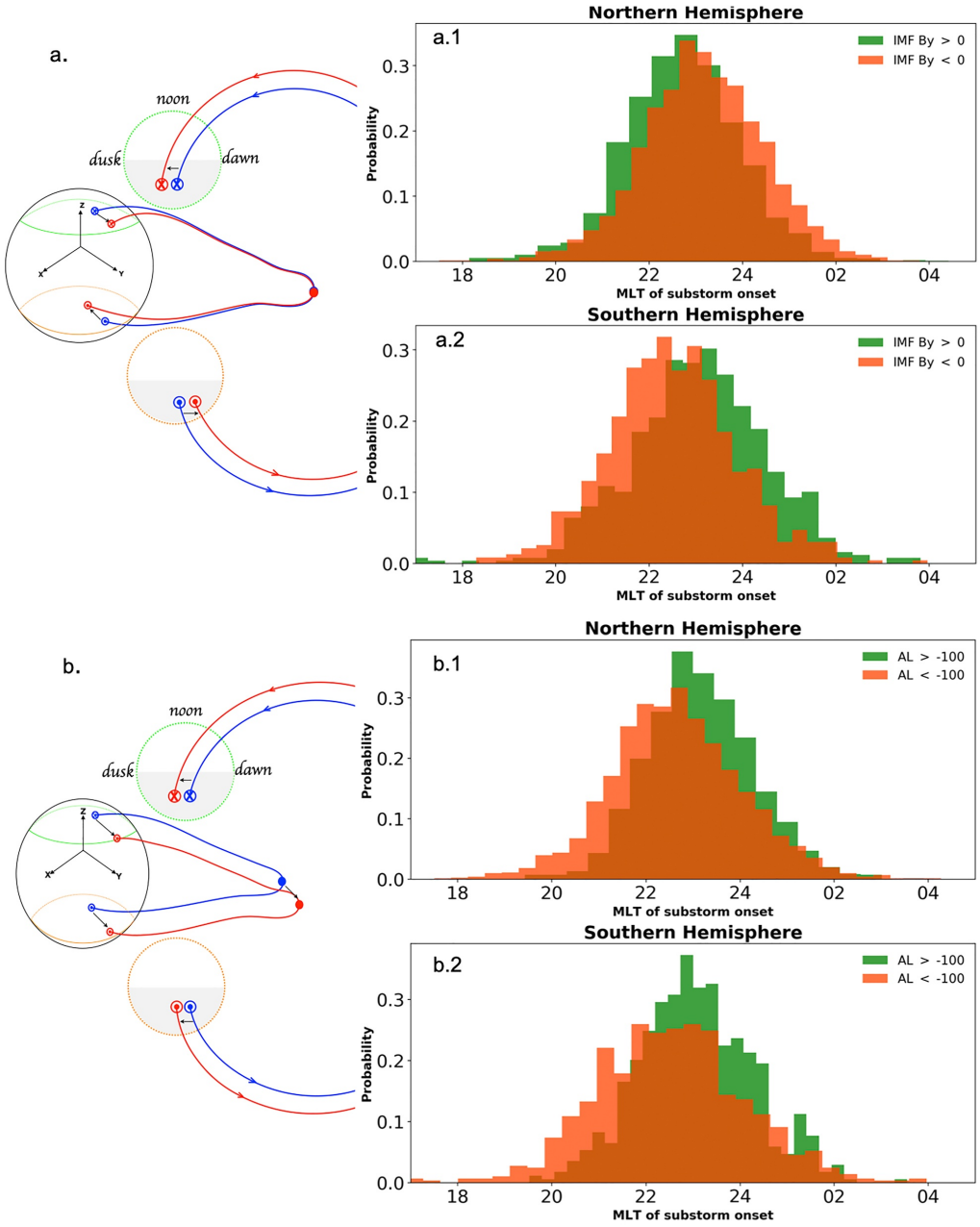

Figure 3.

$$y_n = \begin{cases} a_n + b_n B_y & \text{if } B_y < 0 \\ a_n & \text{if } B_y \geq 0, \end{cases} \quad (1)$$

and for the southern hemisphere,

$$y_s = \begin{cases} a_s & \text{if } B_y < 0 \\ a_s + b_s B_y & \text{if } B_y \geq 0, \end{cases} \quad (2)$$

We find that $a_n(a_s) = 22.75(22.55)$ h, and $b_n(b_s) = 0.11(-0.10)$ hr/nT. Both models explain about 4.5% of the variation in onset MLT.

Figure 2e shows the result of a multivariable regression analysis which includes all the above parameters. The multivariable model combines all the above model representations, and the model parameters are coestimated. In this model, we reverse the signs of B_y and dipole tilt angle Ψ for substorms observed in the Southern hemisphere. The resulting model is $y = 24.63 - 0.10B_y - 1.14AL^{*0.13} - 0.0035\Psi + 0.66\alpha$, where B_y and AL are given in nT, Ψ in degrees, and α in hours. Figure 2e shows each onset plotted against the model prediction as green dots. The dashed line represents where the data would be in the ideal case that the model makes perfect predictions. However, the model only captures 11.3% of the total variance of the MLT of the substorm onsets. The individual data points (green dots) are included in this panel to highlight the large degree of scatter. The standard deviation of the full onset MLT distribution is 1.3 hr, and several substorms also occur outside the bounds of this plot. In the panels above, only binned medians are shown, although the individual data points were used in the regression analyses. The blue dots in Figure 2e also represent binned medians, in 10 bins based on model prediction quantiles, and we see that they follow the dashed line closely. The standard error of the median is too small to be noticed.

3. Discussion and Summary

We have shown that substorm onsets tend to occur at earlier local times during geomagnetically active periods relative to substorm onsets during quiet periods. The regression analyses presented in Figures 2a and 2d show that the AL index before substorm onset is as strongly correlated with onset MLT as the IMF B_y, which has been reported in several earlier studies (Liou & Newell, 2010; Østgaard et al., 2011; Wang et al., 2007).

A key difference from the effect of IMF B_y is that the onset MLT dependence is the same in the two hemispheres with respect to AL. Since the effect of IMF B_y is opposite in the two hemispheres, and since it only explains about 5% of the observed variation in onset MLT, we interpret it as an effect of magnetic mapping. That is, IMF B_y does not influence the location of the substorm onset in the magnetotail, only how it maps to the ionosphere, where we see the auroral emissions. The IMF B_y induces a B_y component in the magnetosphere with the same sign (Tenfjord et al., 2015), which causes the observed substorm onsets to shift in opposite directions in the two hemispheres. This mapping effect is illustrated in Figure 3a. The blue magnetic field line is symmetric between the two hemispheres, and the red magnetic field line illustrates what happens when we introduce a positive B_y in the magnetotail: The footpoint shifts toward dusk in the northern hemisphere and toward dawn in the southern hemisphere. Figure 3a1 (a.2) shows the distribution of substorm onset locations observed in the northern (southern) hemisphere under B_y positive (green) and negative (orange) conditions. We calculated IMF B_y as the

Figure 3. Conceptual figure illustrating (a) the mapping effect and (b) the real shift in the magnetotail. In panels (a) and (b), the green (orange) circle represents the northern (southern) hemisphere's high latitude ionosphere, the blue line is a magnetic field line to be shifted toward either dawn or dusk, appearing as the red line after the shift. The shift is in opposite direction between the northern and southern hemispheres in (a) and in the same direction in (b) Panels (a1) and (a2) represent the distributions of the MLT of substorm onsets in Northern and Southern hemisphere, respectively, the panels show that the substorm onset MLT distribution observed in the northern (southern) hemisphere with positive IMF B_y shifts toward earlier (later) MLT. Panels (b1) and (b2) represent the distributions of the MLT of substorm onsets in Northern and Southern hemisphere, respectively. The panels show that the substorm onset MLT observed in both northern and southern hemispheres shift toward earlier local time in both hemispheres for increased AL.

mean during 1 hr before the substorm onset as used in the linear regression analysis above. We see that the effect is in the opposite direction in the two hemispheres.

Figure 3b illustrates our interpretation of the onset MLT dependence on the AL index: Since the shift is in the same direction in both hemispheres, it is presumably not an effect of mapping, as with IMF B_y. Instead of a mapping effect, there is a real shift of substorm onset location in the magnetotail toward dusk when geomagnetic activity increases. The blue magnetic field line in Figure 3b represents a quiet time situation, and the red magnetic field line represents active times. Figures 3b1 and 3b2 show the distribution of substorm onset locations observed in the northern hemisphere and the southern hemisphere respectively for high (green) and low (orange) activity, quantified in terms of the AL index before the substorm onset. We see that the effect is in the same direction in the two hemispheres.

Two different mechanisms have been proposed to explain dawn-dusk asymmetries in nightside activity: (a) A duskward shift of the plasma convection in the ionosphere due to conductance gradients and associated influence on the magnetotail (Lotko et al., 2014), and (b) a duskward displacement of the tail reconnection region due to Hall effects (Lu et al., 2016, 2018). The two mechanisms are not mutually exclusive, and both may be relevant to understand our observations of an AL control on onset MLT. However, the ionospheric conductance effect is presumably more directly related to the AL index than the magnetotail Hall effect. Considering the ionospheric Ohm's law, the AL index and conductance are proportional; but the conductance can be high even if the magnetotail current sheet is not thin, and vice versa. The ionospheric conductance effect on global magnetospheric dynamics was investigated in detail by Lotko et al. (2014). They used a magnetohydrodynamic simulation of the magnetosphere, with an electrostatic coupling to the ionosphere. They performed three simulation runs using the same solar wind conditions, but three different high-latitude distributions of ionospheric conductance: First, a uniform ionospheric conductance produced symmetric magnetotail activity with respect to the Sun-Earth line. Second, a realistic, empirical distribution with enhanced Hall conductance in the auroral oval produced magnetotail activity shifted toward dusk. Third, an unrealistic distribution of artificially depressed Hall conductance in the auroral oval produced magnetotail activity shifted toward dawn. These simulations clearly illustrate that ionospheric feedback can impact magnetospheric dynamics, and in particular magnetotail reconnection. If, as suggested by Angelopoulos et al. (2008), substorms are triggered by tail reconnection, it is likely that the effect studied by Lotko et al. (2014) and Zhang et al. (2012) may influence the location of the substorm onset and the subsequent expansion.

Wolf (1970) and Atkinson and Hutchison (1978) showed that the conductance gradient associated with the sunlight terminator can imply a clockwise rotation of the ionospheric convection pattern. This rotation could be an additional contributing factor in the duskward shift of magnetospheric activity. However, unlike the auroral gradient effect studied by Lotko et al. (2014), the terminator gradient effect is not expected to change with increasing geomagnetic activity.

Earlier studies, for example, Rostoker (1991) have reported that consecutive auroral brightenings tend to appear at progressively earlier local times. This could be a manifestation of the same mechanism(s) responsible for the observed relationship between the substorm onset MLT and the AL index discussed in this study. Kiehas et al. (2018) related observed duskward shift in magnetotail plasma flow to the high geomagnetic activity of high AL index. They suggested that the near-Earth reconnection is favorably located at the dusk sector as suggested by Lotko et al. (2014), Lu et al. (2016, 2018), and Zhang et al. (2012).

The ionospheric effect observed in the simulations reported by Lotko et al. (2014) relies on electrostatic models to represent the magnetosphere-ionosphere coupling. In reality, this coupling is not electrostatic, and an electrostatic model cannot explain *how* ionospheric feedback causes the magnetospheric activity to shift toward dusk. Determining the process by which ionospheric feedback regulates magnetospheric activity requires solving the equations that describe conservation of mass and momentum for ions and electrons moving through the neutral fluid, as they respond to electromagnetic fields that obey Maxwell's equations (e.g., Dreher, 1997).

Even though we have shown that the AL index is as useful in predictions of substorm onset MLT as IMF B_y, the explanatory power of our regression models (Figure 2) are all very low. A model that combines IMF B_y, the AL index, the aberration angle, and the dipole tilt angle explains about 11% of the observed variation in substorm onset MLT. The timing and location of substorm onsets therefore remain highly unpredictable.

Data Availability Statement

Magnetometer data can be downloaded directly from https://supermag.jhuapl.edu/mag where you need to specify the year to download. In our case, we used the years between 1996 and 2005. Solar wind data can be downloaded from https://cdaweb.gsfc.nasa.gov/sp_phys/data/omni/hro_1min/.

Acknowledgments

This study was supported by the Research Council of Norway/CoE under contracts 223252/F50 and 300844/F50, and by the Trond Mohn Foundation. For the ground magnetometer data the authors gratefully acknowledge: INTERMAGNET, Alan Thomson; CARISMA, PI Ian Mann; CANMOS, Geomagnetism Unit of the Geological Survey of Canada; The S-RAMP Database, PI K. Yumoto and Dr. K. Shiokawa; The SPIDR database; AARI, PI Oleg Troshichev; The MACCS program, PI M. Engebretson; GIMA; MEASURE, UCLA IGPP and Florida Institute of Technology; SAMBA, PI Eftyhia Zesta; 210 Chain, PI K. Yumoto; SAMNET, PI Farideh Honary; IMAGE, PI Liisa Juusola; Finnish Meteorological Institute, PI Liisa Juusola; Sodankylä Geophysical Observatory, PI Tero Raita; UiT the Arctic University of Norway, Tromsø Geophysical Observatory, PI Magnar G. Johnsen; GFZ German Research Centre For Geosciences, PI Jürgen Matzka; Institute of Geophysics, Polish Academy of Sciences, PI Anne Neska and Jan Reda; Polar Geophysical Institute, PI Alexander Yahnin and Yarolav Sakharov; Geological Survey of Sweden, PI Gerhard Schwarz; Swedish Institute of Space Physics, PI Masatoshi Yamauchi; AUTUMN, PI Martin Connors; DTU Space, Thom Edwards and PI Anna Willer; South Pole and McMurdo Magnetometer, PI's Louis J. Lanzarotti and Alan T. Weatherwax; ICESTAR; RAPIDMAG; British Artarctic Survey; McMac, PI Dr. Peter Chi; BGS, PI Dr. Susan Macmillan; Pushkov Institute of Terrestrial Magnetism, Ionosphere and Radio Wave Propagation (IZMIRAN); MFGI, PI B. Heilig; Institute of Geophysics, Polish Academy of Sciences, PI Anne Neska and Jan Reda; University of L'Aquila, PI M. Vellante; BCMT, V. Lesur and A. Chambodut; Data obtained in cooperation with Geoscience Australia, PI Andrew Lewis; AALPIP, co-PIs Bob Clauer and Michael Hartinger; MagStar, PI Jennifer Gannon; SuperMAG, PI Jesper W. Gjerloev; Data obtained in cooperation with the Australian Bureau of Meteorology, PI Richard Marshall. The authors acknowledge as well the use of NASA/GSFC's Space Physics Data Facility's OMNIWeb service, and OMNI data.

References

Akasofu, S. I. (1964). The development of the auroral substorm. *Planetary and Space Science*, *12*(4), 273–282. https://doi.org/10.1016/0032-0633(64)90151-5

Angelopoulos, V., Kennel, C. F., Coroniti, F. V., Pellat, R., Kivelson, M. G., Walker, R. J., et al. (1994). Statistical characteristics of bursty bulk flow events. *Journal of Geophysical Research: Space Physics*, *99*(A11), 21257–21280. https://doi.org/10.1029/94JA01263

Angelopoulos, V., McFadden, J. P., Larson, D., Carlson, C. W., Mende, S. B., Frey, H., et al. (2008). Tail reconnection triggering substorm onset. *Science*, *321*(5891), 931–935. https://doi.org/10.1126/science.1160495

Atkinson, G., & Hutchison, D. (1978). Effect of the day night ionospheric conductivity gradient on polar cap convective flow. *Journal of Geophysical Research*, *83*, 725–729. https://doi.org/10.1029/ja083ia02p00725

Dreher, J. (1997). On the self-consistent description of dynamic magnetosphere-ionosphere coupling phenomena with resolved ionosphere. *Journal of Geophysical Research*, *102*, 85–94. https://doi.org/10.1029/96JA02800

Frey, H. U., Mende, S. B., Angelopoulos, V., & Donovan, E. F. (2004). Substorm onset observations by IMAGE-FUV. *Journal of Geophysical Research: Space Physics*, *109*(A10), 2. https://doi.org/10.1029/2004JA010607

Gérard, J. C., Hubert, B., Grard, A., Meurant, M., & Mende, S. B. (2004). Solar wind control of auroral substorm onset locations observed with the IMAGE-FUV imagers. *Journal of Geophysical Research: Space Physics*, *109*(A3), 1–13. https://doi.org/10.1029/2003JA010129

Gjerloev, J. W. (2012). The SuperMAG data processing technique. *Journal of Geophysical Research: Space Physics*, *117*(9), 1–19. https://doi.org/10.1029/2012JA017683

Greene, W. H. (2003). *Economic Analysis* (5th ed., pp. 1–1054). Pearson Education, Inc.

Grocott, A., Laurens, H. J., & Wild, J. A. (2017). Nightside ionospheric convection asymmetries during the early substorm expansion phase: Relationship to onset local time. *Geophysical Research Letters*, *44*(23), 11696–11705. https://doi.org/10.1002/2017GL075763

Hones, E. W., Zwickl, R. D., Fritz, T. A., & Bame, S. J. (1986). Structural and dynamical aspects of the distant magnetotail determined from ISEE-3 plasma measurements. *Planetary and Space Science*, *34*(10), 889–901. https://doi.org/10.1016/0032-0633(86)90001-2

Kepko, L., McPherron, R. L., Amm, O., Apatenkov, S., Baumjohann, W., Birn, J., et al. (2015). Substorm current wedge revisited. *Space Science Reviews*, *190*, 1–46. https://doi.org/10.1007/s11214-014-0124-9

Kiehas, S. A., Runov, A., Angelopolos, V., Hietala, H., & Korovinksiy, D. (2018). Magnetotail fast flow occurrence rate and dawn-dusk asymmetry at X_{GSM} -60 R_E. *Journal of Geophysical Research: Space Physics*, *123*(3), 1767–1778. https://doi.org/10.1002/2017JA024776

Laundal, K. M., Gjerloev, J. W., Østgaard, N., Reistad, J. P., Haaland, S., Snekvik, K., et al. (2016). The impact of sunlight on high-latitude equivalent currents. *Journal of Geophysical Research: Space Physics*, *121*(3), 2715–2726. https://doi.org/10.1002/2015JA022236

Laundal, K.-M., Reistad, J.-P., Hatch, S.-M., Moretto, T., Ohma, A., Østgaard, N., et al. (2020). Time-scale dependence of solar wind-based regression models of ionospheric electrodynamics. *Scientific reports*, *10*. https://doi.org/10.1038/s41598-020-73532-z

Laundal, K. M., & Richmond, A. D. (2017). Magnetic coordinate systems. *Space Science Reviews*, *206*(1–4), 27–59. https://doi.org/10.1007/s11214-016-0275-y

Liou, K. (2010). Polar Ultraviolet Imager observation of auroral breakup. *Journal of Geophysical Research: Space Physics*, *115*(12), 1–7. https://doi.org/10.1029/2010JA015578

Liou, K., & Newell, P. T. (2010). On the azimuthal location of auroral breakup: Hemispheric asymmetry. *Geophysical Research Letters*, *37*(23), 1–5. https://doi.org/10.1029/2010GL045537

Liou, K., Newell, P. T., Sibeck, D. G., Meng, C. I., Brittnacher, M., & Parks, G. (2001). Observation of IMF and seasonal effects in the location of auroral substorm onset. *Journal of Geophysical Research: Space Physics*, *106*(4), 5799–5810. https://doi.org/10.1029/2000ja003001

Lotko, W., Smith, R. H., Zhang, B., Ouellette, J. E., Brambles, O. J., & Lyon, J. G. (2014). Ionospheric control of magnetotail reconnection. *Science*, *345*(6193), 184–187. https://doi.org/10.1126/science.1252907

Lui, A. T. Y. (1991). A synthesis of magnetospheric substorm models. *Journal of Geophysical Research: Space Physics*, *96*(A2), 1849–1856. https://doi.org/10.1029/90JA02430

Lu, S., Lin, Y., Angelopoulos, V., Artemyev, A. V., Pritchett, P. L., Lu, Q., & Wang, X. Y. (2016). Hall effect control of magnetotail dawn-dusk asymmetry: A three-dimensional global hybrid simulation. *Journal of Geophysical Research: Space Physics*, *121*(12), 11882–11895. https://doi.org/10.1002/2016JA023325

Lu, S., Pritchett, P. L., Angelopoulos, V., & Artemyev, A. V. (2018). Formation of dawn-dusk asymmetry in earth's magnetotail thin current sheet: A three-dimensional particle-in-cell simulation. *Journal of Geophysical Research: Space Physics*, *123*(4), 2801–2814. https://doi.org/10.1002/2017JA025095

McPherron, R. L. (1970). Growth phase of magnetospheric substorms. *Journal of Geophysical Research*, *75*(28), 5592–5599. https://doi.org/10.1029/ja075i028p05592

McPherron, R. L., & Chu, X. (2016). Relation of the auroral substorm to the substorm current wedge. *Geoscience Letters*, *3*(1). https://doi.org/10.1186/s40562-016-0044-5

Mende, S. B., Carlson, C. W., Frey, H. U., Peticolas, L. M., & Østgaard, N. (2003). FAST and IMAGE-FUV observations of a substorm onset. *Journal of Geophysical Research: Space Physics*, *108*(A9). https://doi.org/10.1029/2002JA009787

Milan, S. E., Grocott, A., & Hubert, B. (2010). A superposed epoch analysis of auroral evolution during substorms: Local time of onset region. *Journal of Geophysical Research: Space Physics*, *115*(10), 1–9. https://doi.org/10.1029/2010JA015663

Milan, S. E., Hutchinson, J., Boakes, P. D., & Hubert, B. (2009). Influences on the radius of the auroral oval. *Annales Geophysicae*, *27*(7), 2913–2924. Retrieved from https://angeo.copernicus.org/articles/27/2913/2009/

Østgaard, N., Laundal, K. M., Juusola, L., Åsnes, A., Håland, S. E., & Weygand, J. M. (2011). Interhemispherical asymmetry of substorm onset locations and the interplanetary magnetic field. *Geophysical Research Letters*, *38*(8), 1–5. https://doi.org/10.1029/2011GL046767

Østgaard, N., Mende, S., Frey, H., Immel, T., Frank, L., Sigwarth, J., et al. (2004). Interplanetary magnetic field control of the location substorm onset and auroral features in the conjugate hemisphere. *Journal of Geophysical Research*, *109*. https://doi.org/10.1029/2003JA010370

Østgaard, N., Tsyganenko, N., Mende, S., Frey, H., Immel, T., Fillingim, M., et al. (2005). Observations and model predictions of substorm auroral asymmetries in the conjugate hemispheres. *Geophysical Research Letters*, *32*. https://doi.org/10.1029/2004GL022166

Rostoker, G. (1991). Some observational constraints for substorm models. In *Magnetospheric substorms* (pp. 61–72). American Geophysical Union (AGU). https://doi.org/10.1029/GM064p0061

Tenfjord, P., Østgaard, N., Snekvik, K., Laundal, K. M., Reistad, J. P., Haaland, S., et al. (2015). How the IMF by induces a by component in the closed magnetosphere and how it leads to asymmetric currents and convection patterns in the two hemispheres. *Journal of Geophysical Research - A: Space Physics*, *120*(11), 9368–9384. https://doi.org/10.1002/2015JA021579

Tsyganenko, N. A. (1998). Modeling of twisted/warped magnetospheric configurations using the general deformation method. *Journal of Geophysical Research: Space Physics*, *103*(A10), 23551–23563. https://doi.org/10.1029/98JA02292

Wang, H., Lühr, H., Ma, S. Y., & Frey, H. U. (2007). Interhemispheric comparison of average substorm onset locations: Evidence for deviation from conjugacy. *Annales Geophysicae*, *25*(4), 989–999. https://doi.org/10.5194/angeo-25-989-2007

Wolf, R. A. (1970). Effects of ionospheric conductivity on convective flow of plasma in the magnetosphere. *Journal of Geophysical Research*, *75*(25), 4677–4698. https://doi.org/10.1029/JA075i025p04677

Zhang, B., Lotko, W., Brambles, O., Damiano, P., Wiltberger, M., & Lyon, J. (2012). Magnetotail origins of auroral alfvénic power. *Journal of Geophysical Research: Space Physics*, *117*(A9). https://doi.org/10.1029/2012JA017680

Paper II

Substorm Impact on Dayside Ionospheric Currents.

Elhawary, R. and Laundal, K. M. and Reistad, J. P. and Madelaire, M. and Ohma, A.
Geophysical Research Letters, **50/e2023GL104800** (2023)

AGU ADVANCING EARTH AND SPACE SCIENCES

Geophysical Research Letters

RESEARCH LETTER
10.1029/2023GL104800

Substorm Impact on Dayside Ionospheric Currents

R. Elhawary[1], K. M. Laundal[1], J. P. Reistad[1], M. Madelaire[1], and A. Ohma[1]

[1]Birkeland Centre for Space Science, Department for Physics and Technology, University of Bergen, Bergen, Norway

Key Points:

- Analyses of ground magnetometer data from substorms during northward Interplanetary Magnetic Field (IMF) show that substorms impact the NBZ dayside ionospheric currents
- During substorms under northward IMF conditions, lobe cells are unusually weak before onset and become more distinct after
- We suggest possible mechanisms by which magnetotail dynamics can influence dayside ionospheric currents

Supporting Information:

Supporting Information may be found in the online version of this article.

Correspondence to:

R. Elhawary,
reham.elhawary@uib.no

Citation:

Elhawary, R., Laundal, K. M., Reistad, J. P., Madelaire, M., & Ohma, A. (2023). Substorm impact on dayside ionospheric currents. *Geophysical Research Letters*, *50*, e2023GL104800. https://doi.org/10.1029/2023GL104800

Received 1 JUN 2023
Accepted 5 JUL 2023

Author Contributions:

Conceptualization: R. Elhawary, K. M. Laundal, J. P. Reistad
Formal analysis: R. Elhawary
Investigation: R. Elhawary, A. Ohma
Methodology: R. Elhawary
Software: M. Madelaire
Supervision: K. M. Laundal, J. P. Reistad
Validation: R. Elhawary
Writing – original draft: R. Elhawary
Writing – review & editing: R. Elhawary, K. M. Laundal, J. P. Reistad, M. Madelaire, A. Ohma

Abstract Ionospheric dayside dynamics is strongly controlled by the interaction between the Interplanetary Magnetic Field (IMF) and the Earth's magnetic field near the dayside magnetopause, while nightside ionospheric dynamics depends mainly on magnetotail activity. However, we know little about the influence of magnetotail activity on the dayside ionospheric dynamics. We investigate this by performing superposed epoch analyses of ground magnetic field data for substorms occurring during northward IMF. In such substorms, dayside reconnection is minimized, allowing us to separate the effects of the magnetotail activity on the dayside current system. We find that as nightside activity elevates, the dayside ionospheric current elevates. Our analyses indicate that the lobe cells are less distinct before onset than during non-substorm northward IMF conditions. They become more pronounced after onset, possibly due to magnetospheric reconfiguration or a remote effect of the nightside current. We discuss possible mechanisms that may explain our observations.

Plain Language Summary Aurora in the high latitude upper atmosphere is a major observable illustration of events occurring in the nightside of the Earth's magnetosphere called substorms. Substorms increase the electric current of the upper atmosphere at high latitudes. The increment lasts for tens of minutes before it decays. The impact of substorms on the dayside current system is not known. We study substorms during certain conditions, and we find that the dayside currents also tend to increase with substorms. We discuss potential explanations of that influence on the dayside. Our findings help us understand the origins of the dynamics of the upper atmosphere.

1. Introduction

The interaction between the Interplanetary Magnetic Field (IMF) and the terrestrial magnetic field through magnetic reconnection is the primary driver of magnetosphere dynamics. During southward IMF, the Dungey cycle explains the ionospheric convection pattern in terms of dayside magnetic reconnection between the IMF and Earth's magnetosphere near the dayside magnetopause. Dayside reconnection leads to the opening of magnetic field lines and the expansion of the polar cap. The opened field lines stretch toward the nightside magnetotail equatorial plane. Eventually, the built-up pressure triggers nightside reconnection, causing the contraction of the polar cap as open field lines close. This dynamic process is known as the Expanding/Contracting Polar Cap paradigm (ECPC) (Cowley & Lockwood, 1992).

Although empirical models such as the Average Magnetic field and Polar current System model (AMPS) (Laundal et al., 2018) and the Weimer electric potential model (Weimer, 2005) provide insights into ionospheric dynamics in terms of IMF, their ability to capture the less predictable factors controlling nightside reconnection is limited. Previous studies (Grocott et al., 2002, 2017; Provan et al., 2004) have shown that substorms can dominate over convection driven by dayside reconnection. Additionally, there is evidence that dayside dynamics can influence nightside ionospheric convection via wave propagation mechanisms (Snekvik et al., 2017). While the impact of substorms on the nightside current system is known, the influence of substorms on the dayside current system requires more investigation. In this study, our primary objective is to investigate the influence of substorms on dayside ionospheric currents.

Substorms are a critical process in which the magnetosphere releases magnetic flux by reconnection in the neutral sheet of the magnetotail (Milan et al., 2010). During substorms, especially during southward IMF, both dayside and nightside can be highly dynamic. In-situ measurements of the solar wind and IMF makes it possible to quantify the dayside reconnection rate (Milan et al., 2012), but there is no similar proxy for nightside reconnection. This makes differentiating between the contribution of nightside and dayside reconnection on ionospheric dynamics very challenging to achieve. However, during northward IMF, the dayside experiences a minimal opening of flux and is only affected by IMF in a localized region in the dayside polar cap, while the nightside can

undergo magnetotail reconnection during substorms. Therefore, our study focuses on understanding the influence of substorms on dayside ionospheric convection during northward IMF.

During northward IMF, an intense and localized current system is established in the dayside polar cap (Iijima, 1984; Laundal et al., 2018; Milan, 2015). This current is referred to as the northward-directed B_z (NBZ), or lobe cells, due to its relation to lobe reconnection. We use the two terms interchangeably for the rest of the paper. The NBZ current system consists of two cells; a positive, upward-directed current in the pre-noon sector and a negative, downward-directed current in the post-noon sector, located poleward of the dayside region-1 current. The strength of the lobe cells reflects the reverse dayside convection pattern modulated by ionospheric conductance (Reistad et al., 2019).

In this study, we present a statistical analysis of the ionospheric current during northward IMF substorms by examining ground magnetic field perturbations above 60° latitude. The analysis is based on three substorm lists. Only substorms preceded by 45 min and followed by 20 min of northward IMF are considered in order to isolate substorm-induced dayside activity. Using each list, we perform a superposed epoch analysis using a spherical harmonic (SH) representation of the magnetic field. In Section 2, we discuss substorm lists and data analysis in detail. In Section 3, our findings demonstrate a dayside ionospheric response to the substorm onset. In Section 4, we discuss possible explanations for the influence of nightside dynamics on the dayside ionospheric current.

2. Data and Method

To investigate the ionospheric currents in the dayside during substorms with northward IMF, we used three different substorm lists to ensure that observed trends are not a signature of a specific substorm list. (a) The first list, FL: uses global ultraviolet (UV) imaging to identify substorm onsets. This list consists of two lists provided through Frey et al. (2004) and Liou (2010). (b) NG: is based on the SuperMAG AL (SML) index, which is a ground-based magnetometer index as described in detail in previous works (Newell & Gjerloev, 2011) between years 1990 and 2019. (c) SOPHIE S75 is based on SuperMAG AL (SML) index and uses a different algorithm to identify the substorm phases and the substorm onsets compared to the NG list, as discussed in Forsyth et al. (2015), between years 1990 and 2019.

While it is well-known that substorms are more common under southward IMF conditions, we limit our investigation to northward IMF substorms (Lee, Choi, et al., 2010; Lee, Ohtani, & Lee, 2010; Miyashita et al., 2011; Peng et al., 2013). We obtained solar wind measurements with a 1-min resolution from the OMNI data set which is propagated to represent the solar wind and IMF conditions at the bow shock. The solar wind data is presented in Geocentric Solar Magnetic coordinates. We defined a northward IMF substorm using a 65-min interval of northward IMF from 45 min prior to substorm onset to 20 min after onset. We permitted no data gaps during this interval, but allowed at most a total of 5 min of deviation from northward IMF throughout the interval. We chose the northward IMF 45-min criterion prior to onset to account for uncertainties in the solar wind time shift and to allow for the system reconfiguration due to the northward IMF turning as discussed in Yu and Ridley (2009), while a sufficient number of substorms remain for statistical analysis.

We limited the NG and S75 substorm lists to include only those events that were detected first by a magnetometer on the nightside (i.e., with magnetic local time between 18 and 06). As a slight positive bias in IMF B_y was observed in the substorm lists defined using ground-based indices (Ohma et al., 2021), we imposed an additional constraint that required the absolute value of the IMF clock angle, $\theta_{ca} = \arctan2(B_y, B_z)$, to be $<45°$ from 45 min before substorm onset until 20 min after onset, allowing for a deviation of 5 min and no data gaps. However, the requirements were relaxed for the FL list in order to have sufficient events for a superposed epoch analysis. We implemented $|\theta_{ca}| < 70°$ restriction to minimize the potential effects of closed field line reconnection, as previous studies suggested its occurrence on the dayside equatorward of the cusp at absolute clock angles greater than 70° (Freeman et al., 1993; Senior et al., 2002). The OMNI data set also provided the AL index, which we used as another criterion for the S75 list, with a minimum AL index less than −100 nT to avoid false identification of substorms. With these criteria, the NG list had 236 events, S75 had 164 events, and FL had 143 events.

Although we used a large time window (−45, 20) min to capture the ionospheric response to the northward turning, it is possible that the response could be delayed due to the associated reconfiguration time (e.g., Snekvik et al., 2017; Tenfjord et al., 2017). To distinguish between a delayed influence of the IMF turning and the impact of substorms on the dayside ionospheric current, we applied the same stable northward IMF criterion to a control

group (CG) of non-substorm events. Specifically, we randomly selected 7,000 reference minutes between 1996 and 2005 and applied the same northward IMF and clock angle criteria, resulting in a CG list of 384 events for analysis.

In this study, we analyzed ground magnetic field perturbations from the SuperMAG database to investigate ionospheric currents in the high-latitude (≥60°) northern hemisphere. We used 1-min resolution magnetometer data with the baseline subtracted provided through SuperMAG (Gjerloev, 2012) and converted the magnetic field perturbations to quasi-dipole coordinates following Laundal et al. (2016) which we used in the SH representation.

To study the ionospheric currents based on the ground observations of magnetic field perturbations, we used a mathematical representation called the equivalent horizontal ionospheric current (EHIC) as discussed in Madelaire et al. (2022). The EHIC is related to the equivalent current function Ψ through

$$\vec{j}_{eq} = \hat{r} \times \nabla \Psi \tag{1}$$

where $\hat{r}$ is a unit vector in the upward direction. We calculated Ψ using SH coefficients that describe the modeled field from external sources. According to the Fukushima theorem (Fukushima, 1969), the EHIC will be the divergence-free part of the actual horizontal current field, assuming radial magnetic field lines and uniform conductance. Following for example, Laundal et al. (2016), Ψ is given by

$$\Psi = \frac{a}{\mu_0} \sum_{n,m} \frac{2n+1}{n+1} \left(\frac{a+h}{a} \right)^n P_n^m(\cos(\theta))[q_n^m \cos(m\phi) + s_n^m \sin(m\phi)] \tag{2}$$

where h is the height set at 110 km where the current is evaluated, $a = 6371.2$ km is the radius of the Earth, μ_0 is the permeability constant, ϕ is the magnetic local time converted to radians, and θ is the quasi-dipole colatitude. $P_n^m(\cos(\theta))$ are the Schmidt semi-normalized associated Legendre functions of degree n, and order m, and (q_n^m, s_n^m) are the SH coefficients describing the modeled field from external sources. We also used the Equivalent Field-Aligned Current (EFAC) as a visualization tool to track the evolution of the dayside and nightside current systems. The EFAC (Madelaire et al., 2022) is inferred from the ground assuming a uniform conductance and a ratio of 1 between Hall and Pedersen conductances. EFAC can be defined as the curl of EHIC, where EHIC is clockwise in regions with positive EFAC and anti-clockwise with negative EFAC.

To solve for the model parameters (q_n^m and s_n^m), we use iterative re-weighted least-squares with Huber weights (Madelaire et al., 2022). This reduces the influence of outliers on the final solution, which can be particularly useful in cases where the data contains a few extreme values that would otherwise skew the results (Huber, 1964). By reducing the impact of these outliers, Huber weights help ensure that the model's parameters are more representative of the data. To quantify the uncertainty in our model related to variations between events, we employed the bootstrap technique. This involves repeating the inversion process multiple times with randomly resampled substorm events. We repeated the inversion 50 times while allowing replacement using the same number of substorms. Additionally, we quantified the range of variation in the solar wind data and AL index for each substorm list using the 25th and 75th percentile of the super-posed epoch data for each list.

3. Observations

In Figures 1a and 1b, we compare the temporal evolution of the dayside dynamics between the non-substorm control group (CG) and the Newell and Gerloev (NG) substorms. The colored contours show upward (red) and downward (blue) EFACs, and the black contours show the EHIC. In Figure 1c we observe that all three IMF B_z quartiles are positive for the whole 2-hour interval, even though we applied the −45 to 20 min criterion on the IMF B_z for both CG (navy) and NG (yellow). Figure 1d shows the observed IMF B_y medians for both CG and NG, which are centered nearly around zero. In Figure 1e, we see that the AL index for the CG is almost constant during the analyzed interval of 2 hours, while a sharp change in the AL index of the NG list starts around the onset time shown in all quartiles, as well as the expected development during substorms (Baker et al., 1985; McPherron, 1995; McPherron & Manka, 1985).

Despite the IMF B_z being northward in both cases, there are notable differences between the two groups in the behavior of the dayside NBZ cells. We refer to the positive cell as the P-cell and the negative cell as the N-cell. Figure 1b shows that for the NG list, we observe an increase in the NBZ cells as well as a rise in the nightside

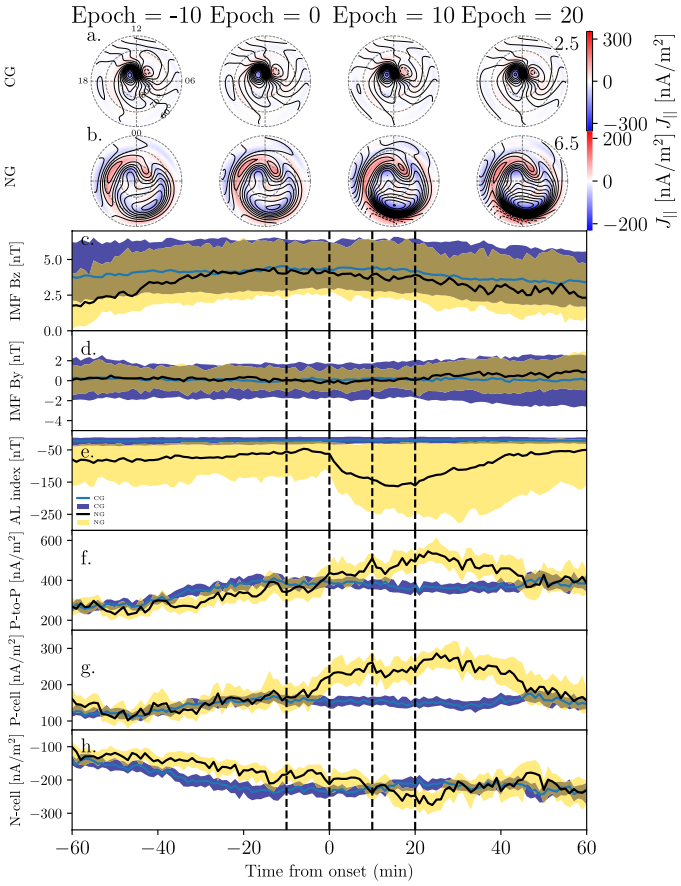

Figure 1. Comparison of the solar wind conditions and ionospheric currents between the CG and NG lists with a northward Interplanetary Magnetic Field (IMF). Panels (a) and (b) show maps of the equivalent horizontal ionospheric current (EHIC) and Equivalent Field-Aligned Current (EFAC), respectively, for the CG and NG lists. The direction of the current is clockwise in regions of downward EFAC and anti-clockwise in regions of upward EFAC. The numbers on the maps indicate the step size of Ψ in kA for CG and NG, respectively. Panels (c–h) present the IMF B_z (c), B_y (d), AL-index (e), the peak-to-peak value (f), the maximum of the P-cell (g), and the minimum of the N-cell (h) for the CG and NG lists. The blue and black lines indicate the median value for the CG and NG, respectively, and the navy and yellow shaded areas enclosed by the first and third quartiles for the CG and NG, respectively, it has been calculated through bootstrap in panels (f–h). The vertical dashed black markers correspond to the snapshots of the EHIC and EFAC maps shown in panels (a and b).

electrojet in response to the substorm onset. At epoch time −10, the NBZ cells for the NG list are weaker compared to the CG lobe cells shown in Figure 1a, and the magnitudes of the N-cell and P-cell increase as the nightside electrojets rise 10 and 20 min after the substorm onset, respectively. In order to investigate the possible influence of the solar wind velocity, density, dynamic pressure, and IMF B_x, we applied a superposed epoch analysis presented in the Supporting Information S1. None of these parameters show large variations.

In Figure 1f, we illustrate the contrasting behavior of the peak-to-peak value between the NG substorms and CG. The peak-to-peak value represents the difference between the maximum of the EFAC P-cell and the minimum of the N-cell. In the case of NG, this value increases a few minutes before substorm onset. However, there is no noticeable change for the CG. The P-cell maximum was calculated from a region between 75 and 90° latitude and 6 and 12 MLT, while the N-cell minimum was calculated from a sector between 75 and 90° latitude and 12 and 18 MLT.

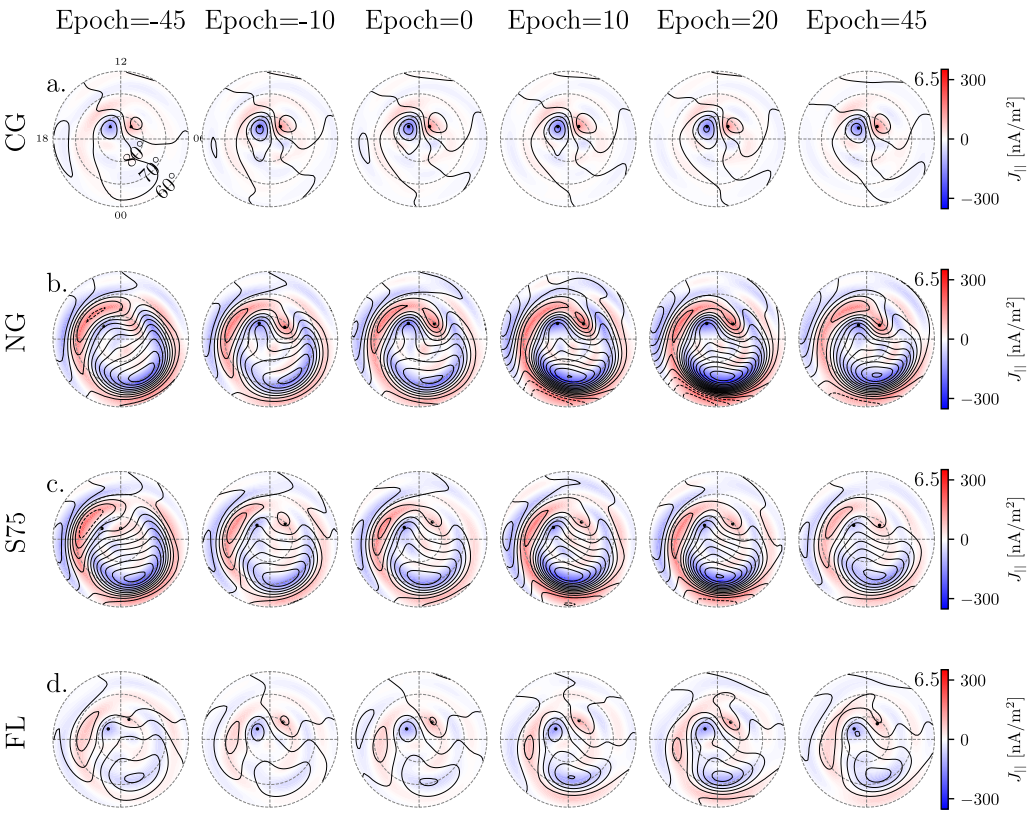

Figure 2. Maps of the Equivalent Field-Aligned Current (red/blue) and equivalent horizontal ionospheric current (black contours) for different lists under northward Interplanetary Magnetic Field conditions. Each map is oriented with magnetic noon up, midnight down, dawn on the right, and dusk on the left. Snapshots are shown at epoch times of −45, −10, 0, 10, 20, and 45 min relative to the onset time at 0. Panel (a) shows the maps for the CG, while Panels (b–d) show the results for the NG, S75, and FL lists, respectively. The numbers on the maps indicate the step size of Ψ in kA for each list.

Figure 1g shows that the P-cell magnitude for the NG list increases slightly earlier than the substorm onset, whereas, for the CG, the P-cell remains constant. Similarly, Figure 1h shows that the N-cell magnitude for the NG list increases also a few minutes prior to substorm onset, while there are no changes observed for the CG.

With the same formatting as Figures 1f–1h and 3d–3f show P-to-p, P-cell and N-cell for the CG, FL, S75, and NG lists with the lines representing the medians while the shaded areas represent the first and third quartiles.

To investigate whether the observed behavior is unique to the NG list, we analyzed two additional substorm lists (S75, FL) along with the CG. Figure 2 displays maps of the EFAC and EHIC at selected epoch times for all lists, while Figure 3 shows the temporal evolution of the IMF and geomagnetic response relative to substorm onset for each list. In Figure 2a, we observe a pronounced dayside NBZ current, while quiet levels of geomagnetic activity are observed at the nightside. All substorm lists at epoch time −45 in Figures 2b–2d show a lack of a pronounced dayside NBZ current. At epoch time −10, no noticeable change is observed for the substorm lists or the CG. However, after epoch time zero, we observe an increase in the magnitude of both the dayside P- and N-cells and the nightside EFAC and EHIC, as quantified in Figures 3c–3f. This increase is a clear response in the NG list, and a small but visible response in S75 and FL lists, although it occurs 6 min prior to onset, which we will discuss in the next section.

Figures 3d–3f shows that the magnitude of the peak-to-peak values, the maximum value of the EFAC P-cell, and the absolute value of the N-cell increase a few minutes before the onset of substorms as indicated by the thick

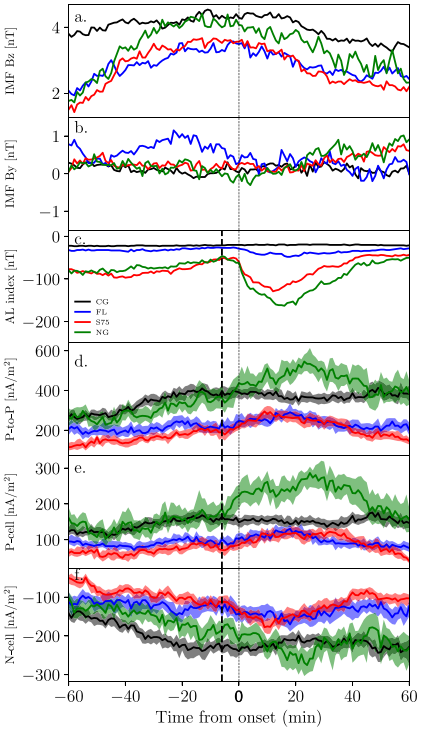

Figure 3. Comparison of solar wind conditions and ionospheric behavior for different substorm lists and a control group (CG). The panels display various parameters, with the median values represented by black (CG), blue (FL), red (S75), and green (NG) lines. The thin dashed line indicates the onset time. Panels (a and b) illustrate the solar wind Interplanetary Magnetic Field B_z and B_y conditions, respectively. Panel (c) shows the auroral lower index, while panel (d) presents the peak-to-peak values of the Equivalent Field-Aligned Current (EFAC) P- and N-cells. Panels (e and f) depict the maximum and minimum values of the EFAC P- and N-cells, respectively. The thick dashed line in panels (c–f) represents the initiation time of the dayside response, 6 min prior to the onset. The shaded areas in panels (d–f) indicate the first and third quartiles for all lists, following the same order as the median values.

dashed vertical line for all three substorm lists, while the AL index magnitude starts to increase with a little dip that increases rapidly starting on the onset. As the substorms progress, the magnitude of both the dayside and nightside current remains higher than before onset, as seen in Figures 2b–2d at epoch times 10 and 20. During the substorm recovery phase at epoch time 45, the nightside current and the dayside lobe cells gradually decay. Moreover, Figures 3d–3f demonstrates a gradual change in the dayside current for both the CG and the substorm lists from −45 to around −20, which may indicate a response to the IMF turning.

Figure 3 provides a comprehensive comparison of the solar wind and geomagnetic response to substorm onsets for both the control group and the three substorm lists. The median value of IMF B_z for the control group and the substorm lists is positive and remains constant during the two-hour interval, as shown in Figure 3a. In Figure 3b, the solar wind IMF B_y is centered around zero for the control group and two substorm lists, but it is slightly shifted toward positive values for the FL substorm list. The AL index drops significantly for the substorm lists, as seen in Figure 3c, with a sharper drop for substorms defined based on ground magnetometers than those defined based on global UV imaging (FL). The different substorm lists exhibit varying strengths of the AL index. The magnitude of the AL index is higher around epoch time 60 min prior to onset than around 45 min prior to onset when we imposed our criteria for the NG and the S75 lists which is expected during northward IMF. The AL index of the NG and S75 lists show stronger dips (below −100 nT) than the FL list. The magnitude of enhancements in NBZ currents following substorm onset also varies across the lists and is correlated with the strength of the AL index during the substorm, with NG and S75 exhibiting the clearest enhancements.

4. Discussion and Summary

We conducted a statistical analysis of ionospheric currents during substorms that occurred under northward IMF conditions. To isolate the substorm-induced dayside activity, we selected substorms with northward IMF for 45 min before onset to 20 min after onset. Since substorm onsets are defined differently based on indices from ground magnetometer measurements or based on satellite images, we studied the response for three different substorm lists using different definitions, two based on ground magnetometers (NG and S75), and one based on optical observations of the UV aurora (FL). For the S75 and NG substorm lists, we additionally restricted the clock angle to be between −45° and 45°. For the S75 list, we also restricted the minimum AL index to be less than −100 nT. Our analysis suggests that the dayside lobe cells respond to substorms, a few minutes prior to the reported onset times. The impact of nightside dynamics on dayside ionospheric currents is observed in all three different substorm lists. We found that the substorm list with the largest drop in the AL index (NG) resulted in the clearest response in the NBZ currents, while the substorm list with the weakest AL drop (FL) only indicated subtle changes in the NBZ currents associated with the onset.

There are various ways in which nightside activity could impact ionospheric electrodynamics on the dayside. One possible explanation suggested by Ohtani et al. (2021) is that FACs could respond to a remote effect of the nightside substorm current wedge, which might account for the dayside response during northward IMF substorms. However, the increase in EFAC lobe cells observed a few minutes prior to substorm onset, as seen in Figures 3c–3f from epoch −6 is inconsistent with the expected immediate response for such a remote effect, suggesting that other explanations should be explored.

Wave propagation is a fundamental process that communicates changes between the magnetosphere and the ionosphere. Different propagation times of the magnetohydrodynamic waves could be a reason for the observed response prior to substorm onset. Wave propagation through the magnetosphere can be either fast (compressive)

or slow (shear Alfvénic) waves. Magnetic reconnection events in the magnetotail generate compressive waves that can propagate along and across magnetic field lines, causing changes in plasma density and pressure. Chi et al. (2009) and Lui (2009) suggested that these fast waves can reach the ionosphere between 1.5 and 5 min after being generated in the magnetotail through the plasma sheet. However (Ferdousi & Raeder, 2016), argued that if the fast waves propagate through the lobes then the waves originating around $X \sim -10$ R_E can arrive almost simultaneously to the high latitude ionosphere and can be delayed for about 20–72 s when originating around $X \sim -20$ to -30 R_E. Snekvik et al. (2017) observed that these waves lead to an almost immediate global response to dayside reconnection. In our analysis, we observe an enhancement in the dayside NBZ current that starts 6 min prior to substorm onset, as shown in Figures 3d–3f, which may be attributed to the arrival of compressive waves and fast plasma flows (Ohtani, 2001; Ohtani et al., 1999; Sergeev et al., 1995). The change in the magnitude of the AL index at the time indicated by the thick dashed line 6 min prior to onset as shown in Figure 3c, may also be related to the compressive waves (Machida et al., 2009; Miyashita et al., 2009).

On the other hand, slow waves are also generated by the motion of the plasma in the magnetosphere and can cause changes in the ionospheric convection pattern and are associated with the establishment of the substorm current wedge. These waves arrive at the ionosphere during the substorm expansion phase after the compressive waves, with a maximum response time of 10–20 min (G. Lu et al., 2002). By this time, the remote effect discussed earlier could partly explain the preserved elevation in the NBZ cells throughout the expansion phase, as shown in Figures 3d–3f.

The observed increase in NBZ currents during northward IMF substorms may be attributed to changes in the lobe reconnection rate, which are influenced by variations in the magnetopause topology. The IMF B_z component strongly affects the degree of flaring of the magnetopause (Shue et al., 1997). When new magnetic flux is added to the lobes, the tail of the magnetosphere extends further. However, during northward IMF conditions, the magnetosphere takes on a more blunt shape (Shue et al. (1997); J. Y. Lu et al. (2011).). Lobe reconnection occurs just tailward of the cusp, where the local geometry differs between the flaring and blunt-shaped magnetosphere. The precise impact of these geometrical changes on the lobe reconnection rate is still unclear. However, it is known that strong lobe reconnection typically occurs during northward IMF conditions. Before a substorm, the magnetotail lobes need to be loaded, resulting in outward flaring of the magnetotail during northward IMF substorms compared to the control group. The substorm process leads to changes in the tail state (Eather et al., 1979), possibly causing a more blunt-shaped magnetopause as magnetic flux becomes closed. Therefore, the observed changes in NBZ currents shown in Figure 2b–2d may reflect variations in the lobe reconnection rate associated with topological changes of the magnetosphere during the substorm.

In summary, we analyzed three substorm lists and found that during northward IMF, the dayside ionospheric currents, as observed with ground magnetometers, respond to substorm activity by increasing the magnitude of the NBZ cells. We found that substorm lists with higher AL index exhibit a higher response in NBZ cells, as shown in Figures 2b–2d and 3c–3f. Interestingly, the NBZ cell response begins a few minutes before substorm onset. We have discussed three possible effects that could account for the observed dayside response to substorms.

- The remote nightside current and the establishment of the substorm current wedge may explain the increase observed in the dayside NBZ cells after onset. However, this factor alone is insufficient to capture the impact prior to substorm onset.
- Compressive and shear Alfvénic waves are mechanisms for communicating between the magnetosphere and the ionosphere. Initially fast mode waves (compressive) could reach the ionosphere before the establishment of a substorm current wedge, and be responsible for the observed dayside enhancement prior to the substorm onset. This is followed by shear Alfvénic waves sustaining the increase during the substorm expansion phase.
- Changes in flaring angle could enhance the lobe reconnection efficiency, maintaining the elevated NBZ cells throughout the substorm.

Data Availability Statement

Magnetometer data can be downloaded directly from https://supermag.jhuapl.edu/mag/ where you need to specify the year to download. Solar wind data (OMNI) can be downloaded from https://cdaweb.gsfc.nasa.gov/sp_phys/data/omni/hro_1min/. Gjerloev and Newell, SOPHIE75, Frey and Liou lists could be downloaded from https://supermag.jhuapl.edu/substorms/ The substorm lists after applying our selection criteria can be downloaded from: https://doi.org/10.5281/zenodo.7990528.

Acknowledgments

This study was supported by the Research Council of Norway/CoE under contracts 223252/F50 and 300844/F50, and by the Trond Mohn Foundation. For the ground magnetometer data we gratefully acknowledge: INTERMAGNET, Alan Thomson; CARISMA, PI Ian Mann; CANMOS, Geomagnetism Unit of the Geological Survey of Canada; The S-RAMP Database, PI K. Yumoto and Dr. K. Shiokawa; The SPIDR database; AARI, PI Oleg Troshichev; The MACCS program, PI M. Engebretson; GIMA; MEASURE, UCLA IGPP and Florida Institute of Technology; SAMBA, PI Eftyhia Zesta; 210 Chain, PI K. Yumoto; SAMNET, PI Farideh Honary; IMAGE, PI Liisa Juusola; Finnish Meteorological Institute, PI Liisa Juusola; Sodankylä Geophysical Observatory, PI Tero Raita; UiT the Arctic University of Norway, Tromsø Geophysical Observatory, PI Magnar G. Johnsen; GFZ German Research Centre For Geosciences, PI Jürgen Matzka; Institute of Geophysics, Polish Academy of Sciences, PI Anne Neska and Jan Reda; Polar Geophysical Institute, PI Alexander Yahnin and Yarolav Sakharov; Geological Survey of Sweden, PI Gerhard Schwarz; Swedish Institute of Space Physics, PI Masatoshi Yamauchi; AUTUMN, PI Martin Connors; DTU Space, Thom Edwards and PI Anna Willer; South Pole and McMurdo Magnetometer, PI's Louis J. Lanzarotti and Alan T. Weatherwax; ICESTAR; RAPIDMAG; British Artarctic Survey; McMac, PI Dr. Peter Chi; BGS, PI Dr. Susan Macmillan; Pushkov Institute of Terrestrial Magnetism, Ionosphere and Radio Wave Propagation (IZMIRAN); MFGI, PI B. Heilig; Institute of Geophysics, Polish Academy of Sciences, PI Anne Neska and Jan Reda; University of L'Aquila, PI M. Vellante; BCMT, V. Lesur and A. Chambodut; Data obtained in cooperation with Geoscience Australia, PI Andrew Lewis; AALPIP, co-PIs Bob Clauer and Michael Hartinger; MagStar, PI Jennifer Gannon; SuperMAG, PI Jesper W. Gjerloev; Data obtained in cooperation with the Australian Bureau of Meteorology, PI Richard Marshall. We acknowledge as well the use of NASA/GSFC's Space Physics Data Facility's OMNIWeb service, and OMNI data.

References

Baker, D. N., Fritz, T. A., McPherron, R. L., Fairfield, D. H., Kamide, Y., & Baumjohann, W. (1985). Magnetotail energy storage and release during the CDAW 6 substorm analysis intervals. *Journal of Geophysical Research*, *90*(A2), 1205–1216. https://doi.org/10.1029/JA090iA02p01205

Chi, P. J., Russell, C. T., & Ohtani, S. (2009). Substorm onset timing via traveltime magnetoseismology. *Geophysical Research Letters*, *36*(8), L08107. https://doi.org/10.1029/2008GL036574

Cowley, S. W. H., & Lockwood, M. (1992). Excitation and decay of solar-wind driven flows in the magnetosphere-ionosphere system. *Annales Geophysicae*, *10*, 103–115. Retrieved from https://centaur.reading.ac.uk/38840/

Eather, R., Mende, S., & Weber, E. (1979). Dayside aurora and relevance to substorm current systems and dayside merging. *Journal of Geophysical Research*, *84*(A7), 3339–3359. https://doi.org/10.1029/JA084iA07p03339

Ferdousi, B., & Raeder, J. (2016). Signal propagation time from the magnetotail to the ionosphere: Openggcm simulation. *Journal of Geophysical Research: Space Physics*, *121*(7), 6549–6561. https://doi.org/10.1002/2016JA022445

Forsyth, C., Rae, I. J., Coxon, J. C., Freeman, M. P., Jackman, C. M., Gjerloev, J., & Fazakerley, A. N. (2015). A new technique for determining substorm onsets and phases from indices of the electrojet (Sophie). *Journal of Geophysical Research: Space Physics*, *120*(12), 10592–10606. https://doi.org/10.1002/2015JA021343

Freeman, M. P., Farrugia, C. J., Burlaga, L. F., Hairston, M. R., Greenspan, M. E., Ruohoniemi, J. M., & Lepping, R. P. (1993). The interaction of a magnetic cloud with the Earth: Ionospheric convection in the northern and southern hemispheres for a wide range of quasi-steady interplanetary magnetic field conditions. *Journal of Geophysical Research*, *98*(A5), 7633–7655. https://doi.org/10.1029/92JA02350

Frey, H. U., Mende, S. B., Angelopoulos, V., & Donovan, E. F. (2004). Substorm onset observations by IMAGE-FUV. *Journal of Geophysical Research*, *109*(A10), 2. https://doi.org/10.1029/2004JA010607

Fukushima, N. (1969). Equivalence in ground geomagnetic effect of chapman–vestine's and Birkeland–Alfven's electric current-systems for polar magnetic storms. *Report of Ionosphere and Space Research in Japan*, *23*, 219–227. Retrieved from https://www.osti.gov/biblio/4755464

Gjerloev, J. W. (2012). The SuperMAG data processing technique. *Journal of Geophysical Research*, *117*(9), 1–19. https://doi.org/10.1029/2012JA017683

Grocott, A., Cowley, S. W. H., Sigwarth, J. B., Watermann, J. F., & Yeoman, T. K. (2002). Excitation of twin-vortex flow in the nightside high-latitude ionosphere during an isolated substorm. *Annales Geophysicae*, *20*(10), 1577–1601. https://doi.org/10.5194/angeo-20-1577-2002

Grocott, A., Laurens, H. J., & Wild, J. A. (2017). Nightside ionospheric convection asymmetries during the early substorm expansion phase: Relationship to onset local time. *Geophysical Research Letters*, *44*(23), 11696–11705. https://doi.org/10.1002/2017GL075763

Huber, P. J. (1964). Robust estimation of a location parameter. *The Annals of Mathematical Statistics*, *35*(1), 73–101. https://doi.org/10.1214/aoms/1177703732

Iijima, T. (1984). Field-aligned currents during northward IMF. In *Magnetospheric currents* (pp. 115–122). American Geophysical Union (AGU). https://doi.org/10.1029/GM028p0115

Laundal, K. M., Finlay, C. C., Olsen, N., & Reistad, J. P. (2018). Solar wind and seasonal influence on ionospheric currents from swarm and champ measurements. *Journal of Geophysical Research: Space Physics*, *123*(5), 4402–4429. https://doi.org/10.1029/2018JA025387

Laundal, K. M., Gjerloev, J. W., Østgaard, N., Reistad, J. P., Haaland, S., Snekvik, K., et al. (2016). The impact of sunlight on high-latitude equivalent currents. *Journal of Geophysical Research: Space Physics*, *121*(3), 2715–2726. https://doi.org/10.1002/2015JA022236

Lee, D., Choi, K., Ohtani, S., Lee, J. H., Kim, K. C., Park, K. S., & Kim, K. H. (2010). Can intense substorms occur under northward IMF conditions? *Journal of Geophysical Research*, *115*(A1), A01211. https://doi.org/10.1029/2009JA014480

Lee, D., Ohtani, S., & Lee, J. H. (2010). On the poleward boundary of the nightside auroral oval under northward interplanetary magnetic field conditions. *Journal of Geophysical Research*, *115*(A8), A08204. https://doi.org/10.1029/2009JA014906

Liou, K. (2010). Polar Ultraviolet Imager observation of auroral breakup. *Journal of Geophysical Research*, *115*(12), 1–7. https://doi.org/10.1029/2010JA015578

Lu, G., Holzer, T. E., Lummerzheim, D., Ruohoniemi, J. M., Stauning, P., Troshichev, O., et al. (2002). Ionospheric response to the interplanetary magnetic field southward turning: Fast onset and slow reconfiguration. *Journal of Geophysical Research*, *107*(A8), SIA2-1–SIA2-9. https://doi.org/10.1029/2001JA000324

Lu, J. Y., Liu, Z.-Q., Kabin, K., Zhao, M. X., Liu, D. D., Zhou, Q., & Xiao, Y. (2011). Three dimensional shape of the magnetopause: Global MHD results. *Journal of Geophysical Research*, *116*(A9), A09237. https://doi.org/10.1029/2010JA016418

Lui, A. T. Y. (2009). Comment on "tail reconnection triggering substorm onset". *Science*, *324*(5933), 1391. https://doi.org/10.1126/science.1167726

Machida, S., Miyashita, Y., Ieda, A., Nosé, M., Nagata, D., Liou, K., et al. (2009). Statistical visualization of the Earth's magnetotail based on geotail data and the implied substorm model. *Annales Geophysicae*, *27*(3), 1035–1046. https://doi.org/10.5194/angeo-27-1035-2009

Madelaire, M., Laundal, K. M., Reistad, J. P., Hatch, S. M., & Ohma, A. (2022). Transient high latitude geomagnetic response to rapid increases in solar wind dynamic pressure. *Frontiers in Astronomy and Space Sciences*, *9*. https://doi.org/10.3389/fspas.2022.953954

McPherron, R. L. (1995). 13 magnetospheric dynamics. In *Chapter 13 introduction to space physics*.

McPherron, R. L., & Manka, R. H. (1985). Dynamics of the 1054ut march 22,1979, substorm event: CDAW 6. *Journal of Geophysical Research*, *90*(A2), 1175–1190. https://doi.org/10.1029/JA090iA02p01175

Milan, S. E. (2015). Sun et lumière: Solar wind-magnetosphere coupling as deduced from ionospheric flows and polar auroras.

Milan, S. E., Gosling, J. S., & Hubert, B. (2012). Relationship between interplanetary parameters and the magnetopause reconnection rate quantified from observations of the expanding polar cap. *Journal of Geophysical Research*, *117*(A3), A03226. https://doi.org/10.1029/2011JA017082

Milan, S. E., Grocott, A., & Hubert, B. (2010). A superposed epoch analysis of auroral evolution during substorms: Local time of onset region. *Journal of Geophysical Research*, *115*(A5), A00I04. https://doi.org/10.1029/2010JA015663

Miyashita, Y., Kamide, Y., Liou, K., Wu, C.-C., Ieda, A., Nishitani, N., et al. (2011). Successive substorm expansions during a period of prolonged northward interplanetary magnetic field. *Journal of Geophysical Research*, *116*(A9), A09221. https://doi.org/10.1029/2011JA016719

Miyashita, Y., Machida, S., Kamide, Y., Nagata, D., Liou, K., Fujimoto, M., et al. (2009). A state-of-the-art picture of substorm-associated evolution of the near-Earth magnetotail obtained from superposed epoch analysis. *Journal of Geophysical Research*, *114*(A1), A01211. https://doi.org/10.1029/2008JA013225

Newell, P. T., & Gjerloev, J. W. (2011). Substorm and magnetosphere characteristic scales inferred from the supermag auroral electrojet indices. *Journal of Geophysical Research*, *116*(A12), A12232. https://doi.org/10.1029/2011JA016936

Ohma, A., Reistad, J. P., & Hatch, S. M. (2021). Modulation of magnetospheric substorm frequency: Dipole tilt and IMF by effects. *Journal of Geophysical Research: Space Physics*, *126*(3), e2020JA028856. https://doi.org/10.1029/2020JA028856

Ohtani, S. (2001). Substorm trigger processes in the magnetotail: Recent observations and outstanding issues. *Space Science Reviews*, *95*(1–2), 347–359. https://doi.org/10.1023/a:1005231122496

Ohtani, S., Creutzberg, F., Mukai, T., Singer, H., Lui, A. T. Y., Nakamura, M., et al. (1999). Substorm onset timing: The December 31, 1995, event. *Journal of Geophysical Research*, *104*(A10), 22713–22727. https://doi.org/10.1029/1999JA900209

Ohtani, S., Imajo, S., Nakamizo, A., & Gjerloev, J. W. (2021). Globally correlated ground magnetic disturbances during substorms. *Journal of Geophysical Research: Space Physics*, *126*(4), e2020JA028599. https://doi.org/10.1029/2020JA028599

Peng, Z., Wang, C., Yang, Y. F., Hu, H. L. Y. Q., & Du, J. (2013). Substorms under northward interplanetary magnetic field: Statistical study. *Journal of Geophysical Research: Space Physics*, *118*(1), 364–374. https://doi.org/10.1029/2012JA018065

Provan, G., Lester, M., Mende, S. B., & Milan, S. E. (2004). Statistical study of high-latitude plasma flow during magnetospheric substorms. *Annales Geophysicae*, *22*(10), 3607–3624. https://doi.org/10.5194/angeo-22-3607-2004

Reistad, J. P., Laundal, K. M., Østgaard, N., Ohma, A., Thomas, E. G., Haaland, S., et al. (2019). Separation and quantification of ionospheric convection sources: 2. The dipole tilt angle influence on reverse convection cells during northward IMF. *Journal of Geophysical Research: Space Physics*, *124*(7), 6182–6194. https://doi.org/10.1029/2019JA026641

Senior, C., Cerisier, J.-C., Rich, F., Lester, M., & Parks, G. K. (2002). Strong sunward propagating flow bursts in the night sector during quiet solar wind conditions: Superdarn and satellite observations. *Annales Geophysicae*, *20*(6), 771–779. https://doi.org/10.5194/angeo-20-771-2002

Sergeev, V. A., Angelopoulos, V., Mitchell, D. G., & Russell, C. T. (1995). In situ observations of magnetotail reconnection prior to the onset of a small substorm. *Journal of Geophysical Research*, *100*(A10), 19121–19133. https://doi.org/10.1029/95JA01471

Shue, J.-H., Chao, J. K., Fu, H. C., Russell, C. T., Song, P., Khurana, K. K., & Singer, H. J. (1997). A new functional form to study the solar wind control of the magnetopause size and shape. *Journal of Geophysical Research*, *102*(A5), 9497–9511. https://doi.org/10.1029/97JA00196

Snekvik, K., Østgaard, N., Tenfjord, P., Reistad, J. P., Laundal, K. M., Milan, S. E., & Haaland, S. E. (2017). Dayside and nightside magnetic field responses at 780 km altitude to dayside reconnection. *Journal of Geophysical Research: Space Physics*, *122*(2), 1670–1689. https://doi.org/10.1002/2016JA023177

Tenfjord, P., Østgaard, N., Strangeway, R., Haaland, S., Snekvik, K., Laundal, K. M., et al. (2017). Magnetospheric response and reconfiguration times following IMF by reversals. *Journal of Geophysical Research: Space Physics*, *122*(1), 417–431. https://doi.org/10.1002/2016JA023018

Weimer, D. R. (2005). Improved ionospheric electrodynamic models and application to calculating joule heating rates. *Journal of Geophysical Research*, *110*(A5), A05306. https://doi.org/10.1029/2004JA010884

Yu, Y., & Ridley, A. J. (2009). Response of the magnetosphere-ionosphere system to a sudden southward turning of interplanetary magnetic field. *Journal of Geophysical Research*, *114*(A3), A03216. https://doi.org/10.1029/2008JA013292

Geophysical Research Letters

Supporting Information for

Substorm Impact on Dayside Ionospheric Currents

R. Elhawary[1], K.M. Laundal[1], J.P. Reistad[1], M. Madelaire[1], A. Ohma[1]

[1]Birkeland Centre for Space Science, Department for Physics and Technology, University of Bergen,

Contents of this file

Figures S1

Introduction

We analyzed different solar wind data obtained from OMNI data set as discussed in the manuscript. No significant impulses around substorm onset (epoch time = 0) are observed in either the median or quantiles of the analyzed parameters.

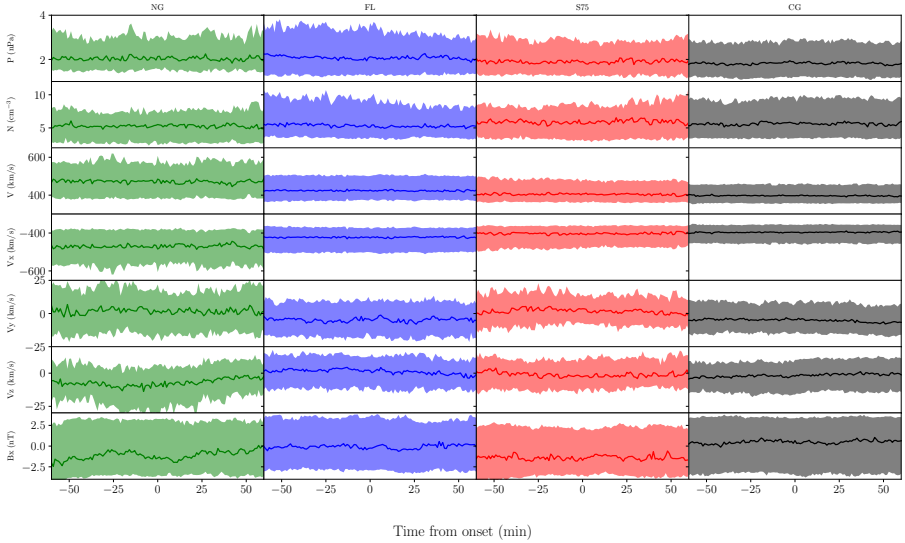

Figure S1. The different solar wind parameter examined to potential influence on the ionospheric current. In all the panels, the median of the solar wind parameters are presented as lines, while the shaded areas represent the 25th and 75th percentiles. the first row represents the pressure of the solar wind. the second row represents the density. then, the following four rows represent V, v_x, v_y and v_z of the solar wind. the last row represents the B_x component. The first column from the left represents the ng list, the second represents the FL list, the third represents the S75 list and the fourth represents the CG.

Paper III

How do substorms influence hemispheric asymmetries in equivalent currents?

Elhawary, R. and Laundal, K. M. and Reistad, J. P. and Madelaire, M
JGR: Space Physics,

Graphic design: Communication Division, UiB / Print: Skipnes Kommunikasjon AS

uib.no

ISBN: 9788230861547 (print)
9788230863220 (PDF)